

AD-A056 978

BOSTON UNIV MASS DEPT OF ASTRONOMY

BEHAVIOR OF THE IONOSPHERIC F-REGION DURING GEOMAGNETIC STORMS (U)

MAR 78 M MENDILLO

F19628-75-C-0044

UNCLASSIFIED

ACBU-SER-III-NO-6

AFGL-TR-78-0092(11)

F/G 4/1

NL

1 of 2

AD  
A056 978



**LEVEL II**

(11)

(6)

BEHAVIOR OF THE IONOSPHERIC F-REGION DURING GEOMAGNETIC STORMS.

(10)

Michael/Mendillo

Department of Astronomy  
Boston University  
725 Commonwealth Avenue  
Boston, Massachusetts 02215

(14) ACBU-SER-III-NO-6

(16) 4643

(17)  $\phi 1$

(18) AFGL

(19) TR-78- $\phi\phi 92(II)$

(15) F19628-75-C- $\phi\phi 44$

DDC  
AUG 3 1978

(9) Final Scientific Report, [redacted]  
1 Sept [redacted] 1974 - 30 Sep [redacted] 1977,

(11)

Mar [redacted] 1978

(12) 166p.

Approved for public release; distribution unlimited.

AIR FORCE GEOPHYSICS LABORATORY  
AIR FORCE SYSTEMS COMMAND  
UNITED STATES AIR FORCE  
HANSCOM AFB, MASSACHUSETTS 01730

AD No. \_\_\_\_\_  
DDC FILE COPY

AD A056978

406 311

JO B

78 07 31 005

UNCLASSIFIED

SECURITY CLASSIFICATION OF THIS PAGE (When Data Entered)

REPORT DOCUMENTATION PAGE		READ INSTRUCTIONS BEFORE COMPLETING FORM
1. REPORT NUMBER AFGL-TR-78-0092(II) <sup>y</sup>	2. GOVT ACCESSION NO.	3. RECIPIENT'S CATALOG NUMBER
4. TITLE (and Subtitle) Behavior of the Ionospheric F-Region During Geomagnetic Storms		5. TYPE OF REPORT & PERIOD COVERED Scientific-Final-Vol.II 1 Sept 1974-30 Sept 1977
		6. PERFORMING ORG. REPORT NUMBER A.C.B.U., Ser III, No 6.
7. AUTHOR(s) Michael Mendillo		8. CONTRACT OR GRANT NUMBER(s) F-19628-75-C-0044
9. PERFORMING ORGANIZATION NAME AND ADDRESS Astronomy Department, Boston University 725 Commonwealth Avenue Boston, MA 02215		10. PROGRAM ELEMENT, PROJECT, TASK AREA & WORK UNIT NUMBERS 62101F 46430107
11. CONTROLLING OFFICE NAME AND ADDRESS Air Force Geophysics Laboratory Hanscom AFB, Bedford, MA 01731 Contract Monitor: J.A. Klobuchar/PHP		12. REPORT DATE MARCH, 1978
		13. NUMBER OF PAGES 164
14. MONITORING AGENCY NAME & ADDRESS (if different from Controlling Office)		15. SECURITY CLASS. (of this report) Unclassified
		15a. DECLASSIFICATION/DOWNGRADING SCHEDULE
16. DISTRIBUTION STATEMENT (of this Report)  Approved for public release; distribution unlimited		
17. DISTRIBUTION STATEMENT (of the abstract entered in Block 20, if different from Report)		
18. SUPPLEMENTARY NOTES		
19. KEY WORDS (Continue on reverse side if necessary and identify by block number) Ionospheric Storms                      Slab Thickness Magnetic Storms                        F-Region Disturbances Total Electron Content                Solar-Terrestrial Relations Peak Density		
20. ABSTRACT (Continue on reverse side if necessary and identify by block number)  The behavior of the ionospheric F-region during geomagnetic storms is addressed by examining many years of total electron content (TEC) data obtained from a semi-global network of TEC observing sites. An analysis procedure is described which leads to the derivation of <u>average disturbance patterns</u> which capture the <u>characteristic features</u> seen during individual storms. These average storm patterns give percentage deviations		

DD FORM 1 JAN 73 1473

EDITION OF 1 NOV 65 IS OBSOLETE

UNCLASSIFIED

SECURITY CLASSIFICATION OF THIS PAGE (When Data Entered)

78 07 31 005

UNCLASSIFIED

SECURITY CLASSIFICATION OF THIS PAGE(When Data Entered)

from monthly median behavior on a local time basis over a 4-day storm period. Primary emphasis is given to disturbance patterns seen over a latitude network spanning the geomagnetic L-shell range  $L \approx 1\frac{1}{2}$  to 5. A clear and recurrent pattern of coupled positive and negative excursions over this latitude range are described on a season by season basis. At lower mid-latitudes ( $L \approx 1\frac{1}{2} - 2$ ), where the largest net changes in ionospheric plasma contents occur, a longitudinal network is used to confirm and contrast the effects observed in the context of the latitudinal patterns.

Multi-year monthly median behavior is given for each site used in the study. A supporting set of average disturbance patterns from previous studies is used to determine solar cycle effects contained in the storm-associated perturbations. The overall picture which emerges suggests that the unified set of average disturbance patterns can be used to update working models of F-region morphology to include storm-time effects. An extensive set of Tables giving the full statistical analyses performed is included as an Appendix.

ACCESSION for	
NTIS	White Section <input checked="" type="checkbox"/>
DOC	Bull Section <input type="checkbox"/>
UNANNOUNCED	<input type="checkbox"/>
JUSTIFICATION.....	
BY.....	
DISTRIBUTION/AVAILABILITY CODES	
Dist.	AVAIL. and/or SPECIAL
A	

UNCLASSIFIED

SECURITY CLASSIFICATION OF THIS PAGE(When Data Entered)

## TABLE OF CONTENTS

I.	Table of Contents . . . . .	iii
II.	Acknowledgements . . . . .	v
III.	List of Figures . . . . .	vi
IV.	List of Tables . . . . .	x
1.	INTRODUCTION . . . . .	1
2.	METHOD OF ANALYSIS . . . . .	3
2.1.	Parameters Examined . . . . .	3
2.2.	Stations Examined . . . . .	5
2.3.	Storm-Period Selection . . . . .	10
2.4.	Storm Analysis Procedure . . . . .	17
2.4.1.	The Control Curve . . . . .	17
2.4.2.	Specifying Departures From the Control Curve . . . . .	19
2.4.3.	Time Resolution . . . . .	20
2.4.4.	Construction of Storm Patterns . . . . .	20
2.4.5.	Analysis Summary . . . . .	24
2.4.6.	Median Data Base Summary for Each Site . . . . .	27
2.4.7.	Assesment of the "Average Storm Pattern" Concept . . . . .	28
3.	F-REGION STORM PATTERNS - THE LATUDINAL NETWORK . . . . .	32
3.1.	Average Storm Patterns -- Narssarssuaq ( $L \approx 5$ ) . . . . .	33
3.2.	Average Storm Patterns -- Goose Bay ( $L \approx 4$ ) . . . . .	51
3.3.	Average Storm Patterns -- Sagamore Hill ( $L \approx 3$ ) . . . . .	66
3.4.	Average Storm Patterns Near $L \approx 2$ . . . . .	82
3.4.1.	Rosman Storm Patterns ( $L \approx 2.2$ ) . . . . .	84
3.4.2.	Kennedy Space Flight Center Storm Patterns ( $L \approx 1.8$ ) . . . . .	87

4.	F-REGION STORM PATTERNS -- THE LONGITUDINAL NETWORK AT MID-LATITUDES ( $L \approx 2$ ) . . . . .	100
4.1.	Average Storm Patterns -- Osan ( $L \approx 1.3$ ) . . . . .	102
4.2.	Average Storm Patterns -- Athens ( $L \approx 1.4$ ) . . . . .	107
4.3.	Average Storm Patterns Near $L \approx 2$ During Solar Maximum Years. . . . .	121
4.4.	Average Storm Patterns Near an $L \approx$ Conjugate Point -- Salisbury ( $L \approx 1.4$ ) . . . . .	125
5.	DISCUSSION AND CASE STUDIES . . . . .	128
5.1.	Summary and General Conclusions . . . . .	128
5.2.	Examples of Storm Effects Along the Latitudinal Network. . . . .	130
5.2.1.	The April 1971 Storm Period . . . . .	130
5.2.2.	The December 1971 Storm Period. . . . .	133
5.2.3.	Latitudinal Distortions Over the $L \approx 3$ to 5 Range . . . . .	137
5.3	Unified Description of Storm Effects Using Average Storm Patterns from $L \approx 1$ to 5 . . . . .	150
6.	LIST OF REFERENCES . . . . .	152
7.	APPENDIX -- Station Summaries of Statistical Patterns of Storm-Induced Perturbations . . . . .	

## ACKNOWLEDGEMENTS

The results contained in this report could not have been achieved without the able assistance of many individuals. Mr. Michael Buonsanto spent two years as a graduate student research assistant, and one year as a full-time research associate, working on several aspects of the study: (1) description of the L=4 ionosphere, (2) the tedious analysis required to establish the TEC data base at each site and (3) extensive computer graphics work for displaying median and disturbed behavior. Mr. Francis X. Lynch worked as a graduate student research assistant during the third year of the study and carried out all of the computer analyses needed to derive the "disturbances patterns" at each site. These conscientious and competent efforts of Mike and Frank are gratefully acknowledged.

All of the total electron content data used in this study were provided by the Air Force Geophysics Laboratory in cooperation with the following individuals and institutions: (a) Narassarssuaq data - Dr. Ib Steen Mikkelsen of the Danish Meteorological Institute, (b) Goose Bay data - personnel of Canadian Marconi Limited, (c) Sagamore Hill data - Mr. Chester Malik and personnel of the Air Weather Service (Detachment 2, 12<sup>th</sup> Weather Squadron), (d) Rosman data - Dr. A.V. daRosa of Stanford University, (e) Kennedy Space Flight Center data - personnel of Pan American World Airways (Meteorology Division), (f) Osan data - personnel of the Air Weather Service (Detachment 15, 30<sup>th</sup> Weather Squadron, and (g) Athens data - Dr. Dimitris Matsoukas of the University of Athens and personnel of the Air Weather Service (Detachment 3 of the Second Weather Wing); a small amount of data from Rhodesia was also furnished by Dr. Matsoukas.

At many stages during the course of this study, colleagues at the Air Force Geophysics Laboratory offered their time and efforts to help address a specific topic or problem. Dr. Jules Aarons was a continued source of support and encouragement; Dr. L. Kersley, Dr. Santimay Basu and Dr. Sunnanda Basu, working under NAS/NRC Fellowships, aided in several discussions; Mr. J. Johanson and Ms. E. Martin of Emmanuel College helped in several areas of computer work and data reduction and presentation.

A special note of thanks is due to the members of the Boston University Astronomy Department who helped in the technical aspects of assembling this report: Ms. Karen Stuart (Department Secretary), Ms. Kem Wefer (Department Librarian), Ms. Joan Kelley (Work-Study Program) and Ms. Barbara Schwartz (Work-Study Program).

It is a pleasure to make the final acknowledgement, in a long litany of thanks, to John Klobuchar, the technical monitor for these investigations under AFGL contract. The overall guidance, years of experience and close collegial fellowship Jack brings to a study under his mentorship surely accounts in a most fundamental and substantive way for the ultimate success of the research program -- and for this we are continually grateful.

78 07 31 005

## LIST OF FIGURES

FIGURE 1.	Network of Total Electron Content (TEC) Observing Sites Spanning the 70°W Meridian Discussed in This Report . . . . .	6
FIGURE 2.	Full Network of Total Electron Content (TEC) Observing Sites Discussed in This Report . . . . .	8
FIGURE 3.	Example of Local Time Distribution Scheme of Storm Commencement Times Used to Obtain Average Local Time Patterns -- taken from AFCRL ATLAS of 75 storm periods at Sagamore Hill (Mendillo and Klobuchar, 1974) . . . . .	25
FIGURE 4a.	Monthly Median Behavior at Narssarssuaq - TEC, 1972 . . . . .	34
" "b.	" " " " " " - " , 1973 . . . . .	35
" "c.	" " " " " " - " , 1974 . . . . .	36
FIGURE 5.	Average Local Time Disturbance Variations, SD(%), in TEC at Narssarssuaq Obtained From 70 Storm Periods . . . . .	38
FIGURE 6a.	SD(TEC) Pattern at Narssarssuaq for 18 Winter Storms . . . . .	39
" "b.	" " " " " " 14 Spring " . . . . .	40
" "c.	" " " " " " 24 Summer " . . . . .	41
" "d.	" " " " " " 14 Fall " . . . . .	42
" "e.	" " " " " " 28 Equinox " . . . . .	43
FIGURE 7a.	Monthly Median Behavior at Goose Bay - TEC, 1972 . . . . .	46
" "b.	" " " " " " - " , 1973 . . . . .	47
" "c.	" " " " " " - " , 1974 . . . . .	48
" "d.	" " " " " " - " , 1975 . . . . .	49
" "e.	" " " " " " - " , 1976 . . . . .	50
FIGURE 8.	Average Local Time Disturbance Variations, SD(%), in TEC, $N_{max}$ and $\tau$ at Goose Bay Obtained From 67 Storm Periods . . . . .	52
FIGURE 9a.	SD(TEC, $N_{max}$ , $\tau$ ) Patterns at Goose Bay for 22 Winter Storms . . . . .	58
" "b.	" " " " " " 13 Spring " . . . . .	59
" "c.	" " " " " " 21 Summer " . . . . .	60
" "d.	" " " " " " 11 Fall " . . . . .	61
" "e.	" " " " " " 24 Equinox " . . . . .	62

FIGURE 10a.	Monthly Median Behavior of TEC at Goose Bay and Sagamore Hill (Hamilton), 1971-1975 . . . . .	67
FIGURE 10b.	Monthly Median Behavior of $N_{\max}$ at St. John's and Wallops Island, 1972-1975 . . . . .	68
FIGURE 11.	Average Local Time Disturbance Variations, SD(%), in TEC at Sagamore Hill Obtained From 109 Storm Periods . . . . .	70
FIGURE 12.	(a) SD(TEC, $N_{\max}$ , $\tau$ ) Patterns at Sagamore Hill Obtained From 75 Storm Periods in 1967-1972 (Hamilton-B data, Mendillo, 1974) . . . . .	72
	(b) SD (TEC, $N_{\max}$ , $\tau$ ) Patterns at Sagamore Hill Obtained From 28 Storm Periods in 1967-1969 (Hamilton-C data, Mendillo et al., 1972) . . . . .	72
FIGURE 13a.	SD(TEC) Pattern at Sagamore Hill for 34 Winter Storms . . . . .	75
" " b.	" " " " " " 21 Spring " . . . . .	76
" " c.	" " " " " " 35 Summer " . . . . .	77
" " d.	" " " " " " 19 Fall " . . . . .	78
" " e.	" " " " " " 40 Equinox " . . . . .	79
FIGURE 14.	Monthly Median Behavior of TEC at Rosman, N.C. - 1972 . . . . .	85
FIGURE 15.	Average Local Time Disturbance Variations, SD(%), in TEC at Rosman Obtained From 13 Storm Periods . . . . .	86
FIGURE 16a.	Monthly Median Behavior at Cape Kennedy - TEC, 1974 . . . . .	88
" " b.	" " " " " " - " , 1975 . . . . .	89
" " c.	" " " " " " - " , 1976 . . . . .	90
FIGURE 17.	Average Local Time Disturbance Variations, SD(%), in TEC at Cape Kennedy Obtained From 70 Storm Periods . . . . .	91
FIGURE 18a.	SD(TEC) Pattern at KSFC For 26 Winter Storms . . . . .	93
" " b.	" " " " " " 15 Spring " . . . . .	94
" " c.	" " " " " " 22 Summer " . . . . .	95
" " d.	" " " " " " 7 Fall " . . . . .	96
" " e.	" " " " " " 22 Equinox " . . . . .	97

FIGURE 19a.	Monthly Median Behavior at Osan - TEC, 1974 . . . . .	103
" " b.	" " " " " " - " , 1975 . . . . .	104
" " c.	" " " " " " - " , 1976 . . . . .	105
FIGURE 20.	Average Local Time Disturbance Variations, SD(%), in TEC at Osan Obtained From 31 Storm Periods . . . . .	106
FIGURE 21a.	Monthly Median Behavior at Athens - TEC, 1972 . . . . .	108
" " b.	" " " " " " - " , 1973 . . . . .	109
" " c.	" " " " " " - " , 1974 . . . . .	110
" " d.	" " " " " " - " , 1975 . . . . .	111
" " e.	" " " " " " - " , 1976 . . . . .	112
FIGURE 22.	Average Local Time Disturbance Variations, SD(%), in TEC at Athens Obtained From 63 Storm Periods . . . . .	114
FIGURE 23a.	SD(TEC) Pattern at Athens For 16 Winter Storms . . . . .	115
" " b.	" " " " " " 10 Spring " . . . . .	116
" " c.	" " " " " " 20 Summer " . . . . .	117
" " d.	" " " " " " 17 Fall " . . . . .	118
" " e.	" " " " " " 27 Equinox " . . . . .	119
FIGURE 24.	(a) Average Local Time Disturbance Variations for 28 Storm Periods in 1967-1969 at Stanford (from Mendillo, 1976) . . . . .	123
	(b) Average Local Time Disturbance Variations for 12 Storm Periods in 1968-1970 at Arecibo (Lanzerotti et al., 1975) . . . . .	123
FIGURE 25.	Average Local Time Disturbance Variations, SD(%), in TEC at Salisbury (Conjugate Point to Athens) Obtained From 6 Daytime SC Periods . . . . .	126

FIGURE 26.	Map of TEC Observing Stations and 400 km Sub-Ionospheric Points Showing Invariant Latitudes . . . . .	131
FIGURE 27.	Three-Site TEC Observations During the Geomagnetic Storm Period 14-15 April 1971 . . . . .	132
FIGURE 28.	Contour of TEC Monthly Median Diurnal Behavior Over the $\Lambda \approx 45^\circ - 75^\circ$ Latitude Range For April 1971 . . . . .	134
FIGURE 29.	Daily TEC Contours Giving Latitude/Local Time Behavior Near $70^\circ\text{W}$ on 14-15 April 1971 . . . . .	135
FIGURE 30.	Summary of Storm-Induced Perturbations (in %) For TEC Latitude/Local Time Behavior Near $70^\circ\text{W}$ on 14-15 April 1971 . . . . .	136
FIGURE 31.	Four-Site TEC Observations During the Geomagnetic Storm Period 17-18 December 1971 . . . . .	138
FIGURE 32.	Contours of TEC Monthly Median Diurnal Behavior Over the $\Lambda \approx 35^\circ - 75^\circ$ Latitude Range For December 1971 . . . . .	139
FIGURE 33.	Daily TEC Contours Giving Latitude/Local Time Behavior Near $70^\circ\text{W}$ on 17-18 December 1971 . . . . .	140
FIGURE 34a.	TEC Median Diurnal Behavior, $L \approx 3-5$ -- May, Jun, 1972 . . .	141
" " b.	" " " " " " -- Jul, Aug, 1972 . . .	142
" " c.	" " " " " " -- Sep, Oct, 1972 . . .	143
" " d.	" " " " " " -- Nov, Dec, 1972 . . .	144
" " e.	" " " " " " -- Jan, Feb, 1973 . . .	145
" " f.	" " " " " " -- Mar, Apr, 1973 . . .	146
FIGURE 35.	Four-Site TEC Observations During The Geomagnetic Storm Period 15-16 May, 1972 . . . . .	147
FIGURE 36.	Four-Site TEC Observations During The Geomagnetic Storm Period 31 Oct-1 Nov, 1972 . . . . .	149
FIGURE 37.	Unified Summary of Latitude/Local Time Average Storm Patterns . . . . .	151

## List of Tables

Table I - Summary of TEC Observing Sites, Satellites Observed and Sub-Ionospheric Point Parameters . . . . .	9
Table II - Storm Periods Examined - 1971 . . . . .	12
Table III - Storm Periods Examined - 1972 . . . . .	12
Table IV - Storm Periods Examined - 1973 . . . . .	13
Table V - Storm Periods Examined - 1974 . . . . .	14
Table VI - Storm Periods Examined - 1975 . . . . .	15
Table VII - Storm Periods Examined - 1976 . . . . .	16
Table VIII - Summary of Station/Parameter Data Coverage and Storm Periods Examined . . . . .	18
Table IX - Summary of Storm Classification Scheme Used in Deriving Average Local Time Patterns SD(%) at Each Site . . . . .	26
Table X - Seasonal Characteristics of the TEC Afternoon Increase at Narssarssuaq (L=5) . . . . .	45
Table XI - Seasonal Characteristics of the TEC Afternoon Increase at Goose Bay (L=4) . . . . .	63
Table XII - Seasonal Characteristics of the TEC Nighttime Increase at Goose Bay (L=4) . . . . .	63
Table XIII - Seasonal Characteristics of the TEC Afternoon Increase at Sagamore Hill (L=3) Using Three Different Data Sets . . . . .	80
Table XIV - Seasonal Characteristics of the TEC Nighttime Depletion on the 3 <sup>rd</sup> Day of a Storm at Sagamore Hill (L=3) Using Three Different Data Sets . . . . .	81
Table XV - Seasonal Characteristics of the Daytime and Nighttime Enhancements in TEC at Cape Kennedy (L=2) on the 1 <sup>st</sup> Day of a Storm Period . . . . .	98
Table XVI - Seasonal Characteristics of the TEC Nighttime Depletion on the 3 <sup>rd</sup> Day of a Storm at Cape Kennedy (L=2) . . . . .	98
Table XVII - Seasonal Characteristics of the Daytime and Nighttime Enhancements in TEC at Athens (L=2) on the 1 <sup>st</sup> Day of a Storm Period . . . . .	120

## 1. INTRODUCTION

This report describes the final results of a major (3-year) study of ionospheric storms. While the phrase "Ionospheric Storm" is a commonly used one, it should be made clear that the disturbance effects under study are those ionospheric perturbations found to be associated with a wide range of simultaneous environmental disturbances which are ultimately launched by changing characteristics of the solar wind. Thus, the "Ionospheric Storm" is not an internal response to a self-generated stress (as might be said, for example, for a meteorological storm), but rather a pure and simple response to an imposed stress.

From a historical perspective, the first widely studied solar-terrestrial disturbance was the geomagnetic storm, and thus one is often faced with the tendency to label an ionospheric storm as "the response of the ionosphere to a geomagnetic storm". This is a perfectly reasonable phrase as long as one keeps in mind that the ionospheric perturbations are not caused by the magnetic variations (as would be the case, for example, if we spoke of the "current storm" induced in high voltage wires during a magnetic storm).

Ionospheric storms are thus associated with magnetic storms, as are auroral displays and perhaps even some aspects of meteorological storms. In this study, we follow the traditional practice of using the geomagnetic storm as the indicator of a solar-terrestrial active period and then seek to document those

ionospheric disturbance effects which accompany the geomagnetic storm.

It is, of course, well known that in the absence of storm-time perturbations the ionosphere still undergoes a so-called "day-to-day variability". The much larger variations seen during storms define the maximum possible range for an ionospheric parameter. This is one of the major reasons for studying ionospheric storms, in that knowledge of this sort impacts both the user of ionospherically supported radio systems, as well as the search for the correct physical processes which account for observed effects.

There are many similarities between the character of storm-time perturbations of the ionosphere and those variations which are normally associated with the solar cycle, seasonal and even day-to-day effects. The mechanisms which act during storms are thus expected to be nothing more than concentrated doses of physical processes which normally affect the ionosphere in more subtle ways. Throughout our storm studies, our goal has been to determine the coupled spatial and temporal characteristics of the ionospheric disturbances in the hope of using the derived morphologies to isolate the physical processes most capable of influencing ionospheric variability in general.

In the following chapters we describe the complete analysis procedure used in these studies (Chapter 2), and then present average results for storm patterns as a function of latitude (Chapter 3) and longitude (Chapter 4). In Chapter 5 we discuss a unified picture of the overall results, and present several "case studies" showing latitudinal effects.

## 2. METHOD OF ANALYSIS

### 2.1 Parameters Examined.

This study of F-region storm effects relies almost exclusively upon the ionospheric parameter total electron content (TEC). The ionospheric TEC refers to the height integral of the ionospheric electron density profile,  $N_e(h)$ , and therefore contains contributions from all of the various ionospheric regions (D, E, F1 and F2). Since the F-region  $N_e$  values easily account for more than 90% of the integral, TEC is rightly considered a measure of the F-region total plasma content. This columnar content is obtained by continuously monitoring the amount of Faraday rotation (polarization twist) a VHF radiowave wave experiences in traversing the ionosphere. Since the amount of Faraday rotation depends on the geomagnetic field strength, most of the rotation occurs within the first few thousand kilometers above the Earth's surface. It is generally agreed that, within an accuracy of 5-10%, the Faraday technique gives the ionospheric content up to a height of approximately 2000 km. Thus, in spite of the fact that the VHF signals monitored come from geostationary satellites at  $\approx 6\frac{1}{2}$  earth radii, the Faraday measurement yields only the ionospheric content (TEC, or sometimes given the symbols  $N_T$ ,  $N_F$  or  $N_I$ ).

Details of the interpretation and data reduction methods of Faraday rotation observations are given by Titheridge (1972), Mendillo and Klobuchar (1974) and Papagiannis et al. (1975). Most of the experimental arrangements and actual data taking and initial

data reduction for the TEC measurements examined in this study were carried out by J. A. Klobuchar of the Air Force Geophysics Laboratory (AFGL). The reader is referred to Klobuchar's description of these procedures in the report recently published by Eis, Klobuchar and Malik (1977).

The TEC parameter is a quantity well suited for storm studies. The major reason for this is the fact that the occurrence of a disturbed ionosphere does not interfere with the continuous monitoring of the Faraday effect. Thus, while severe distortions of the  $N_e(h)$  profile may occur, while the VHF signal may suffer amplitude scintillations due to  $N_e$  irregularities, or some absorption effects may occur, the measurement is basically unaffected by these often drastic processes. Conventional ionosonde measurements, on the other hand, can suffer severe degradations during storm periods, and thus the events of most interest can be lost to the very effects under study.

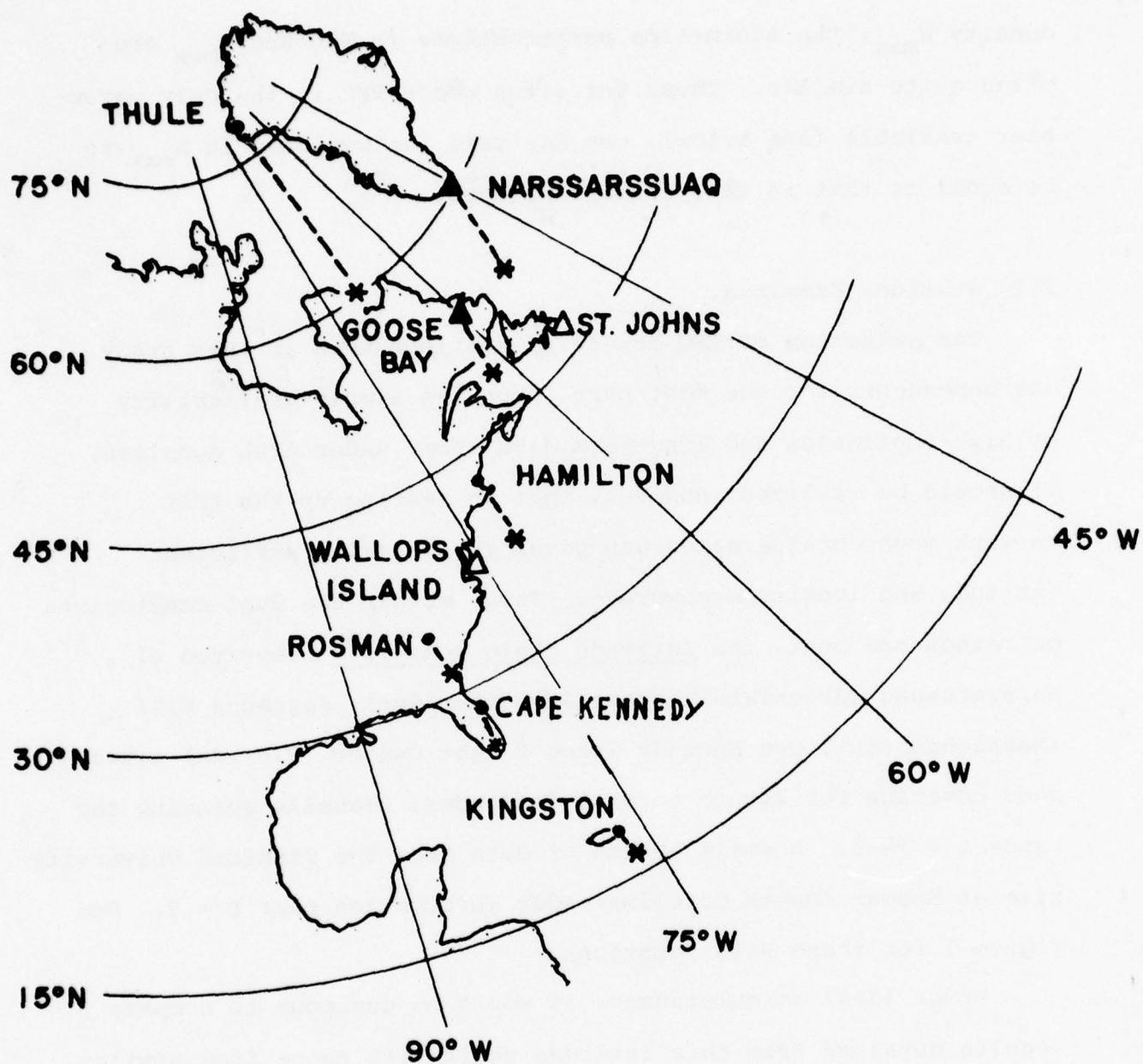
When possible, we have tried to incorporate ionosonde data into our storm studies. Specifically, foF2 (the F-region's critical or penetration frequency) has been used to obtain the peak electron density of the ionosphere ( $N_{\max}$  at  $h_{\max}$ ) at sites close to the TEC observing sites. The availability of both TEC and  $N_{\max}$  data for a given site permits one to form the parameter equivalent slab thickness ( $\tau \equiv \text{TEC}/N_{\max}$ ), which gives a first-order measure of the width or thickness of the  $N_e(h)$  profile. In summary, then, the F-region parameters examined in this study are TEC,  $N_{\max}$ , and  $\tau$ . Since the TEC refers to the integral of a  $N_e(h)$  profile of peak

density  $N_{\max}$ , the storm-time perturbations in TEC and  $N_{\max}$  are often quite similar. Thus, for sites where TEC is the only parameter available (see below), one may take the response in  $N_{\max}$  to be equal to that in TEC, ceteris paribus.

## 2.2 Stations Examined.

The selection of TEC observing stations used in this study was dependent, for the most part, upon the simple availability of high-confidence and long-term data taken under AFGL auspices. It should be realized, however, that in setting up the AFGL network much consideration was given to obtaining sufficient latitude and longitude coverage. Thus, within the dual constraints of reason and cost, the latitude chain near 70°W comprised of Narssarssuaq (Greenland), Goose Bay (Labrador), Sagamore Hill (Massachusetts), and Kennedy Space Flight Center (Florida) gives good coverage for low to auroral latitudes, L-shells spanning the range  $L = 1\frac{1}{2}$ -5. A small amount of data from the Stanford University site at Rosman (North Carolina) adds information near  $L = 2$ . See Figure 1 for these site locations.

Under ideal circumstances, it would be desirable to compare results obtained from this latitude chain with those from similar chains at other longitudes. The reason for this lies in the fact that ionospheric processes (quiet as well as disturbed time effects) depend upon both geographic and geomagnetic coordinates. Since the geomagnetic axis is tilted to the Earth's axis of rotation, the difference between geographic and geomagnetic latitudes is a



TEC OBSERVING STATIONS •

TEC 420 KM SUB-ION. PTS. \*  
(ATS - 3 AT 70° W)

IONOSONDE STATIONS Δ

FIGURE 1.

strong function of longitude. Thus, while solar production effects depend only on geographic latitude, plasma transport depends on geomagnetic coordinates, and therefore the resultant ionospheres at identical latitudes can often exhibit noticeably different characteristics.

Our analysis of the longitudinal effects associated with ionospheric disturbances was limited to low latitudes -- latitudes characterized by  $L \approx 1\frac{1}{2}$ . This choice was motivated by the availability of AFGL data, as well as the realization that storm effects at low latitudes often involve the largest net changes in total plasma content. The impact of storms upon ionospheric - dependent radio propagation systems (e.g., trans-ionospheric ranging networks) are therefore largest at low latitudes, and consequently longitudinal effects are of considerable interest. In this study, we used TEC observations from Athens (Greece) and Osan (Korea) to compare low-latitude average storms effects at widely separated longitudes with those obtained at Cape Kennedy. A small amount of data from Salisbury (Rhodesia) was also used to examine low-latitude storm patterns at geomagnetic conjugate points (i.e., the Athens/Salisbury sites). See Figure 2 for site comparisons.

In Table I, we present a comprehensive summary of the TEC observing sites. For each station, the geographic coordinates of the antenna site used in the observations are given. The geostationary satellite(s) under observation are given, with nominal position values, together with antenna-to-satellite elevation and azimuth angles. The 420-km sub-ionospheric coordinates are given in geo-

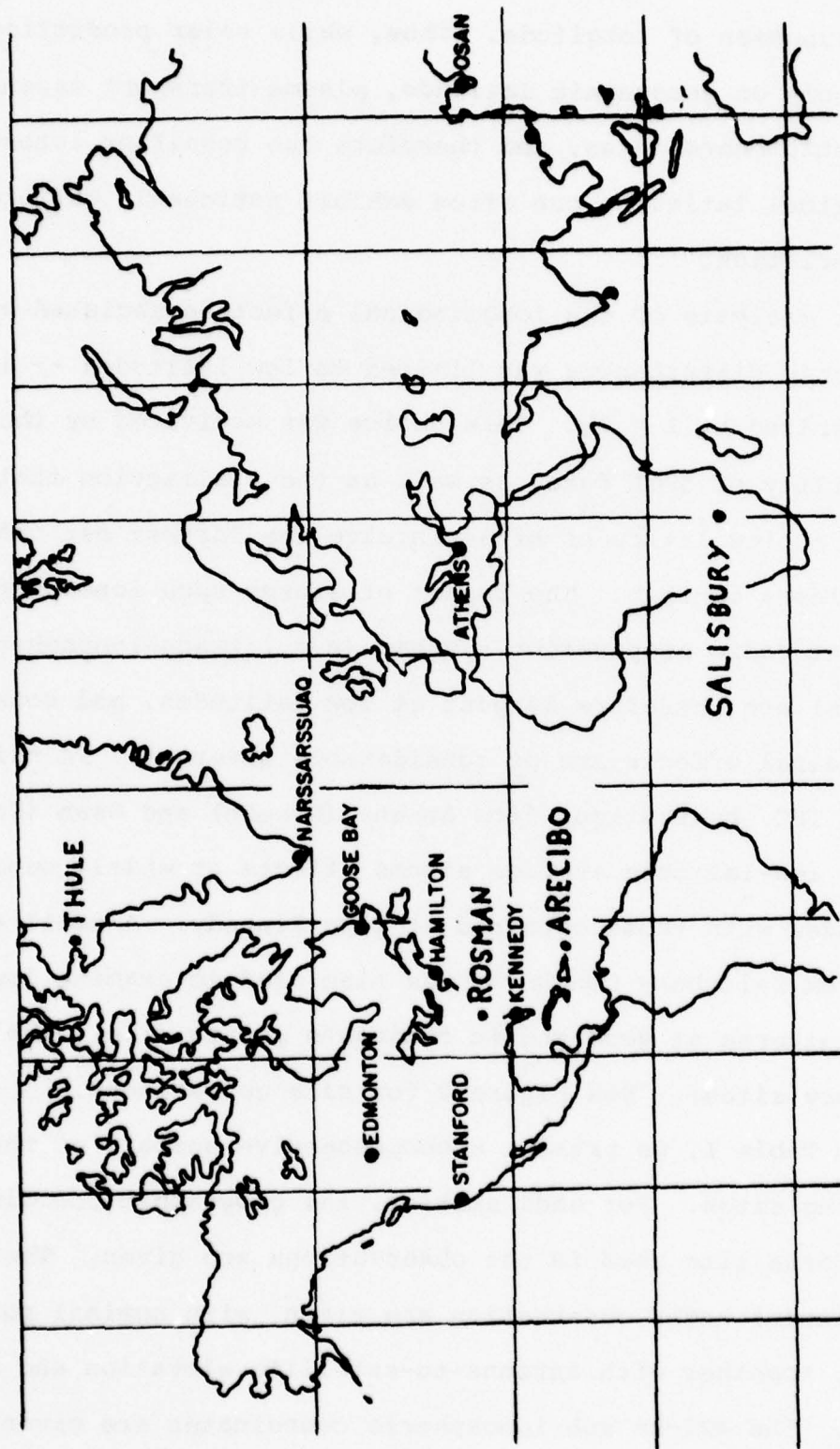


FIGURE 2.

Table I

ANTENNA SITES			SATELLITE INFORMATION				
STATION NAME	LAT	LONG	NAME OF SAT	LAT	LONG	ELEV (°)	AZIMUTH (°)
	(°N)	(°E)		Nominal Values	(°E)		
NARSSARSSUAQ	61.2	-45.4	ATS-3	0	-70*	17.9	207.6
GOOSE BAY	53.3	-60.3	ATS-3	0	-70*	28.7	192.0
HAMILTON	42.6	-70.8	ATS-3	0	-70*	41.0	178.8
ATHENS	38.0	23.7	152F2	0	-34 to 97	4to46 (34.2)†	133.0†
OSAN	37.2	127.10	152F2	0	135 to 200	5to46 (18.4)†	112.3†
ROSMAN, N.C.	35.1	-82.9	ATS-3	0	-70*	42.7	158.2
KENNEDY SFC	28.6	-80.6	ATS-3	0	-70*	54.8	158.5
SALISBURY, RHODESIA	-17.5	31.05	152F3	0	-16†	33.3	285.5

420 Km Sub-ionospheric point parameters					Solar Positions			
STATION NAME	LAT	LONG	Dip(I)	Inv(A)	X at sub-ion point			
					L	S SOL	W SOL	EQUINOX
						(12 LT)		
NARSSARSSUAQ	53.1	-52.2	74.9	63.03	4.86	29.7	76.5	54.4
GOOSE BAY	47.5	-62.2	74.1	59.75	3.94	24.1	70.9	48.8
HAMILTON	38.7	-70.7	69.9	52.79	2.94	15.3	62.1	40.0
ATHENS	33-35	13 to 43 +(28)†	48.5	31.03	1.36	10.6	57.4	35.3
OSAN	33-34	128 to 146 +(137)†	45.7	26.76	1.25	10.6	57.4	35.3
ROSMAN, N.C.	32.1	-81.5	64.6	46.51	2.11	8.7	55.5	35.4
KENNEDY SFC	26.3	-79.6	59.3	41.39	1.78	2.9	49.7	27.6
SALISBURY,	-15.9	26.0	-50.2	29.86	1.33	39.3	7.5	14.6

\*Nominal value; changes in the ATS-3 satellite position were small ( $\approx$  few degrees) after mid-1971; position varied by  $\approx 40^\circ$  before then. ATS-3 began moving again in July 1976.

† Nominal Value

graphic positions, together with three specifications of geomagnetic coordinates: the dip angle ( $I$ ), the invariant latitude ( $\Lambda$ ) at 420 km and its associated  $L$  - shell. In order to gauge solar production conditions at the sub-ionospheric point, the noontime solar zenith angle ( $\chi$ ) is given for summer solstice, winter solstice and equinox conditions.

### 2.3. Storm-Period Selection.

As mentioned in the Introduction, our concept for ionospheric storm selection rests upon the definition of well defined geomagnetic storm periods. In our earlier studies of storm effects in the Sagamore Hill TEC, we defined a geomagnetic storm severity criterion in the hope of studying only strong events in which the ionospheric perturbations would be clear and easily identified. These criteria were described in detail in the AFCRL ATLAS of storm effects (Mendillo and Klobuchar, 1974). For this study we use a slightly modified scheme which permits a few weaker storms to be included and does not limit the examination of geomagnetic storm commencement times to a single, nearby observatory (Fredericksburg). Since we consider a data base which spans the years 1971-1976, years which overlap those covered in the ATLAS (1967-1972), we decided to keep to the same numbering sequence started in the ATLAS (#'s 1-75).

In selecting geomagnetic storms we consider both sudden storm commencements (SSCs), gauged to the nearest minute, and gradual storm commencements (GSC's), gauged to the nearest hour. The existence criterion for a substantial geomagnetic perturbation

was taken to be either a storm during which the planetary magnetic index  $A_p$  was  $\geq 30$  for at least one day of the storm period (equivalent to  $K_p = 4^+$  all day), or a storm during which the 3-hr planetary magnetic index  $K_p$  was  $\geq 5$  during the storm period. Since primary emphasis was to be placed on studying the TEC response from the latitude chain of stations at  $70^\circ$  W, the magnetometer station at Fredericksburg (Va) was used as the primary site to define SSC and GSC times. When Fredericksburg did not record a clear storm commencement time, we turned to the records from Boulder, Tucson, San Juan, Newport or College for the SC time. For SSC events, the selection of a station's commencement time matters little since the very nature of the event means global simultaneity. The GSC events do present a problem since even relatively close stations (FRED, BOUL or TUCS) can differ by several hours or more in specifying the UT beginning time of the disturbance (hence the "G" for gradual!)

In using a list of SC events determined for a latitude network to study longitude effects again presents a problem for the GSC periods. We feel that since the number of storm periods examined at Osan and Athens is large, the comparison of their results with Cape Kennedy data (at a longitude appropriate to the GSC selections) is a reasonable way of assessing longitudinal differences in simultaneous events.

In Tables II through VII we list the storm periods examined, separated by year (1971-1976). We note that the number of events tends to increase as solar minimum approaches (annual events

Table II

## STORM PERIODS EXAMINED - 1971

<u>STORM NUMBER</u>	<u>DATE</u>	<u>S.C. TIME (U.T.)</u>	<u>STATION NAME</u>	<u>MAX. VALUE OF K<sub>p</sub></u>	<u>MAX. VALUE OF A<sub>p</sub></u>
46	27 January	SSC = 04:30	FRED	5	39
47	15 February	GSC = 13:--	FRED	5	29
48	24 February	GSC = 21:--	FRED	7	43
49	12 March	GSC = 20:--	FRED	5	39
50	3 April	SSC = 21:39	FRED	6	27
51	9 April	SSC = 04:29	FRED	6	53
52	14 April	SSC = 12:43	FRED	7	39
53	5 May	GSC = 16:--	FRED	6	50
54	16 May	GSC = 23:--	FRED	6	73
55	25 June	GSC = 05:--	FRED	5	32
56	17 September	GSC = 18:--	FRED	5	47
57	26 September	GSC = 16:--	FRED	6	38
58	8 October	SSC = 17:03	FRED	5	37
59	22 November	GSC = 18:--	FRED	6	45
60	17 December	SSC = 14:18	FRED	6	67

Table III

## STORM PERIODS EXAMINED - 1972

<u>STORM NUMBER</u>	<u>DATE</u>	<u>S.C. TIME (U.T.)</u>	<u>STATION NAME</u>	<u>MAX. VALUE OF K<sub>p</sub></u>	<u>MAX. VALUE OF A<sub>p</sub></u>
61	21 January	SSC = 11:51	FRED	5	32
62	24 February	SSC = 06:42	SJUA	5	33
63	6 March	SSC = 21:08	SJUA	7	45
64	29 April	GSC = 03:--	FRED	6	42
65	15 May	SSC = 18:49	FRED	6	38
66	17 June	SSC = 13:12	FRED	8	126
67	24 July	GSC = 19:--	FRED	6	33
68	4 August	SSC = 01:19	FRED	9	182
69	8 August	SSC = 23:54	FRED	6	74
70	13 September	SSC = 12:40	FRED	8	54
71	18 October	SSC = 17:46	FRED	5	34
72	31 October	SSC = 16:58	FRED	7	98
73	15 November	GSC = 09:--	NEWP	5	31
74	12 December	SSC = 21:45	BOUL	5	30
75	15 December	GSC = 19:--	FRED	5	33

Table IV

## STORM PERIODS EXAMINED - 1973

<u>STORM NUMBER</u>	<u>DATE</u>	<u>S.C. TIME (U.T.)</u>	<u>STATION NAME</u>	<u>MAX. VALUE OF Kp</u>	<u>MAX. VALUE OF A<sub>p</sub></u>
76	27 January	GSC=04:--	FRED	5	33
77	21 February	GSC=16:--	BOUL	6	54
78	1 March	GSC=15:--	TUCS	5	40
79	18 March	GSC=12:--	FRED	6	82
80	31 March	GSC=13:--	BOUL	6	91
81	13 April	SSC=04:34	FRED	6	57
82	26 April	GSC=12:--	FRED	5	59
83	13 May	GSC=17:--	FRED	7	80
84	21 May	SSC=02:54	FRED	6	46
85	10 June	GSC=15:--	FRED	5	34
86	17 June	GSC=19:--	FRED	5	38
87	28 June	GSC=21:--	FRED	5	41
88	14 July	GSC=15:--	FRED	5	32
89	26 July	GSC=03:--	FRED	5	36
90	23 August	GSC=12:--	FRED	6	46
91	9 September	GSC=08:--	TUCS	5	44
92	22 September	GSC=21:--	FRED	6	63
93	2 October	GSC=05:--	FRED	6	48
94	16 October	SSC=05:20	TUCS	5	30
95	21 October	GSC=01:--	FRED	5	37
96	28 October	GSC=07:--	FRED	6	86
97	24 November	GSC=13:--	FRED	6	42
98	4 December	GSC=15:--	FRED	5	29
99	19 December	GSC=08:--	BOUL	5	34

Table V

## STORM PERIODS EXAMINED - 1974

<u>STORM NUMBER</u>	<u>DATE</u>	<u>S.C. TIME (U.T.)</u>	<u>STATION NAME</u>	<u>MAX. VALUE OF Kp</u>	<u>MAX. VALUE OF A<sub>p</sub></u>
100	24 January	GSC=03:--	FRED	6	50
101	11 February	GSC=13:--	FRED	5	40
102	22 February	GSC=21:--	FRED	5	44
103	9 March	GSC=03:--	BOUL	6	33
104	16 March	GSC=05:--	BOUL	5	42
105	20 March	GSC=19:--	FRED	6	68
106	2 April	GSC=19:--	FRED	5	39
107	18 April	GSC=02:--	FRED	6	48
108	4 May	GSC=01:--	FRED	5	35
109	16 May	GSC=17:--	FRED	6	38
110	31 May	GSC=03:--	FRED	5	30
111	10 June	SSC=18:49	FRED	5	32
112	25 June	SSC=23:29	FRED	6	54
113	4 July	SSC=15:33	FRED	9	74
114	6 July	SSC=03:21			130
115	8 July	GSC=06:--	FRED	5	36
116	22 July	GSC=21:--	FRED	6	82
117	2 August	GSC=13:--	FRED	5	35
118	18 August	GSC=21:--	FRED	6	46
119	29 August	GSC=03:--	BOUL	6	31
120	15 September	SSC=13:43	FRED	7	88
121	18 September	SSC=14:34	FRED	6	43
122	24 September	GSC=04:--	FRED	5	38
123	12 October	SSC=12:44	FRED	6	86
124	14 October	SSC=16:34	BOUL	6	68
125	23 October	GSC=19:--	FRED	6	38
126	8 November	SSC=14:14	FRED	6	39
127	11 November	GSC=07:--	FRED	5	70
128	8 December	GSC=15:--	TUCS	5	42
129	17 December	GSC=15:--	TUCS	4	28

Table VI

## STORM PERIODS EXAMINED - 1975

<u>STORM NUMBER</u>	<u>DATE</u>	<u>S.C. TIME (U.T.)</u>	<u>STATION NAME</u>	<u>MAX. VALUE OF K<sub>p</sub></u>	<u>MAX. VALUE OF A<sub>p</sub></u>
130	6 January	SSC=19:58	BOUL	7	44
131	7 January	SSC=23:22	FRED	5	36
132	13 January	GSC=01:--	BOUL	5	33
133	16 January	GSC=14:--	BOUL	5	29
134	31 January	GSC=11:--	BOUL	5	37
135	9 February	GSC=21:--	BOUL	6	38
136	23 February	GSC=06:--	BOUL	6	32
137	5 March	GSC=02:--	BOUL	5	30
138	9 March	GSC=23:--	FRED	6	80
139	27 March	GSC=13:--	FRED	5	38
140	7 April	GSC=15:--	FRED	5	52
141	20 April	GSC=16:--	BOUL	6	25
142	4 May	GSC=23:--	FRED	6	35
143	16 May	SSC=03:08	FRED	6	28
144	19 May	SSC=19:50	FRED	6	23
145	1 June	GSC=13:--	FRED	5	28
146	11 June	GSC=08:--	BOUL	5	27
147	29 June	GSC=13:--	FRED	5	26
148	8 July	GSC=02:--	BOUL	6	37
149	24 July	GSC=21:--	FRED	6	33
150	5 August	GSC=01:--	BOUL	5	29
151	28 August	GSC=21:--	FRED	5	27
152	9 September	GSC=02:--	BOUL	6	26
153	7 October	GSC=01:--	FRED	6	45
154	2 November	GSC=15:--	FRED	6	65
155	9 November	SSC=07:53	BOUL	5	37
156	21 November	SSC=23:05	FRED	5	50
157	29 November	GSC=04:--	FRED	5	36
158	25 December	GSC=23:--	FRED	5	34

Table VII

## STORM PERIODS EXAMINED - 1976

<u>STORM NUMBER</u>	<u>DATE</u>	<u>S.C. TIME (U.T.)</u>	<u>STATION NAME</u>	<u>MAX. VALUE OF Kp</u>	<u>MAX. VALUE OF A<sub>p</sub></u>
159	10 January	GSC = 06:--	FRED	8	47
160	21 January	GSC = 01:--	BOUL	5	23
161	31 January	GSC = 04:--	BOUL	6	29
162	7 February	GSC = 09:--	BOUL	5	29
163	26 February	GSC = 22:--	FRED	5	26
164	27 February	GSC = 14:--	BOUL	6	26
165	5 March	GSC = 21:--	FRED	6	33
166	7 March	GSC = 00:--	BOUL	6	42
167	25 March	SSC = 20:51	FRED	8	138
168	1 April	GSC = 01:--	FRED	7	107
169	2 April	GSC = 17:--	NEWP	6	44
170	2 May	GSC = 09:--	FRED	7	94
171	10 June	GSC = 19:--	NEWP	6	26
172	30 June	GSC = 03:--	FRED	6	29
173	23 August	GSC = 01:--	FRED	5	30
174	17 September	GSC = 19:--	FRED	5	33
175	19 September	GSC = 10:--	FRED	6	51
176	15 October	GSC = 04:--	FRED	5	33
177	30 October	GSC = 06:--	BOUL	5	34
178	12 November	SSC = 10:25	COLL	7	31
179	17 December	GSC = 23:--	BOUL	5	28
180	28 December	GSC = 20:--	FRED	6	45

numbering 15, 15, 24, 30, 29, and 22), but we are not convinced by any explanation for it. In any event, this only tends to enhance the statistical results which follow.

Table VIII contains an overall summary of a station-by-station list of the ionospheric parameters examined, the number of storm periods analyzed, and the time periods covered (with storm numbers).

## 2.4 Storm Analysis Procedure.

### 2.4.1. The Control Curve.

The question of how to characterize ionospheric disturbances in a quantitative, meaningful way is not a simple one to answer. Over the course of our studies, we have used various schemes which employ some sort of diurnal control curve from which excursions are reckoned. Reasonable candidates for a control curve are: (1) the monthly mean pattern, (2) the monthly median pattern, (3) the mean of n-days prior to a storm, with the value of n typically 7, or larger, (4) the mean of the 5 or 10 magnetically quiet (QQ or Q) days of the month or (5) a single quiet-day prior to the storm. There are various arguments for and against each of these candidates. Mendillo and Klobuchar (1974) discussed this topic in the AFCRL ATLAS, and the reader is referred to that work for further discussion. Our final decision was to use the monthly median diurnal pattern as the control curve. Since the concept behind our study was to determine the contribution of geomagnetic activity to the spread or variability of F-region

Table VIII

<u>STATION</u>	<u>PARAMETER</u>	<u>NUMBER OF STORMS</u>	<u>TIME PERIOD</u>	<u>STORM NUMBERS</u>
Goose Bay, Lab.	TEC	67	Nov 71-Apr 75	59-141
Goose Bay, Lab.	Slab Thickness	65	Nov 71-Mar 75	59-139
St. John's, Nfld.	N <sub>max</sub>	65	Nov 71-Mar 75	59-139
Narssarssuaq, Gnld.	TEC	70	Apr 71-Dec 75	50-129
Kennedy SFC, Fla.	TEC	70	Nov 73-Sep 76	97-175
Athens, Greece	TEC	63	Oct 72-Dec 76	71-180
Osan, Korea	TEC	31	Jan 74-Jun 76	100-172
Rosman, N.C.	TEC	13	Jan 72-Dec 72	61- 75
Hamilton (A), Ma.*	TEC	109	Jan 71-Dec 75	46-158
Hamilton (B), Ma.*	TEC	75	Dec 67-Dec 72	1- 75
Hamilton (B), Ma.*	N <sub>max</sub>	75	Dec 67-Dec 72	1- 75
Hamilton (B), Ma.*	Slab Thickness	75	Dec 67-Dec 72	1- 75
Hamilton (C), Ma.**	TEC	28	Dec 67-Dec 69	1- 28
Salisbury, Rhodesia	TEC	9	Jul 73-Oct 73	88- 96

\* The Hamilton (A) analysis represents a local-time, percentage comparison of hourly TEC values with corresponding hourly monthly medians. The Hamilton (B) analysis is a local-time, percentage comparison of hourly TEC, N<sub>max</sub> and slab thickness values with corresponding hourly mean values for the seven days prior to storm commencement, as described in the AFCRL Atlas of the Midlatitude F-Region Response to Geomagnetic Storms (Mendillo and Klobuchar, 1974).

\*\*The Hamilton (C) analysis used monthly median behavior as the control curve (Mendillo, 1971a,b).

parameters, we felt that the median would be less contaminated from drastic storm effects, in comparison to the mean value patterns. Again, since the artificial division of the year into calendar months is so commonly used in statistical and user-oriented studies, we felt it appropriate to examine storm effects within the context of the monthly median behavior.

It should be emphasized that since we are searching for large-scale storm perturbations, the choice of the control curve should not be so crucial a decision. Long-term studies of the Sagamore Hill TEC storm effects have employed, over the years, each of the control curves mentioned above. The dominant and characteristic patterns always appear in nearly identical ways, and thus the selection of storm periods and averaging techniques are probably more important than the selection of the control curve. The fact that the standard deviations of monthly mean F-region parameters (TEC and  $N_{\max}$ ) are typically  $\approx 20\%$  shows that slight variations in the choice of control curves cannot appreciably affect results for the type of large data-base statistical studies presented here.

#### 2.4.2. Specifying Departures From the Control Curve.

The question of how to measure storm-induced perturbations comes down to two standard options: (1) a pure differential measure of the storm-time values from the control curve, yielding variations in absolute units or (2) forming percentage deviations from the control curve. The differential measure is free from problems of absolute calibration, but in gauging the importance

of these deviations (either from the physical processes viewpoint or the user community's), one invariably wants to compare the results in a more relative way to the control curve. The main drawback of using percentage deviations lies in the trap of "small changes in small numbers" causing large percentage variations, especially during the nighttime hours and during solar minimum years. We decided upon this latter choice -- blissful in the assumption that readers of this report are well aware of the necessity to interpret percentage effects with proper caution.

#### 2.4.3. Time Resolution.

Storm-time perturbations (computed in percent from monthly median patterns) were formed at hourly intervals, in local time, over four days of each storm period. All of our previous studies, as well as those carried out by others, show that an hourly time resolution is more than adequate for characterizing F-region storm effects. This might not be the case for the more localized perturbations which accompany magnetospheric substorms, and four days is insufficient to study plasmaspheric storm effects (Kersley, L., private communication); but for F-region effects, 96 hours per storm presents no problem for the definition of statistical patterns.

#### 2.4.4. Construction of Storm Patterns.

The construction of average storm patterns for this study follows identically the scheme developed for the Sagamore Hill TEC (see Mendillo, 1971b, 1973 and Mendillo and Klobuchar, 1974). While the method employed was developed for a single mid-latitude site, its generalization to other latitudes and longitude sectors

seems straight-forward enough, as the present study will hopefully show.

From a historical perspective, ionospheric storm patterns have traditionally been computed following classic procedures formulated to study geomagnetic variations. Thus, ionospheric disturbances may be analyzed following storm-time (and hence a Dst pattern is constructed), or the disturbances may be scrutinized following local or solar time (and hence a DS pattern is obtained). Following this guideline, for each storm period chosen, the storm commencement (SC) time was rounded off to the nearest local time hour for the station in question, and then the calendar day of this SC time was considered to be DAY 1 of the storm period. Data values for the parameter under consideration (denoted  $P(t)$ ) were then selected from the SC time on DAY 1 through the subsequent four days. The percentage change in  $P(t)$  for each hour of this 4-5 day storm period was computed as

$$\Delta P(t) \equiv \frac{P(t) - \text{Median}(t)}{\text{Median}(t)} \times 100\% \quad (1)$$

The disturbance variation according to storm-time, Dst, for an individual storm was defined to be the sequence of the hourly variation ( $\Delta P(\%)$ ) reckoned from the time of the SC to 96 hours elapsed time, i.e.,

$$\text{Dst}(P, t) \equiv \Delta P(\text{SC}), \Delta P(\text{SC} + 1), \dots, \Delta P(\text{SC} + 95) \quad (2)$$

The average storm-time variation was defined to be

$$\langle \text{Dst}(P, t) \rangle \equiv \frac{\sum_{n=1}^N \text{Dst}(P, t, n)}{N}$$

where  $N$  is the total number of storms used. The median storm-time pattern,  $MDst$ , was simply the set of hourly median values computed from the  $Dst(p,t,n)$  array.

There are several methods which might be employed to investigate the diurnal effects included in the storm variations. Traditional geomagnetic analyses would call for the subtraction of the  $\langle Dst \rangle$  pattern from the storm days in the hope of isolating LT effects. Our early analyses clearly showed that LT effects dominate the disturbance patterns at mid-latitudes and thus we decided upon a method which combines both storm-time and LT effects -- namely following the storm-induced perturbations on a day-by-day basis from DAY 1 (when the SC occurred) through the next three days. Alternate schemes have been discussed (see Hargraves and Baganel, 1977) which do not change in any fundamental way the characteristic patterns obtained by the present method.

In our scheme, we first define the first day of a storm to be the local time period 0000 to 2300 LT which contained the SC time. For a mid-latitude station such as Sagamore Hill, we had found that this period contained most (but not all) of the positive excursion ( $\Delta P > 0$ ) while days 2, 3 and 4 contained the negative phase excursions. For individual storms, the notation used for this disturbed-solar (i.e., local time) variation was  $DS_i(LT) = \Delta P_i(LT)$  where  $i$  is day number,  $i = 1$  to 4. The average disturbed daily variation is then simply given by

$$SD_i(P,LT) = \frac{\sum_{n=1}^N DS_i(P,LT,n)}{N}, \quad i = 1, 2, 3, 4.$$

Again, the median local time pattern,  $MSD_1$ , was obtained by determining the set of median values of the  $DS_1(P,LT,n)$  array.

The average and median patterns obtained in this way yielded a "first-look" at the characteristic features for an ionospheric parameter's storm behavior at a given site. Our earlier work with Sagamore Hill data showed that these characteristic features (such as the "Dusk Effect" enhancement on Day 1 and the "Trough-Associated" minima on Days 2 and 3) could be enhanced (in their average specification) by slightly modifying the analysis procedure. As an example, consider the Sagamore Hill situation. It was found that while a SC during daylight hours generally produced a TEC increase of some sort, a storm which began in the dusk to dawn hours generally followed one of two patterns: (a) the TEC response went directly to the negative phase or (b) a small TEC enhancement occurred during the afternoon of the following day. We realized that if case (a) were deleted from consideration, the  $SD_1$  pattern of a "Dusk Effect" (positive phase) would be enhanced due to the loss of "inconsistent" negative values -- values more typical of the  $SD_2$  pattern (negative phase). Similarly, if case (b) storms were deleted, the  $SD_2$  pattern would be enhanced by omitting "inconsistent" positive values -- values more typical of the  $SD_1$  pattern. Obviously, the solution was not to delete storms from the analysis but rather, for the purpose of averaging, shift their SC times by the appropriate 24 hours. In this way, our statistical description would enhance the feature of interest rather than "average it out" -- and thus provide the desired result of an

average pattern which truly captured the essence of the F-region's characteristic response at a given site.

It should be emphasized that the majority of SC times do not require shifting, as is evidenced by the fact that the unshifted results still point to the correct characteristic features. For the set of TEC data described in the AFCRL ATLAS (75 events), 7 were classified as no-positive-phase storms ( $SC \rightarrow SC + 24$  hr) and 8 as delayed-positive-phase storms ( $SC \rightarrow SC - 24$  hr; see Figure 3). Thus 20% of the storms were modified in their assignment of averaging bins.

Finally, for low latitude stations where the negative phase may be weak or all together absent, shifting of individual SC events for the purpose of averaging was either carried out on the basis of other features or not at all (see Table IX).

#### 2.4.5. Analysis Summary.

For each of the data sets listed in Table VIII, we performed the statistical analyses described above to determine characteristic storm patterns. Specifically, these included (a) Average Storm-Time Patterns,  $\langle Dst \rangle$ , with standard deviations, (b) Median Storm-Time Patterns,  $MDst$ , (c) Average Local-Time Patterns,  $SD$ , with standard deviations and (d) Median Local-Time Patterns,  $MSD$ .

In addition to computing the above patterns for the total number of storms at each site, a seasonal analysis was carried out for those sites where a sufficient data base existed. The seasonal break-down was the standard division of the year into Summer (May, June, July, August), Winter (November, December,

# LOCAL TIME DISTRIBUTION OF SC TIMES USED FOR AVERAGE DIURNAL (SD) ANALYSIS

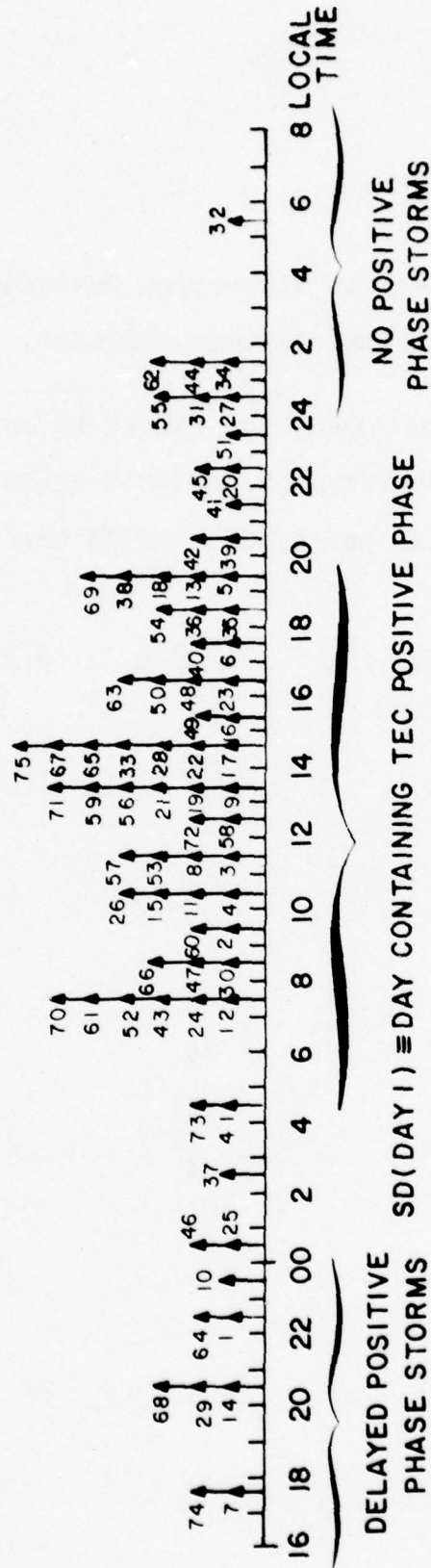


FIGURE 3.

Table IX. Summary of Storm-type Designations For Average  
Local Time Pattern, SD(TEC).

RPP = Regular positive phase (SC at LT on Day 1)

DPP = Delayed positive phase (SC + SC-24 hr, Day 2 + Day 1, etc.)

NPP = No positive phase (SC + SC+24 hr, no Day 1 values)

<u>STATION</u>	<u># of RPP</u>	<u># of DPP</u>	<u># of NPP</u>
Narssarssuaq	54	10	6
Goose Bay	58	6	3
Sagamore Hill (A)	83	22	4
Sagamore Hill (B)	60	8	7
Rosman	11	1	1
Cape Kennedy	58	14	0
Osan	26	5	0
Athens	34	25	4
Salisbury	8	1	0

January, February), Spring (March, April), and Fall (September, October); Spring and Fall storms were also combined into a third 4-month season, Equinox (March, April, September, October).

The four storm analyses,  $\langle \text{Dst} \rangle$ , MDst, SD and MSD, performed on the storm data sets All, Summer, Fall, Winter, Spring and Equinox for each parameter at each site represents an extraordinary amount of results to present. We have decided to include tabulated results for all parameters for all seasons and sites, plus standard deviations (when appropriate), in an extensive set of Tables attached as an Appendix. Since the local time patterns are more closely linked to the understanding of the physical processes responsible for storm effects, and also represent the patterns which could be used to update ionospheric morphology models, we decide to give graphical presentations only for the local time patterns. Moreover, since the median patterns, MSD, do not have standard deviations associated with them, our full focus was given to the average local time patterns,  $\text{SD}_i (P, LT)$ ,  $i = 1$  to 4.

#### 2.4.6. Median Data Base Summary for Each Site.

In order to carry out the above analyses, a great deal of effort was needed to first establish a reliable data base for each site to be investigated. Since storm perturbations are measured with respect to monthly median patterns, the importance of the storm effects can only be judged by having available the monthly median data. We decided that the most compact way of presenting many station-years of median behavior was to construct contours of TEC on a local time/monthly grid for each year of

observation. Thus, as each site is investigated in subsequent chapters, the annual summaries of the median behavior will be presented prior to the disturbance patterns.

#### 2.4.7. Assessment of the "Average Storm Pattern" Concept.

Any casual observer of ionospheric storms knows that, quite literally, no two storms exhibit identical behavior. Indeed, one of the main reasons for publishing the AFCRL ATLAS of Sagamore Hill storm effects was the goal of displaying the great variety of F-region responses which occur at a single site due to increase in geomagnetic activity. The question naturally arises, then, of the real usefulness (and meaning) of average storm patterns. The answer to this dilemma may be approached along two avenues: (1) from the point of view of understanding the physical processes most responsible for storms, it would be foolish to concentrate on a single event, given the realization that single events differ so from one another. The notion of specifying the mechanism which causes storm effects is now known to be a fruitless concept. The fact that perturbations exhibit positive and negative phases, with considerable variations according to season and latitude, shows that a blend of mechanisms operates, with perhaps a dominance of one over the others from event to event and site to site. If, however, the average behavior of a set of storm events exhibits a clear and recognizable pattern--and one reminiscent of many individual events--then the average pattern must point to features and processes truly characteristic of that site. Thus, the average pattern will identify the features most common at a given site

and the search for operative processes will be limited to those capable of causing such effects. Clearly, individual storms will exhibit characteristic features much more pronounced than they appear in the average, and these therefore set the limiting tests for the identification of correct mechanisms.

(2) From the point of view of wishing to update F-region morphology models, there is little choice from using average storm patterns. To base predictions upon individual events would be clearly unjustifiable, for the reasons mentioned above. Average patterns, constructed on a local time basis with seasonal breakdown, offer the only reasonable way of providing an estimate of how a model predicting the mean or average behavior should be modified to include disturbance effects. The correct role of individual events is, once again, to set the limit of "worst-case" conditions for a given parameter and/or site.

Finally, we would like to comment on the absolute values of the percentage variations to be presented in subsequent figures and tables. Perhaps the most frustrating aspect of storm investigations is the realization that, once the goal of obtaining clear and representative storm patterns is achieved, the absolute values of the patterns are often small and, moreover, the standard deviations of those values are invariably greater than the perturbation values themselves. We suggest that results characterized, for example, by variation values of  $+35\% \pm 45\%$  or  $-5\% \pm 30\%$  are not vague or meaningless numbers. One must realize that the standard deviations of a typical mid-latitude monthly mean diurnal pattern

are generally near  $\pm 20\%$ . Thus, if an SD(%) value is obtained which is larger than this "normal variability"--even if its standard deviation is large--a significant storm-associated feature has been identified. As in the above case, a  $\Delta\text{TEC}$  of say  $+35\% \pm 45\%$  surely points to the likelihood of a substantial TEC enhancement--a potentially valuable update to an ionospherically-supported propagation system. Similarly, a small average value with a large uncertainty (such as the  $\Delta\text{TEC} = -5\% \pm 30\%$  quoted above) provides the information that while a monthly mean pattern cannot be significantly updated, the normal variability of  $\approx \pm 20\%$  should now be taken with caution.

Both examples treated above referred to the interpretation of a single storm-associated SD(%) value. A third case exists, namely a string (from several hours to a few days) of consistently positive or negative SD values of small absolute value (say  $\leq |10\%|$ ). This typically happens, for example, during the negative phase of mid-latitude storm effects when daytime SD values might be characterized by  $-5$  to  $-10\%$  for two to three days. Such consistencies point to the reality of the negative phase and its longevity. Yet, in striving to theoretically model neutral atmosphere effects upon F-region loss processes, one would clearly not aim to reproduce only a  $-5\%$  effect.

The best evidence we have for believing in the meaning and utility of "Average Storm Patterns" is once again a return to the Sagamore Hill/Wallops Island studies of the past decade. No site on Earth has received more scrutiny than this  $L \approx 3$  location near

70° W during periods of geomagnetic activity. Characteristic features, first seen in 1965 storm data, followed during subsequent solar maximum and minimum year, repeated in average patterns for 1968-1969, 1968-1972, and now 1971-1976, always point to a consistency between average and individual storm effects. The reality and utility of our average storm patterns was never more obvious than in the correct identification of the "SKYLAB effect" of a "large-scale F-region hole" (Mendillo et al., 1975) which occurred during a severe geomagnetic storm.

### 3. F-REGION STORM PATTERNS -- THE LATITUDINAL NETWORK

In this chapter we present average storm patterns obtained from sites distributed along the North American/Atlantic Coast region. The stations are Narssarssuaq (NSSQ), Goose Bay (GB), Sagamore Hill/Hamilton (Sag Hill), Rosman (ROS) and Kennedy Space Flight Center (KSFC). Tables I and VIII summarized all of the pertinent station/satellite geometry and the parameters/periods covered. With the exception of Rosman, all stations have at least 65 individual storm periods in their analyses, and thus separate storm patterns for each season were computed. At Rosman, where only 13 storm periods in 1972 were available, the pattern for all storms was found to be remarkably consistent for its location between Sagamore Hill and Cape Kennedy, and thus it was kept in the study for discussions of overall behavior.

It should be remembered that the data base for these studies involves satellite radio beacon values of the ionospheric total electron content (TEC). Thus, while a station-name is used to identify a specific data set, the TEC values themselves refer to an equivalent vertical column some distance equatorward of the station, i.e., at the 420-km sub-ionospheric point. As an example, the Narssarssuaq results refer to a point  $\approx 8^{\circ}$  south of Narssarssuaq (and not over Narssarssuaq), while a low latitude site like KSFC has its sub-ionospheric point only  $\approx 2^{\circ}$  from the antenna site. In summary, then, the chain of stations near  $70^{\circ}\text{W}$

gives average storm patterns at the geomagnetic L-shell values of approximately 5, 4, 3 and 2 -- and thus only equatorial and polar cap effects are excluded.

### 3.1. Average Storm Patterns -- Narssarssuaq ( $L \approx 5$ )

The TEC data base for Narssarssuaq spans a little more than four years on the declining side of the 20th solar cycle. The monthly median patterns for the site are given in Figure 4 (a-c) by way of iso-TEC contours (in  $10^{12}$  el/cm<sup>2</sup>) on a local time vs. calendar month grid. In examining these figures, we will not dwell at length on descriptions of the median behavior, but rather comment only on a few features which characterize the site in relation to well known F-region morphologies:

- (1) The solar cycle dependence may be easily seen in the peak TEC values from the afternoon period.
- (2) The so-called "seasonal anomaly" (lower daytime TEC values in summer than in winter), so common at mid-latitudes, and especially in high sunspot years, is not so well defined in the  $L \approx 5$  data for 1972 on.
- (3) A semi-annual component of the daytime maxima is obvious, with peaks in late Spring and Fall.
- (4) The monthly progression in sunrise/sunset times is, of course, most pronounced at high latitudes. The TEC contours in the 0300-0900 LT sector are obviously closely linked to the sunrise pattern (given by arrows)-- indicating that solar radiations, rather than energetic

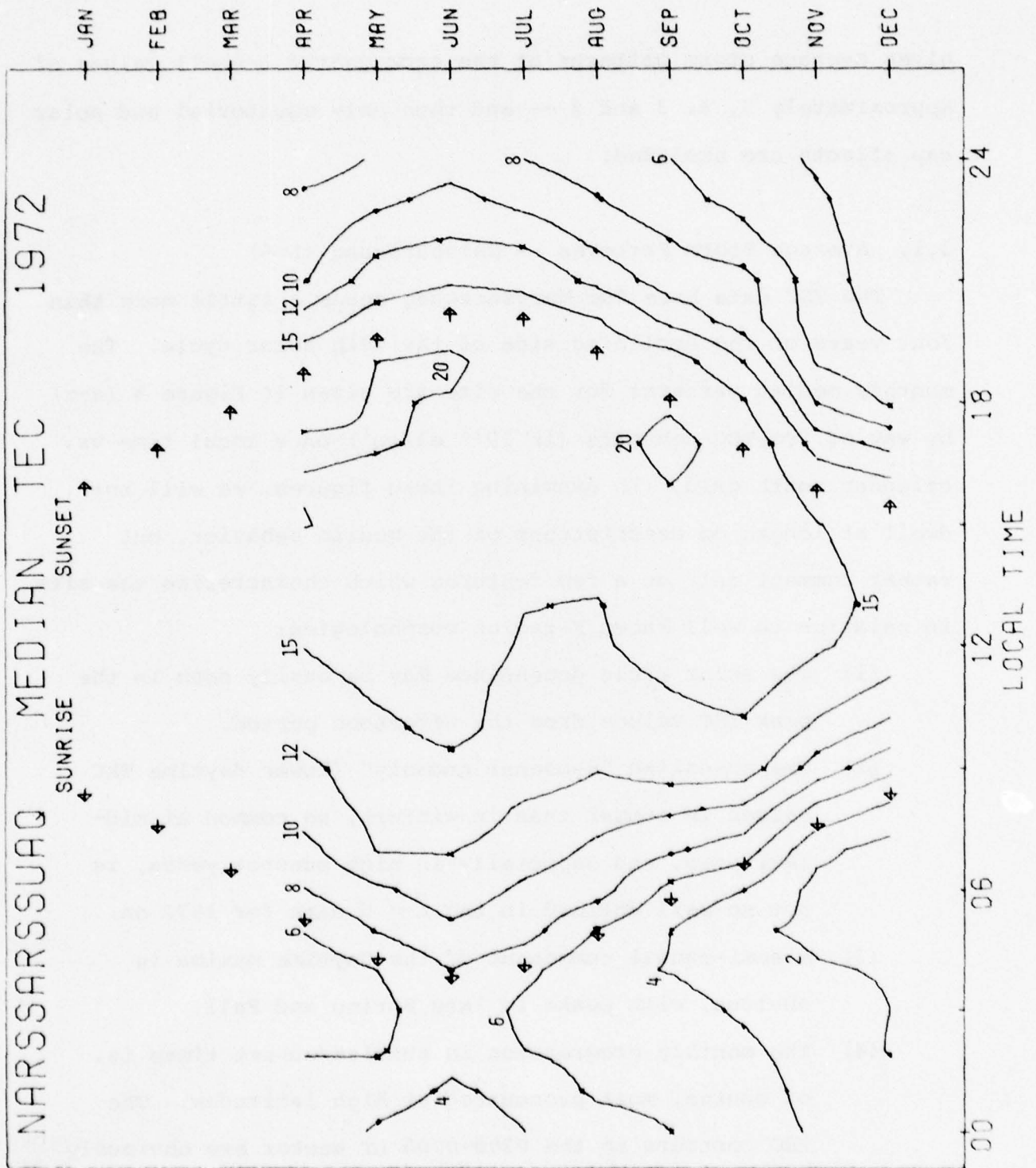


FIGURE 4a.

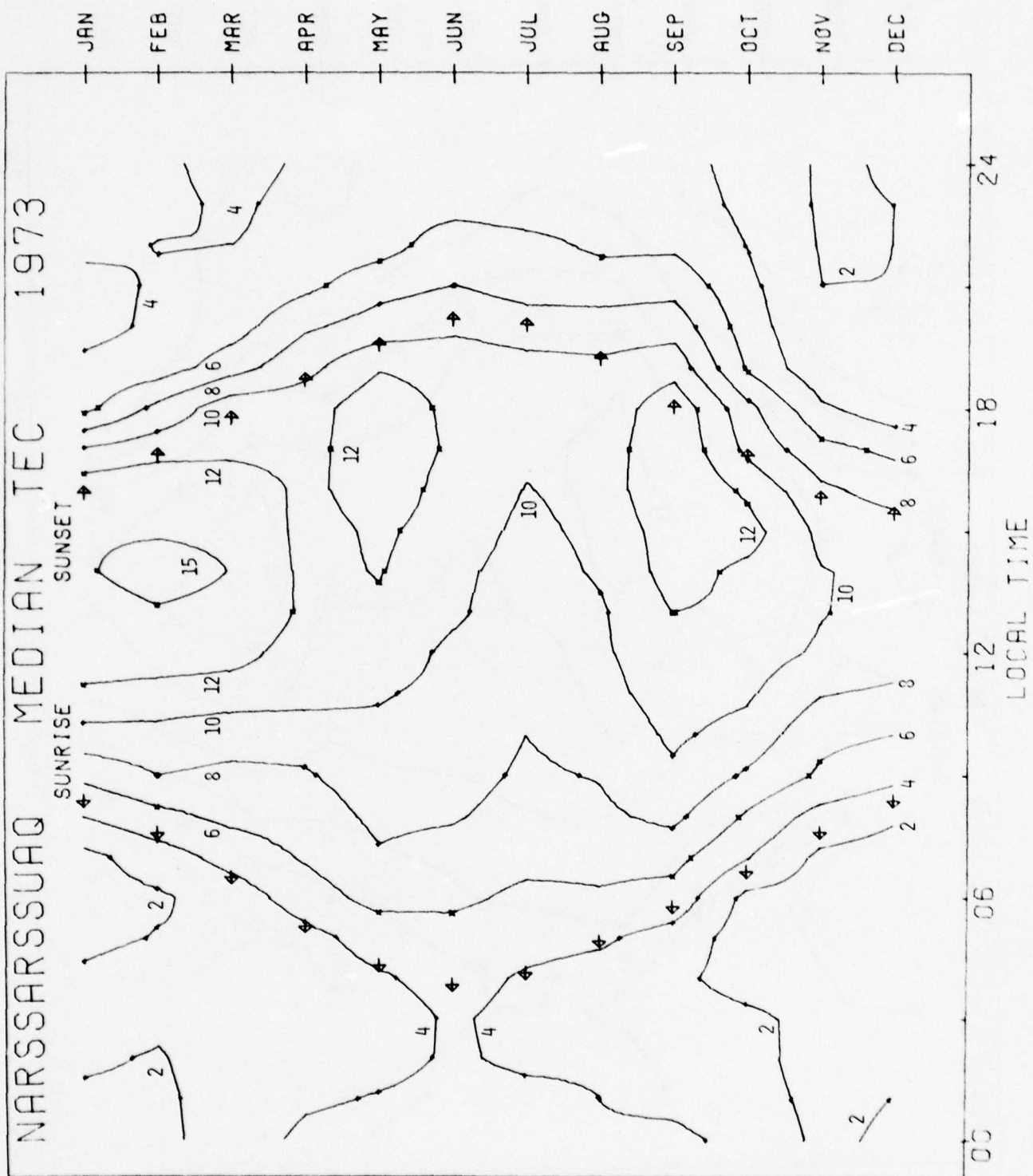


FIGURE 4b.

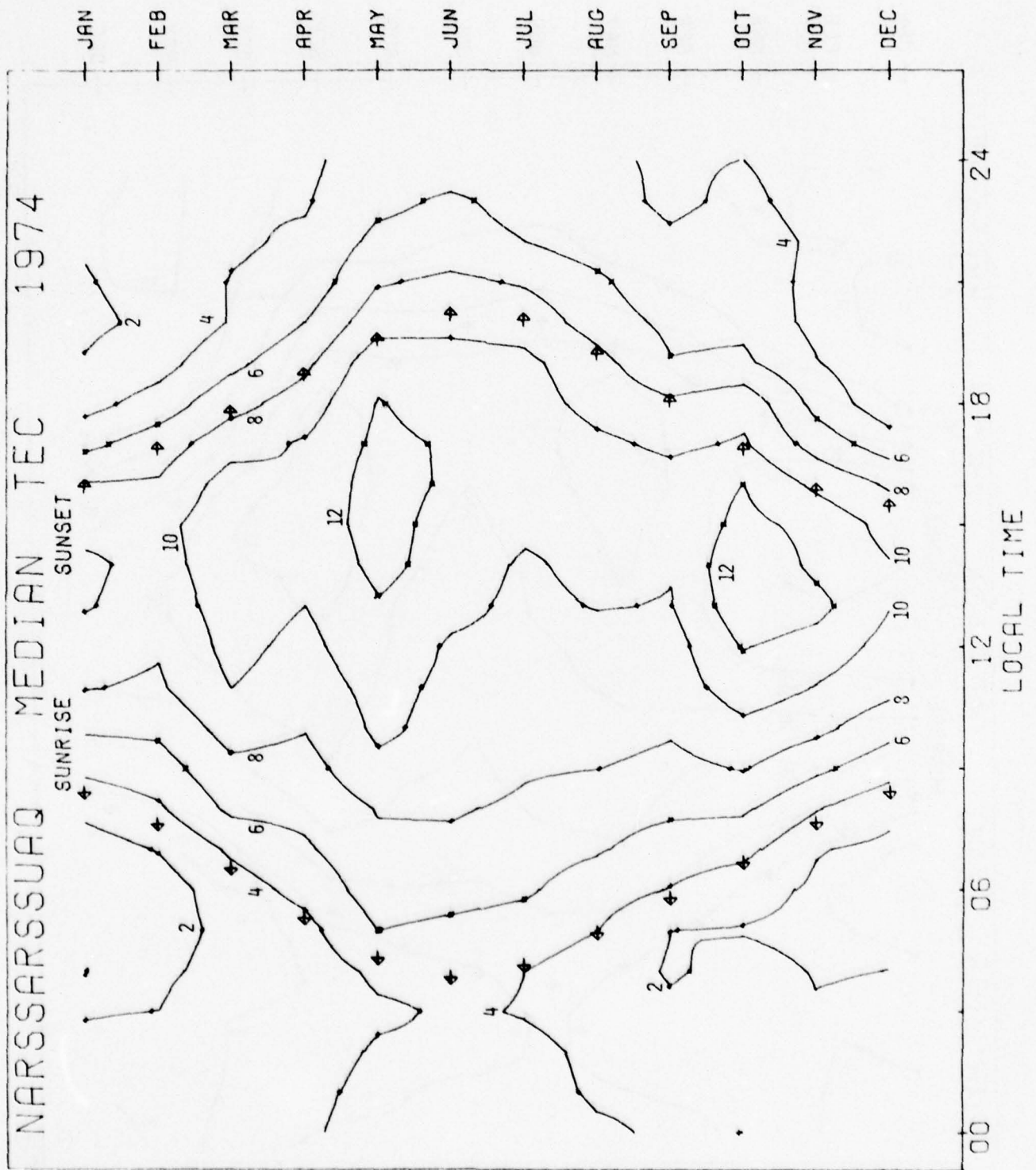


FIGURE 4c.

particle precipitations, are still the dominant source of ionization at  $L \approx 5$ .

The average local time storm pattern,  $SD(TEC, LT)$ , for all 70 storm periods is given in Figure 5. This curve defines the "Characteristic Pattern" for the response of the F-region at  $L \approx 5$  to geomagnetic storms. In examining this and subsequent curves, we will identify what we feel to be the dominant features; quantitative information about selected features will then be tabulated for easy referral. The results in Figure 5 draw attention to the following features:

- (1) Daytime Effects. On the day of the storm commencement, SD1, there is quite a pronounced and well-defined F-region enhancement. The TEC increase begins in the forenoon hours, steadily increasing to a maximum effect of +22% at 1400 LT. While this seemingly small perturbation (in %) is dwarfed by much larger effects at night, it should be recalled that 20% of a daytime TEC value involves substantially more plasma than 50% of a nighttime TEC value. As will be discussed in subsequent sections, this "afternoon increase" is the high-latitude counter-part of the "Dusk effect" enhancement so well documented by our earlier studies of mid-latitude effects. This positive phase on Day 1 at  $L \approx 5$  is abruptly terminated after 1500 LT, and is completely gone by 1700 LT.

On Day 2, the SD2 pattern shows a negative phase

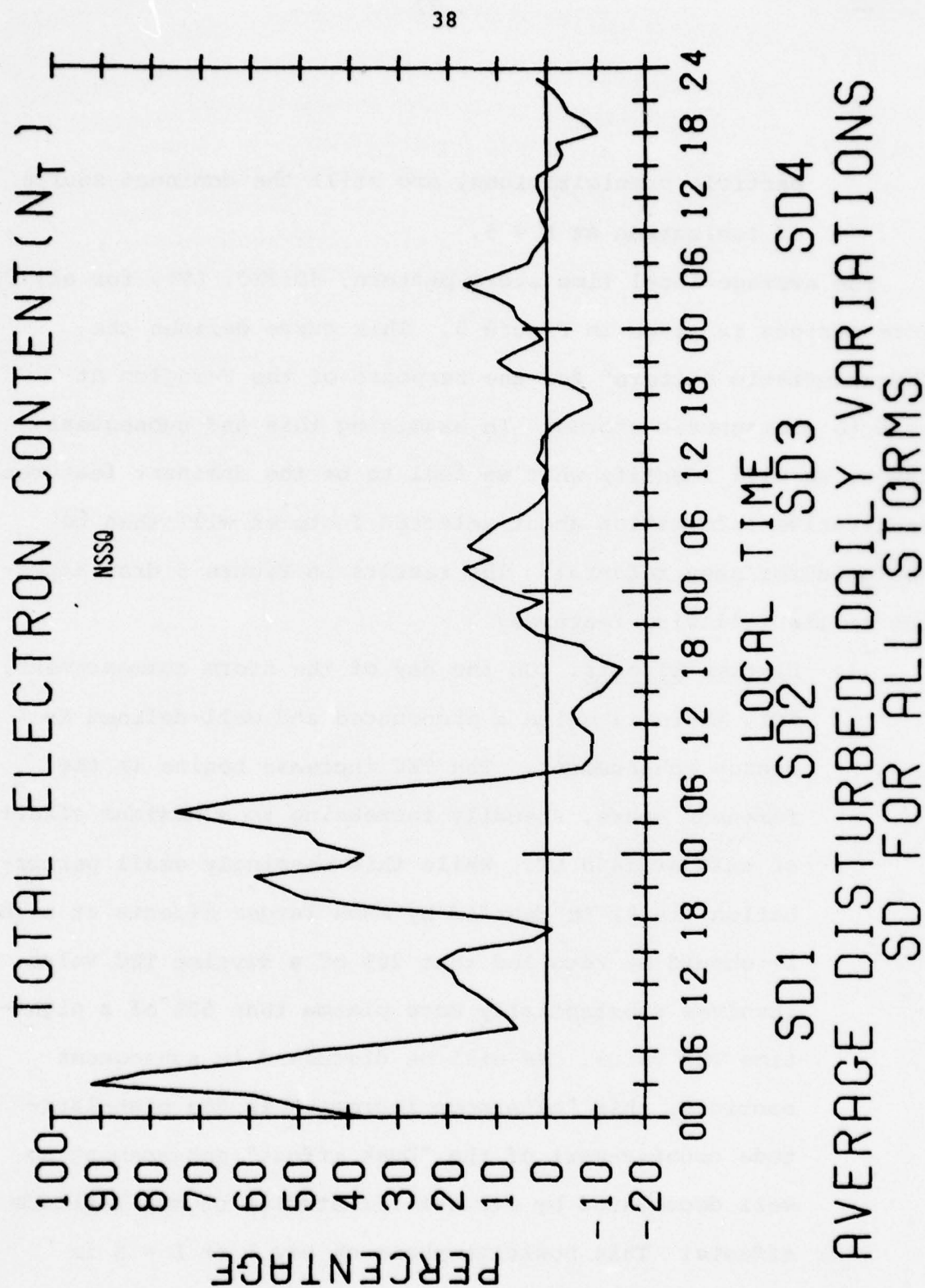


FIGURE 5.

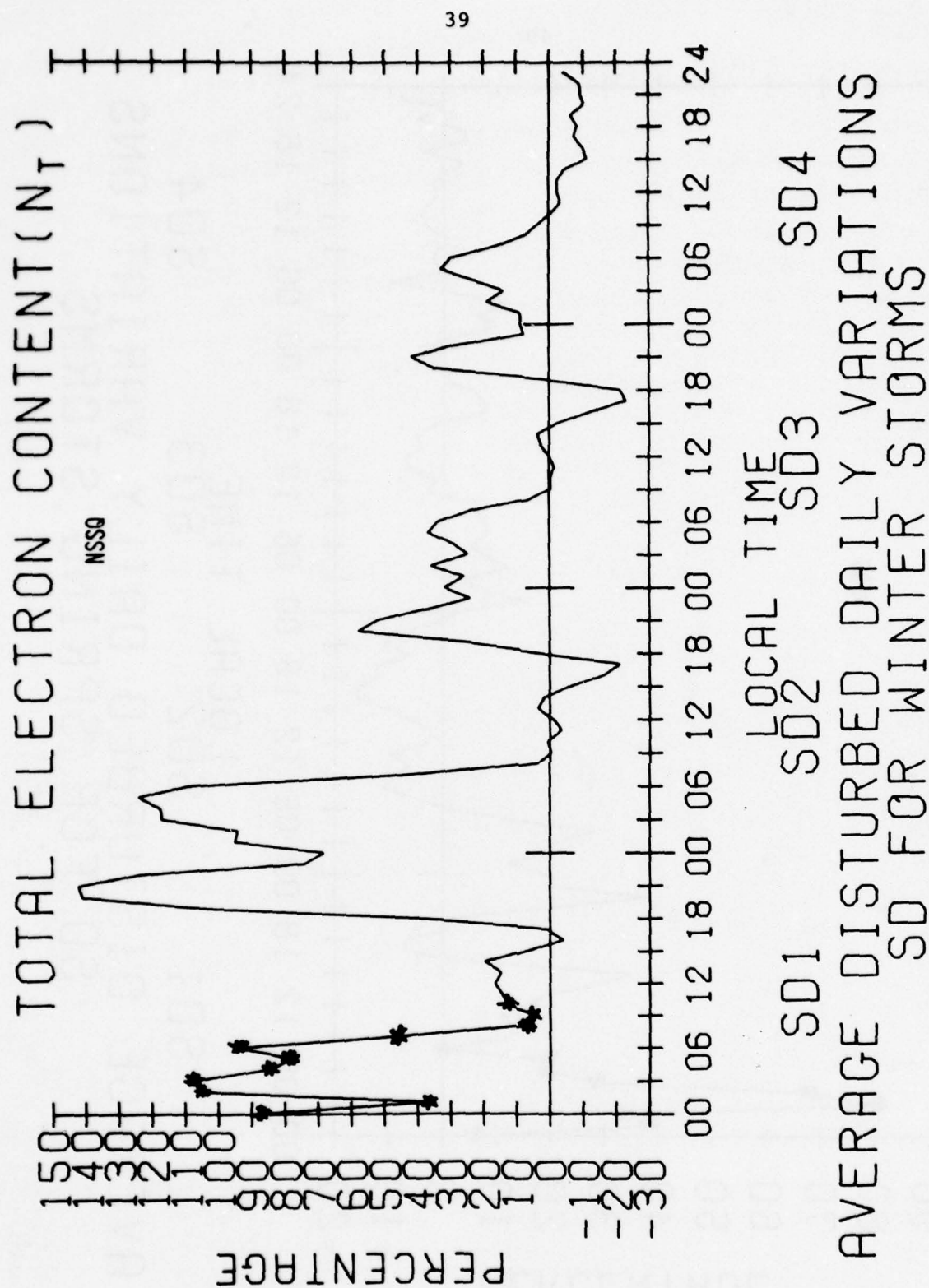


FIGURE 6a.

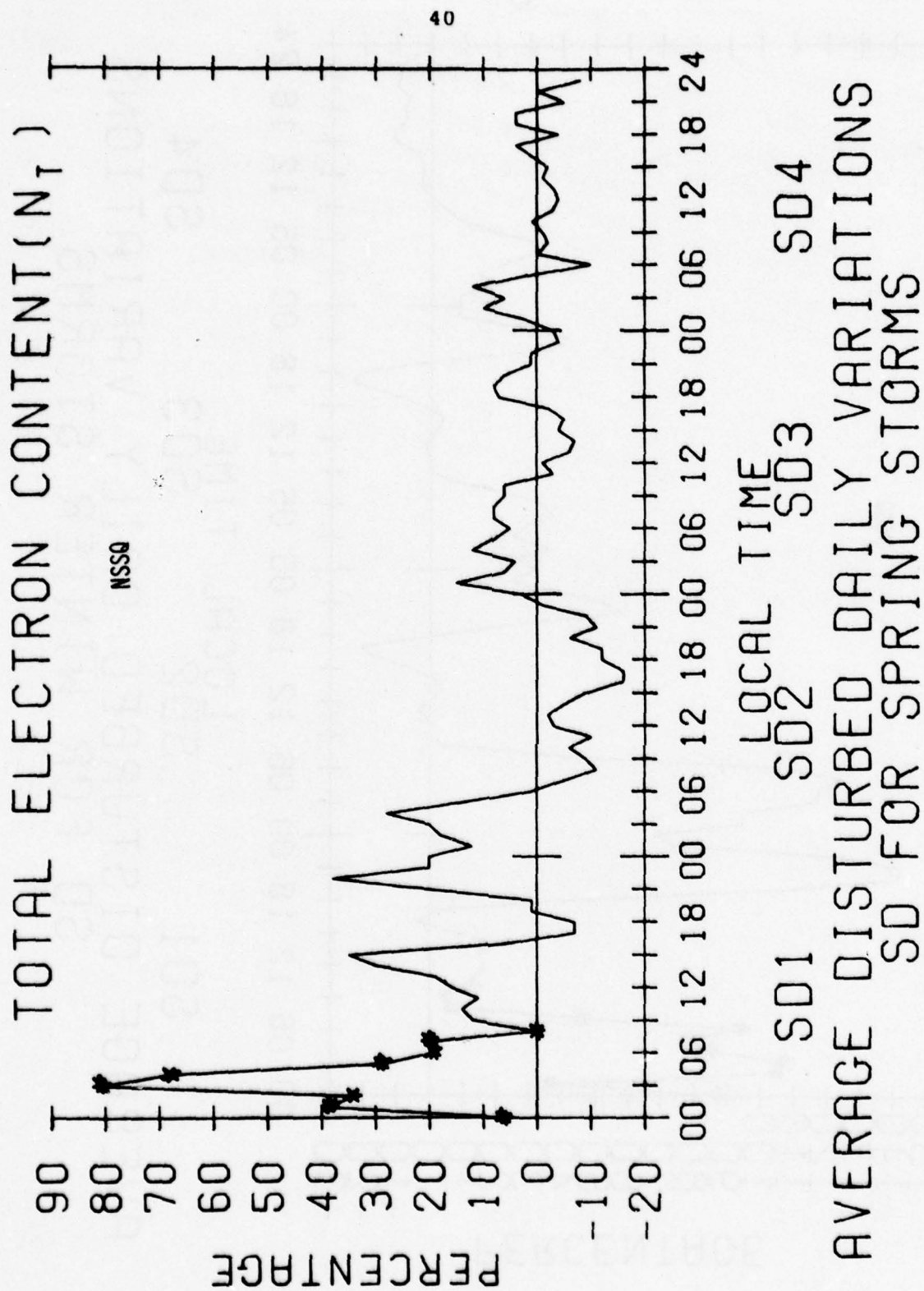


FIGURE 6b.

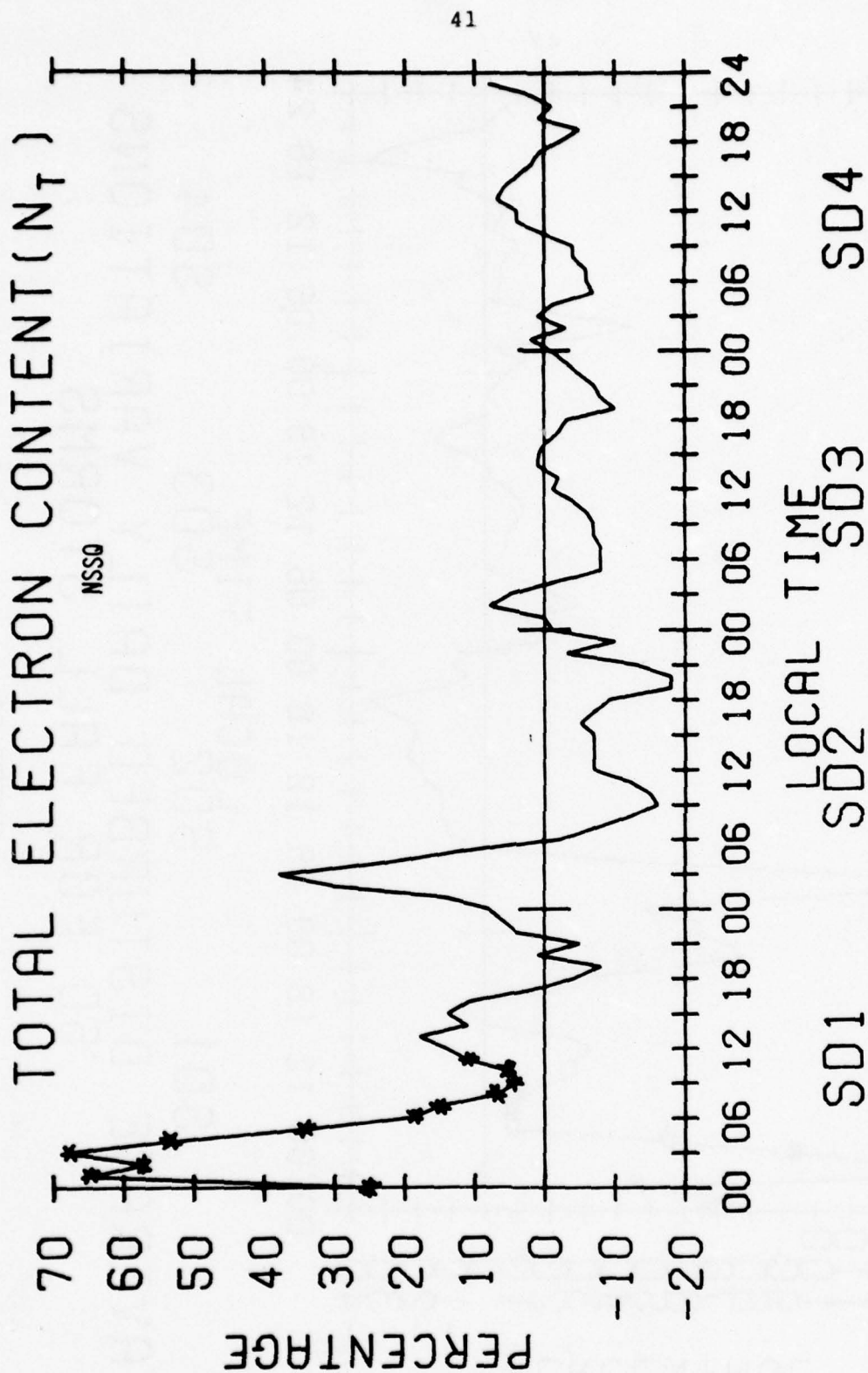


FIGURE 6c.

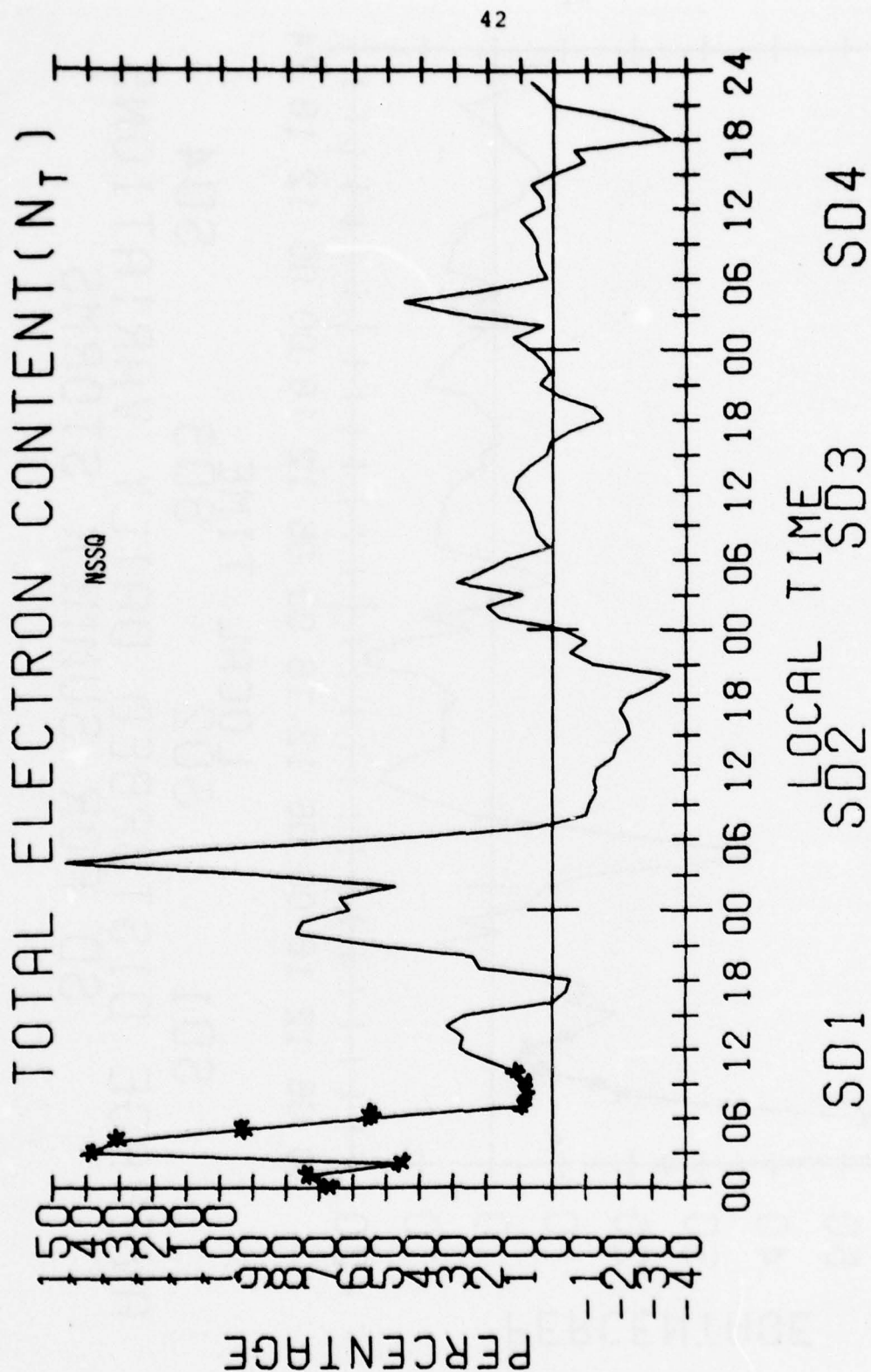


FIGURE 6d.

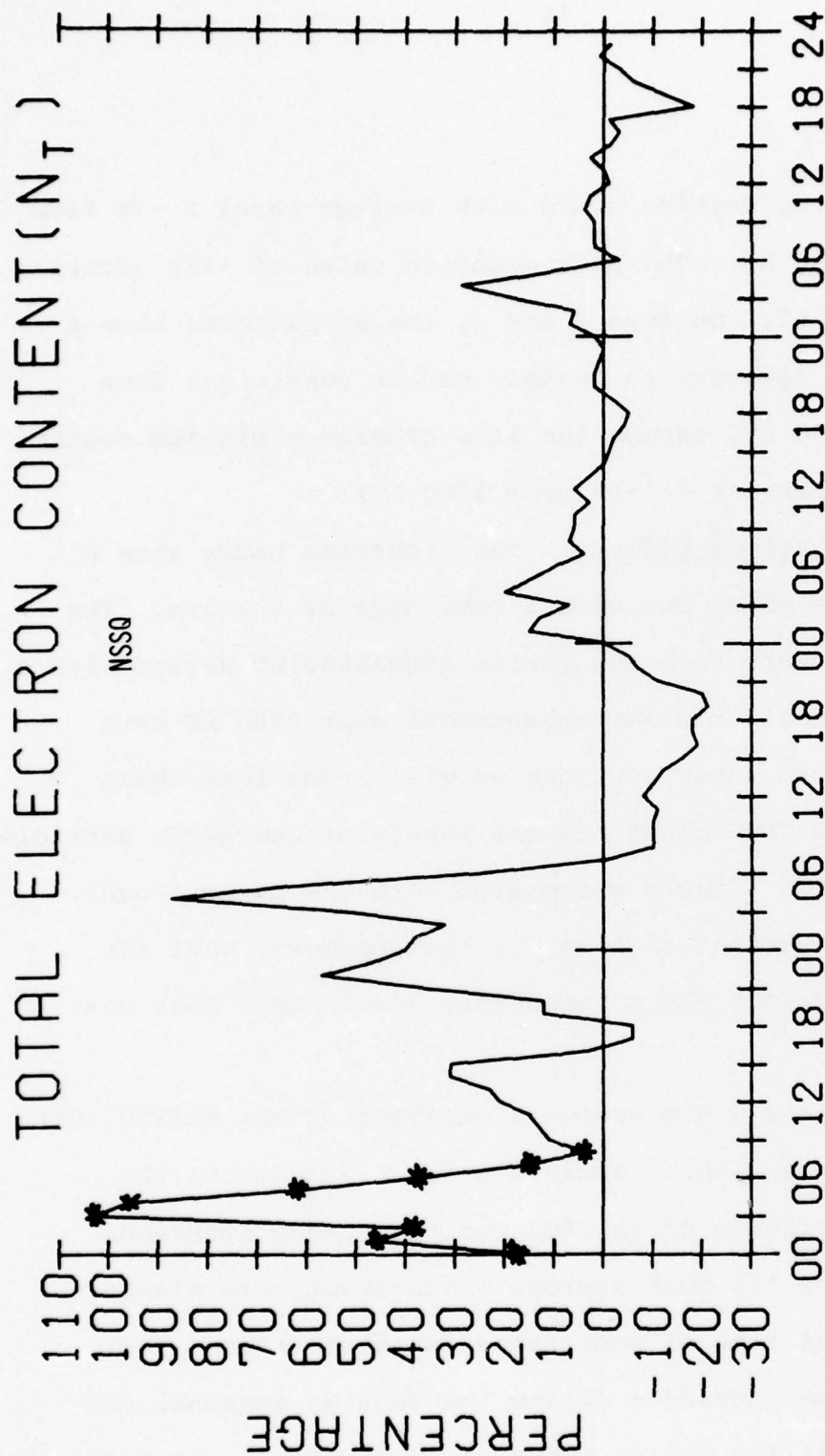


FIGURE 6e.

during the daytime hours with average level  $\approx -7\%$  from 1000-1500 LT. The peak negative value of  $-15\%$  occurs at 1700 LT. On days 2 and 3, the SD patterns show a daytime recovery to monthly median conditions from 1000-1500 LT, though the late afternoon minimum continues to persist ( $\sim -9\%$  near 1700 LT).

(2) Nighttime Effects. The nighttime hours show a positive phase during all four days of a storm. The enhancements span the entire 1900-0600 LT period with a consistently minimum enhancement near 0000 LT each night. In later sections we will argue that these enhanced TEC values are the result of energetic particle ionization effects associated with the auroral oval. It is important to note, in that context, that the post-midnight TEC enhancements reach their peak near 0400 LT.

In Figure 6 (a-e), the seasonal analyses of the SD(TEC, LT) effects at  $L \approx 5$  are given. Table X gives a summary of the seasonal characteristics of the SD1 positive phase afternoon increase by quoting the peak average enhancement, its standard deviation and local time of occurrence for each season. Note that the storm-time increases follow the regular seasonal daytime trends seen in the median behavior in Figure 4. Specifically, the enhancements are largest during the equinoxes, with not much of a difference between the summer and winter values. The times of the maxima are confined to the  $1400 \pm 0001$  LT period.

Table X. Seasonal Characteristics of the TEC afternoon  
Increase at Narssarssuaq ( $L \approx 2$ ).

Season (with # of storms)	( $\Delta$ TEC)max in %	Time of ( $\Delta$ TEC)max LT
Winter (18)	20 $\pm$ 25	14:00
Spring (14)	35 $\pm$ 48	15:00
Summer (24)	18 $\pm$ 18	13:00
Fall (14)	32 $\pm$ 30	14:00
All (70)	22 $\pm$ 32	14:00

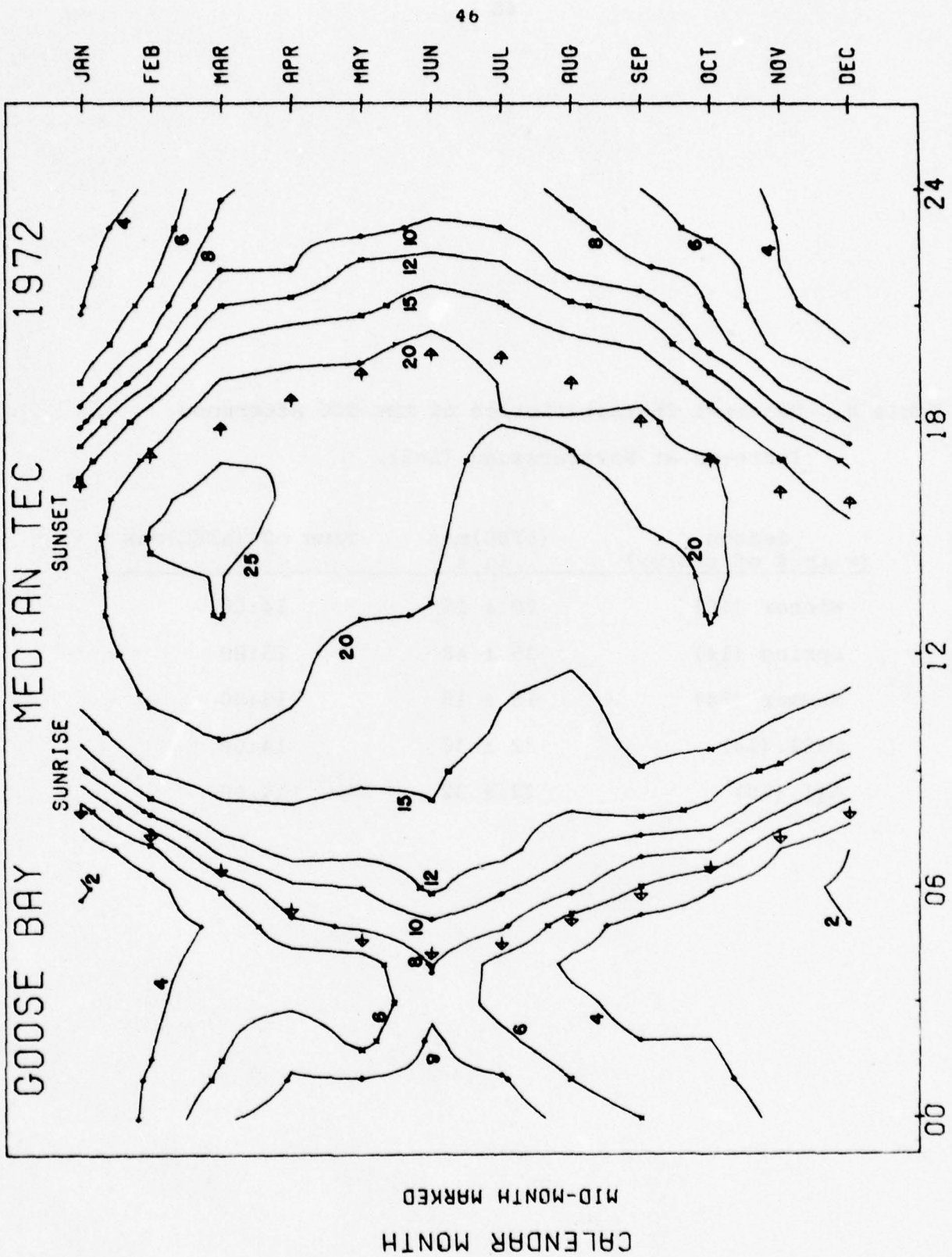


FIGURE 7a.

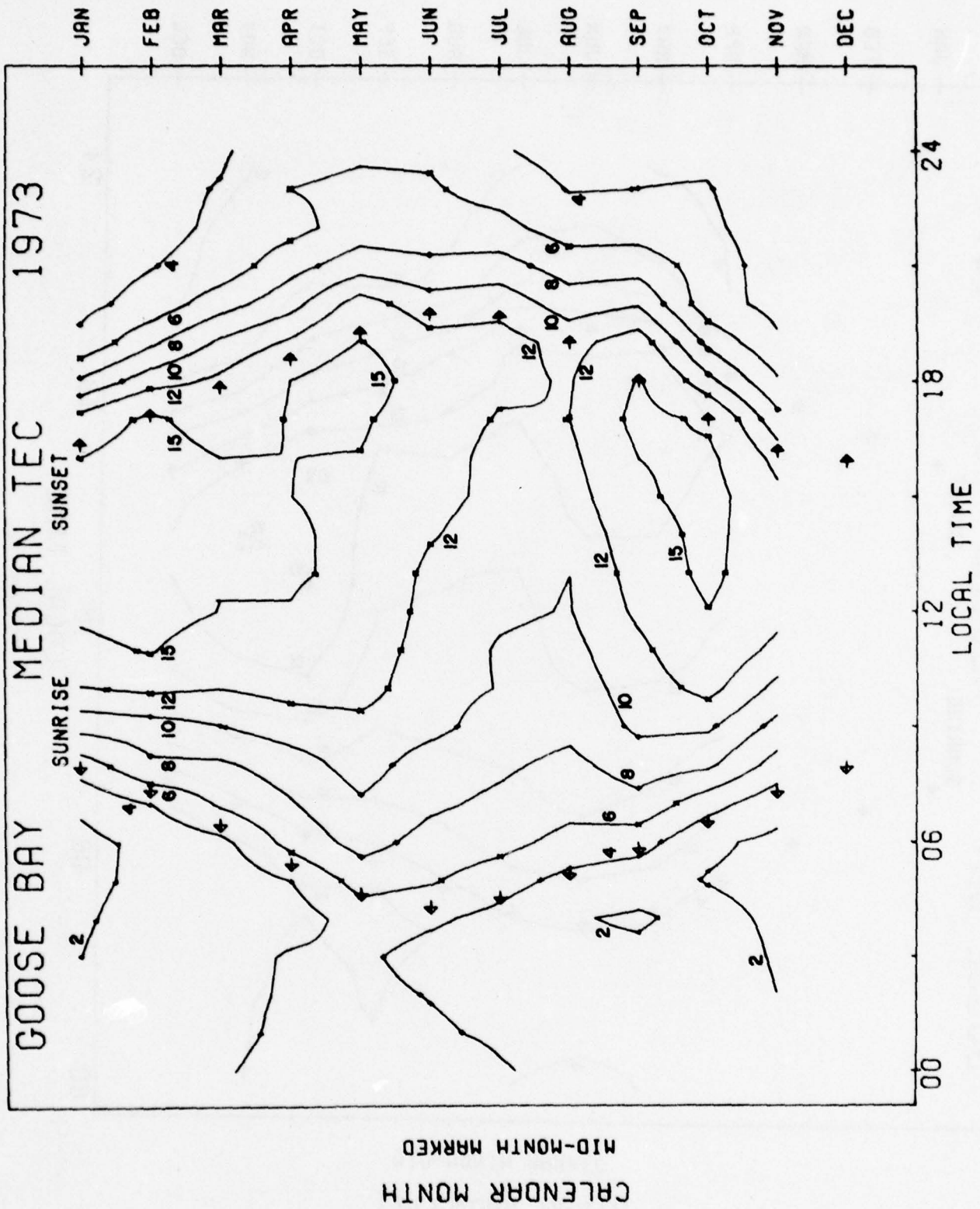
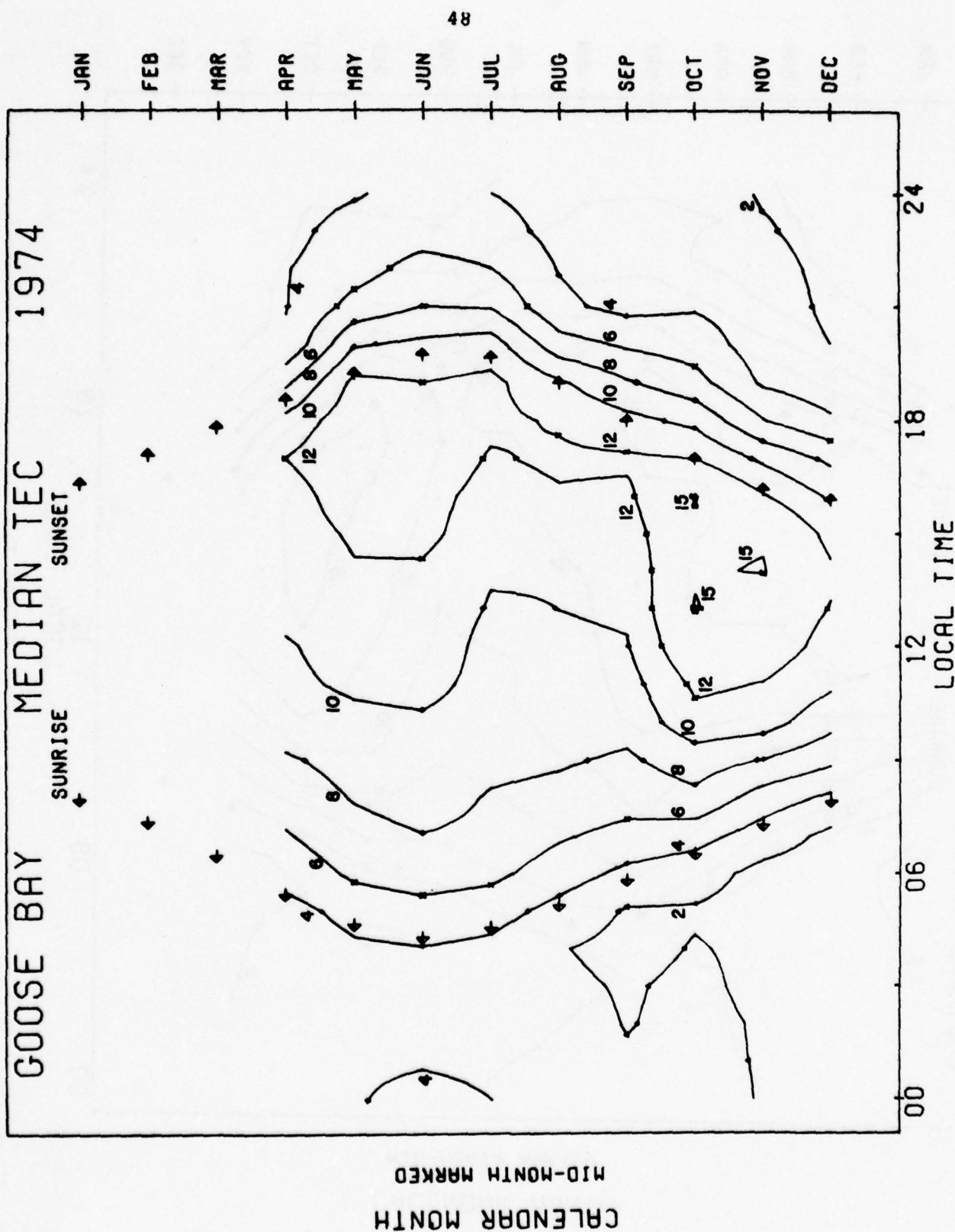


FIGURE 7b.



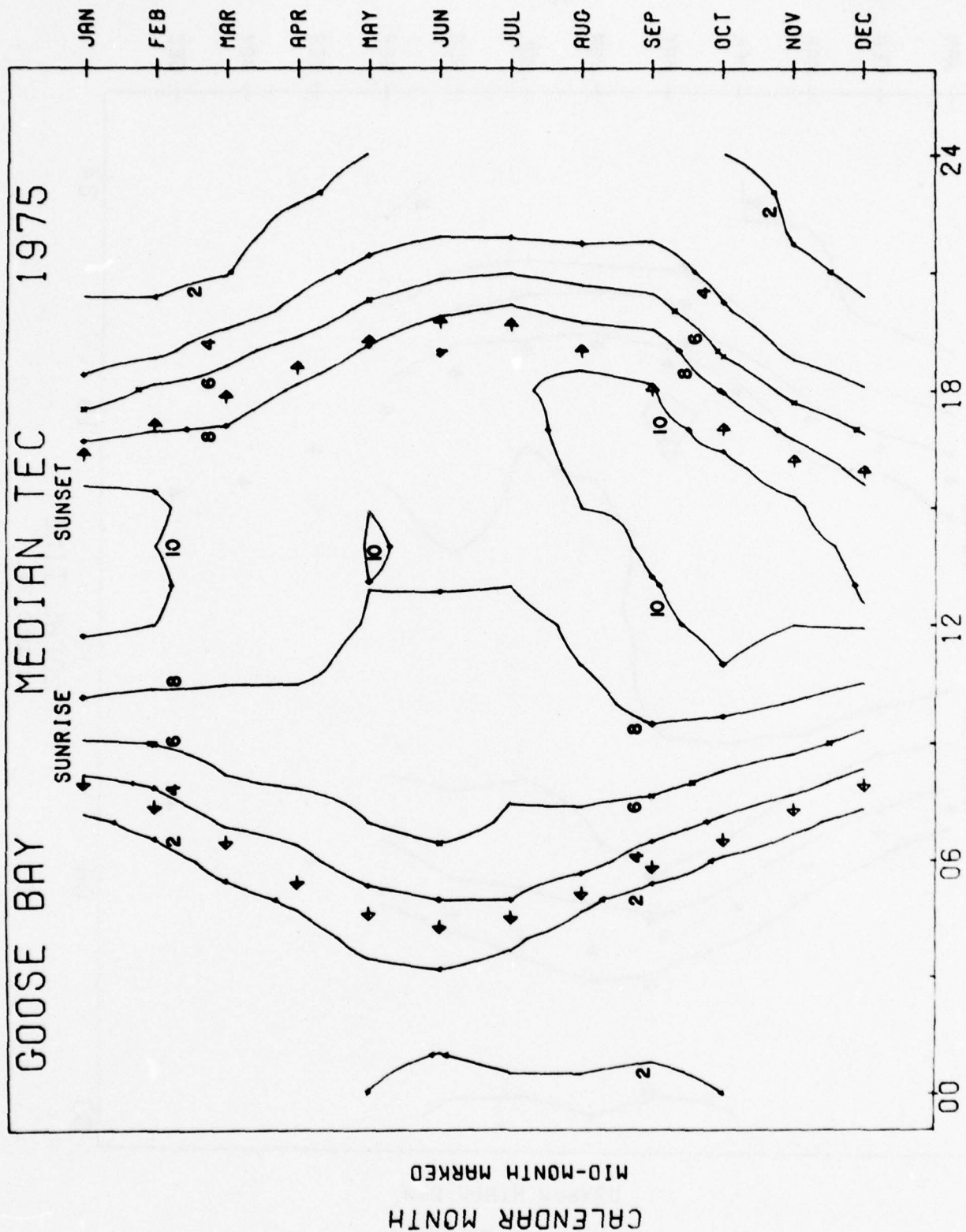


FIGURE 7d.

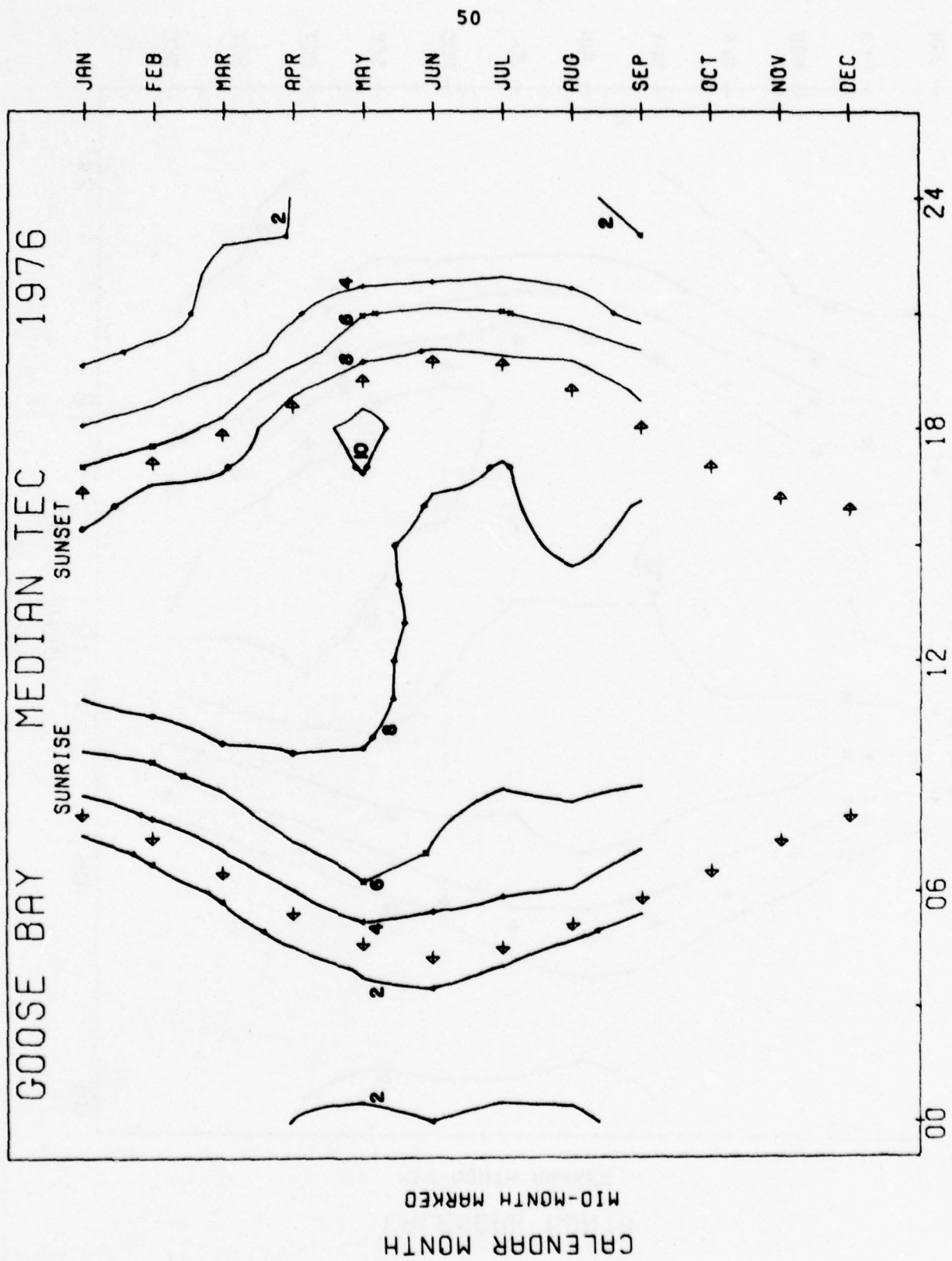


FIGURE 7e.

In Appendix A, the full set of tabulated results for  $L \approx 5$  are given. These include  $SD(TEC, LT)$ ,  $MSD(TEC, LT)$ ,  $\langle Dst(TEC, t) \rangle$  and  $MDst(TEC, t)$ .

### 3.2. Average Storm Patterns -- Goose Bay ( $L \approx 4$ ).

The AFGL observing site at Goose Bay, Labrador, has recorded TEC data since November 1971. As pointed in Figure 1 (and Table 1), the 420 km sub-ionospheric point falls very close to the ionosonde station at St. John's, Newfoundland. This provides the opportunity to examine three F-region parameters ( $TEC$ ,  $N_{max}$  and  $\tau = TEC/N_{max}$ ) at a location of great interest ( $L \approx 4$ ), due to the fact that the  $L = 4$  field line typically marks the location of the plasmopause. Our long-term studies of  $TEC$ ,  $N_{max}$  and  $\tau$  at  $L \approx 3$  (Sagamore Hill) revealed consistent storm morphologies capable of addressing changes in the entire  $Ne(h)$  profile (see, for example, Mendillo et al., 1972; Mendillo and Klobuchar, 1974, 1975), and thus a great deal of effort was put into an attempt to extract similar 3-parameter results for the  $L = 4$  site. It should be emphasized that very little quantitative information exists on the F-region at  $L = 4$ , and thus this new set of extensive F-region data makes possible the first serious examination of the ionosphere at such a location.

In keeping to our guideline of presenting a brief overview of the median behavior of  $TEC$  at each station, we present in Figure 7 (a-e) annual summaries of iso- $TEC$  contours on a  $LT$  vs. month grid. These curves show the type of ambient ionosphere upon which the storm-induced  $SD(\%)$  patterns fall. The solar cycle dependence in

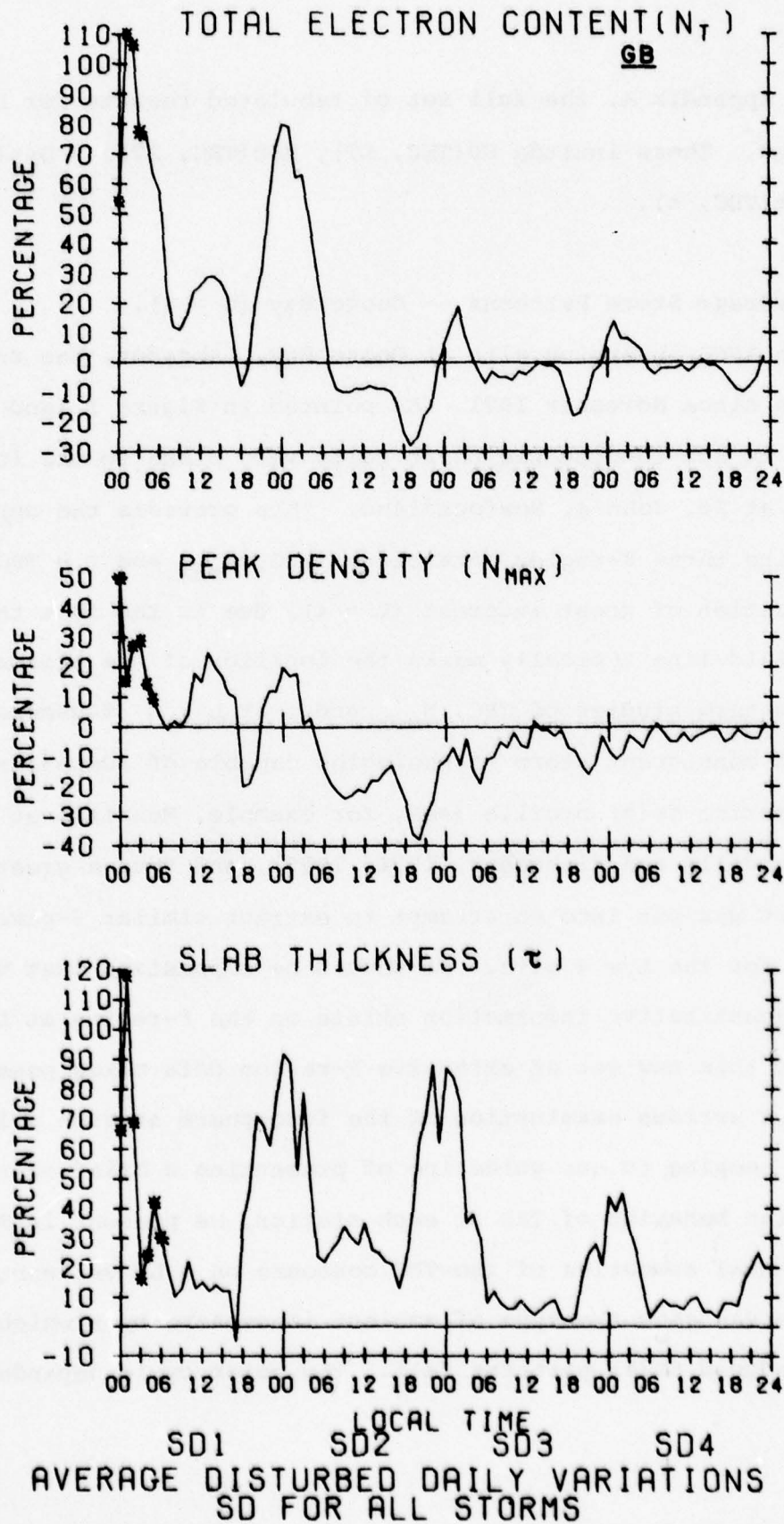


FIGURE 8

TEC is seen clearly in both daytime and nighttime values: the afternoon TEC values in 1972 are more than twice the corresponding 1975-76 data, while in the pre-dawn hours enhancement factors of 3 to 4 are seen. The "seasonal anomaly" and the "semi-annual variation" in the daytime behavior, effects very typical at mid-latitudes, are also seen at  $L = 4$ , particularly during high solar flux years. In summary, then, the daytime TEC behavior at  $L = 4$  appears to be consistent with well-documented effects at mid-latitudes (e.g., at  $L = 3$ ). The larger solar zenith angles (see Table I) result in a noticeable latitude gradient (see Figure 10 in next section), but the main character of the seasonal and local time morphologies are the same.

The main distinguishing feature about the  $L = 4$  ionosphere is the low nighttime TEC values, particularly during winter nights. A TEC  $\lesssim 2$  units (i.e., in  $10^{12}$  el/cm<sup>2</sup> or  $10^{16}$  el/m<sup>2</sup>) is generally associated with a low foF2 value ( $\lesssim 2$  MHz) and thus such data suggest that the  $L = 4$  ionosphere clearly falls within the F-region trough which straddles the average location of the plasmapause on winter nights (Mendillo and Chacko, 1977). The existence of the trough, and its proximity to auroral processes, are characteristics unique to  $L = 4$  and, being dynamic features, exert a dominant influence of the storm-induced perturbations seen at that site.

The TEC,  $N_{\max}$  and  $\tau$  local time disturbance patterns SD (%) for all 67 storms are presented in Figure 8. The asterisks in this and similar figures denote average values based on less than 10 storms or less than half the total number of storms, whichever is

smaller. The TEC curve (top panel) shows an afternoon positive phase on Day 1 with a maximum value of approximately + 30% from 1300-1400 LT. This period of enhancement is "cut off " after 1600 LT, approximately an hour later than seen at  $L \approx 5$  and, as will be shown in the next section, before the termination of the positive phase at  $L \approx 3$ .

The most dramatic SD(TEC) characteristic seen in Figure 8 is the large nighttime peak which occurs between days 1 and 2. This 80% enhancement occurs near 00 LT, at a time when smaller TEC enhancements occur at  $L \approx 5$  (see Figure 5). The timing and relative magnitudes of this TEC increase (i.e., in comparing Figures 5 and 8) give clear evidence of the extent to which auroral induced F-region enhancements move equatorward during storms. Smaller "midnight peaks" also occur between nights 2 and 3 and nights 3 and 4, indicating once again the long-lived nature nighttime disturbance effects.

A daytime negative phase in SD(TEC) is seen at  $L \approx 4$ , with a smooth recovery trend from Day 2 to Day 4. Recall that the  $L \approx 5$  results (Figure 5) showed a daytime negative phase only on Day 2. Such differences are probably related to the latitudinally dependent recovery processes for the neutral atmosphere, specifically to the time required for the  $O/N_2$  ratio to return to pre-storm conditions. During the 10:00 - 15:00 LT period,  $SD_2(TEC)$  at  $L \approx 4$  is  $\sim -9\%$ ; at  $L \approx 5$ , the corresponding value is  $\sim -8\%$  indicating little difference in the average specification of the negative phase magnitude. We do feel, however, that the persistence of a small negative phase

on Days 3 and 4 at Goose Bay is significant; in addition to neutral atmosphere effects, dynamic processes replenishing plasmaspheric tubes near  $L \approx 4$  might also contribute to the longer recovery time at  $L \approx 4$ .

The deep TEC minimum of approximately -30% near 19:00 LT on Day 2 represents the strongest case of an effect which occurs on all four days of the storm period. Re-examination of Figure 5 shows that similar minima occur just prior to 18:00 LT at  $L \approx 5$  on all four days of the storm. This suggests a dynamic process linking the  $L = 4$  and 5 sites, rather than  $O/N_2$  chemistry effects. Indeed, the  $L = 3$  results to be presented in the next section will further support the concept of repeated trough/plasmapause boundary crossings as a function of latitude and local time on each night of the storm period. It will be seen that while daytime positive F-region enhancements only occur early in the storm period (i.e., during the afternoon on Day 1), nighttime effects over the  $L \approx 3-5$  range are dominated by trough motions which yield the largest negative phase values during nighttime period between days 2 and 3 of the storm.

The peak density ( $N_{\max}$ ) pattern in Figure 8 is similar to the TEC results, except that the nighttime peaks are not as prominent and the daytime depletions are greater. Such differences in the response of TEC and  $N_{\max}$  imply that the F-region profile undergoes significant changes in shape during disturbed periods (Papagiannis et al., 1975). On Day 2, the daytime depletions in  $N_{\max}$  are two times larger than those seen in TEC, while at night-

time  $\Delta\text{TEC}$  (%) is nearly four times greater than  $\Delta N_{\text{max}}$  (%). This represents an excellent example of the difficulty in trying to relate similar F-region parameters to each other during storms. Thus, it is important to re-emphasize that attempts to interpret and/or use average storm patterns should be tempered by the following points:

(1) TEC data is an integral parameter, and thus changes at any one height (e.g.,  $h_{\text{max}}$ ) may easily be larger or smaller than changes in the integral over all heights.

(2) The  $N_{\text{max}}$  parameter is measured by a vertical sounding device while TEC is obtained along a slant ray path. Latitudinally dependent processes can thus affect the TEC measurement at different heights along the slant ray path, and vertical redistributions may drastically change  $N_{\text{max}}$  with TEC unaffected.

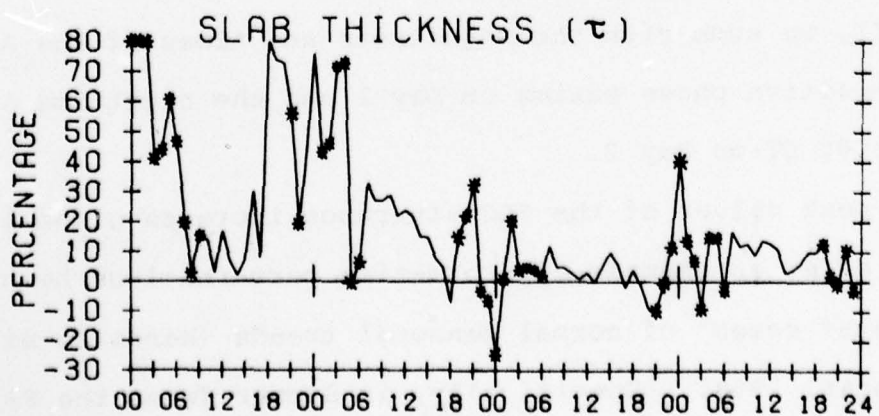
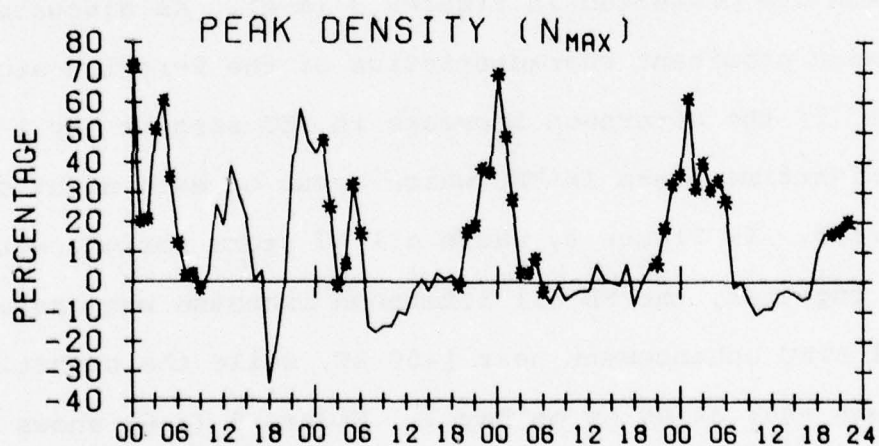
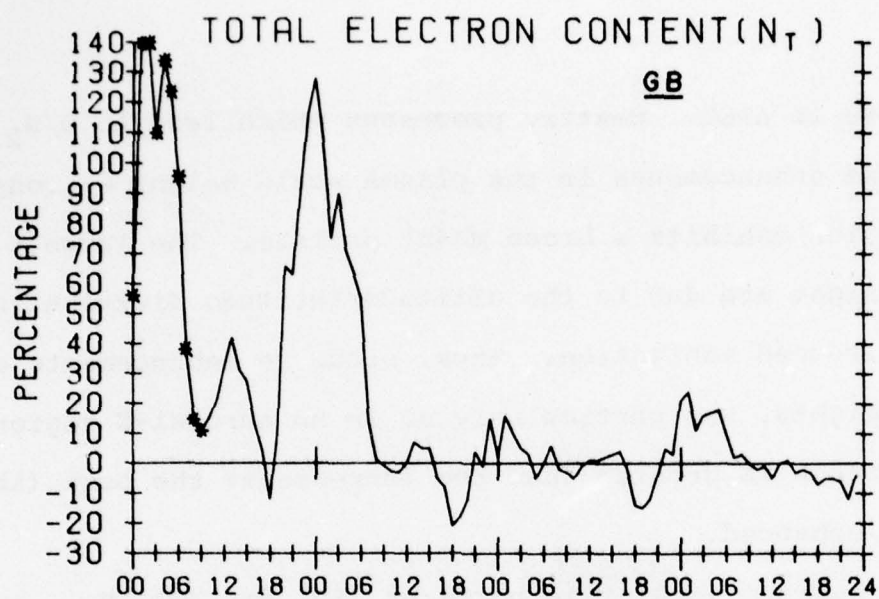
(3) Ionosonde degradation is always a problem, particularly during the nighttime hours. For the 67 events used to derive Figure 8, the "midnight peak" is defined by 60 TEC events and 35  $N_{\text{max}}$  events, while the  $\text{SD}_2$  "negative phase" comes from 61 TEC events and 48  $N_{\text{max}}$  events.

The final panel in Figure 8 gives the slab thickness patterns  $\text{SD}(\tau)$ . It should be recalled that  $\tau$  values can be formed only when both TEC and  $N_{\text{max}}$  data are simultaneously available. The  $\tau$  patterns in Figure 8 show two clear features: a general enhancement during all four days of the storm period, and large  $\Delta\tau$  (%) peaks during the nighttime hours. During the daytime periods,  $\tau$  is enhanced because the  $\Delta N_{\text{max}}$  depletions are deeper

than those in  $\Delta\text{TEC}$ . Heating processes which lead to  $\text{O}/\text{N}_2$  decreases also cause enhancements in the plasma scale height -- consequently the F-region exhibits a broad  $\text{Ne}(h)$  profile. The large  $\tau$  increases seen at night are due to the altitude/latitude distribution of auroral induced ionization. Thus, since Ne enhancements can occur at all heights, and particularly so in an auroral-E region, the  $\Delta\text{TEC}$  increase is greater than the increase at the peak ( $\Delta N_{\text{max}}$ ), and  $\tau$  is enhanced.

The average local-time patterns (SD) for TEC,  $N_{\text{max}}$  and  $\tau$  for each season are presented in Figures 9 (a-e). As discussed above, the two most prominent characteristics of the F-region storm at  $L = 4$  are (1) the afternoon increase in TEC seen on Day 1 and (2) the nighttime peaks in TEC which occur on each night of the storm period. In Figure 8, where all 67 storm periods were analyzed together, the SD (1) afternoon increase was characterized by a  $\approx 30\%$   $\Delta\text{TEC}$  enhancement near 1400 LT, while the nighttime peak in  $\Delta\text{TEC}$  was  $\approx 80\%$  at 00 LT on Day 2. Figure 9 (a-e) shows that these features undergo systematic seasonal variations. In Tables XI and XII, we summarize the magnitudes and times of the  $\Delta\text{TEC}$  daytime positive phase maxima on Day 1 and the nighttime  $\Delta\text{TEC}$  peak near 00 LT on Day 2.

The peak values of the TEC afternoon increase given in Table XI again offer an example of storm-time perturbations being "exaggerated cases" of normal seasonal trends (Mendillo et al., 1969; Duncan, 1969). Specifically, in Summer (when the F-region daytime contents reach their annual minimum) the storm associated



LOCAL TIME  
SD1 SD2 SD3 SD4  
AVERAGE DISTURBED DAILY VARIATIONS  
SD FOR WINTER STORMS

FIGURE 9a.

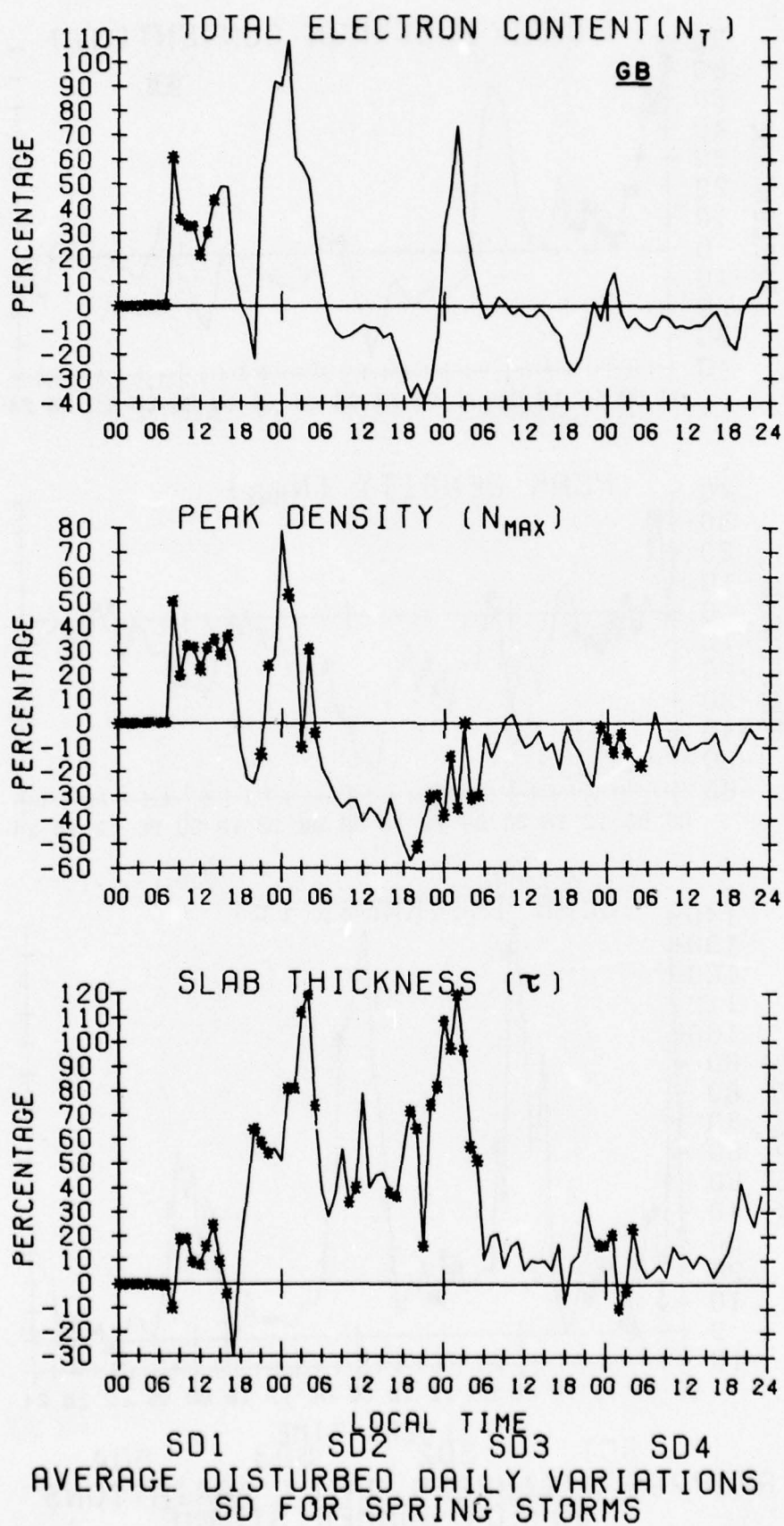


FIGURE 9b.

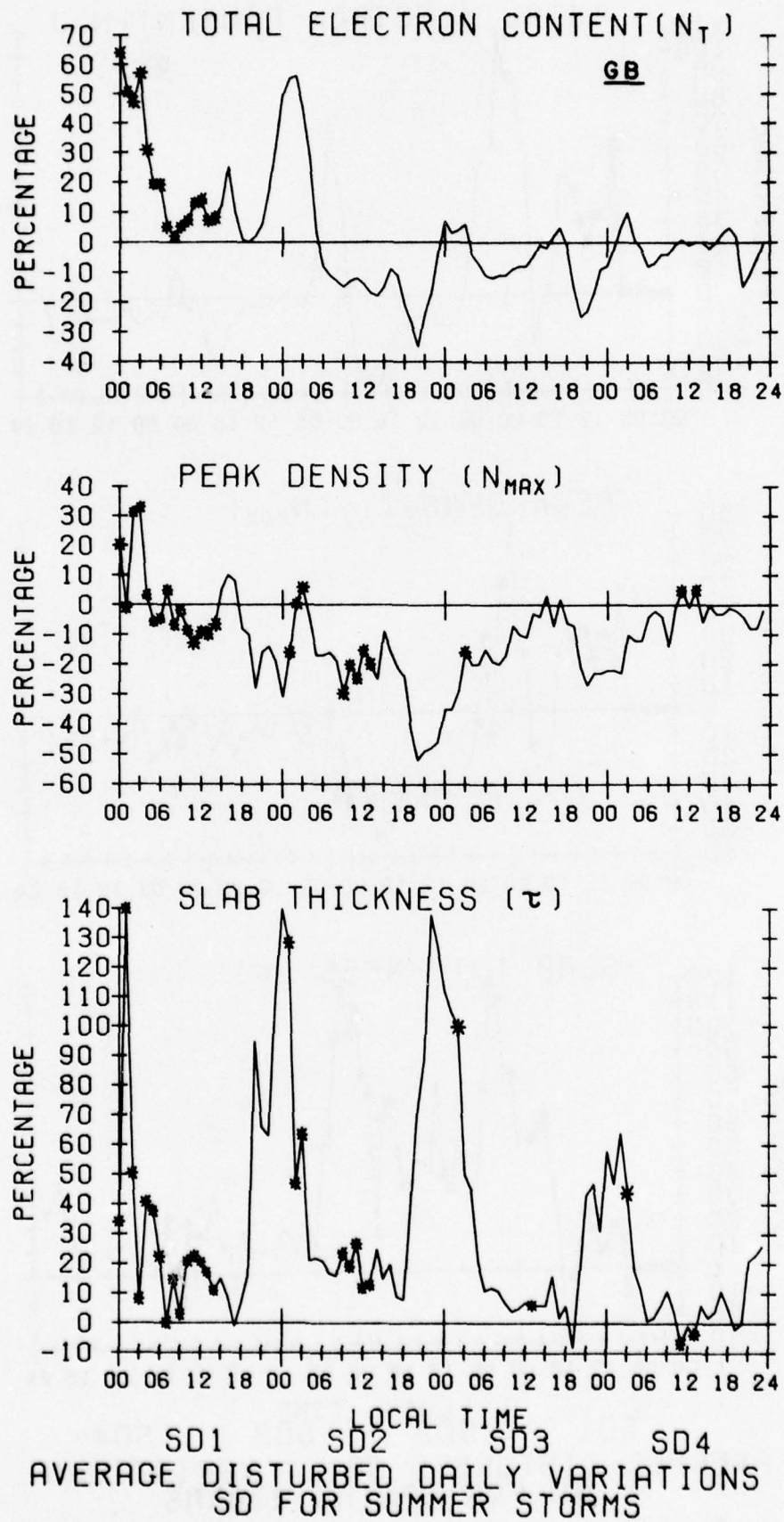
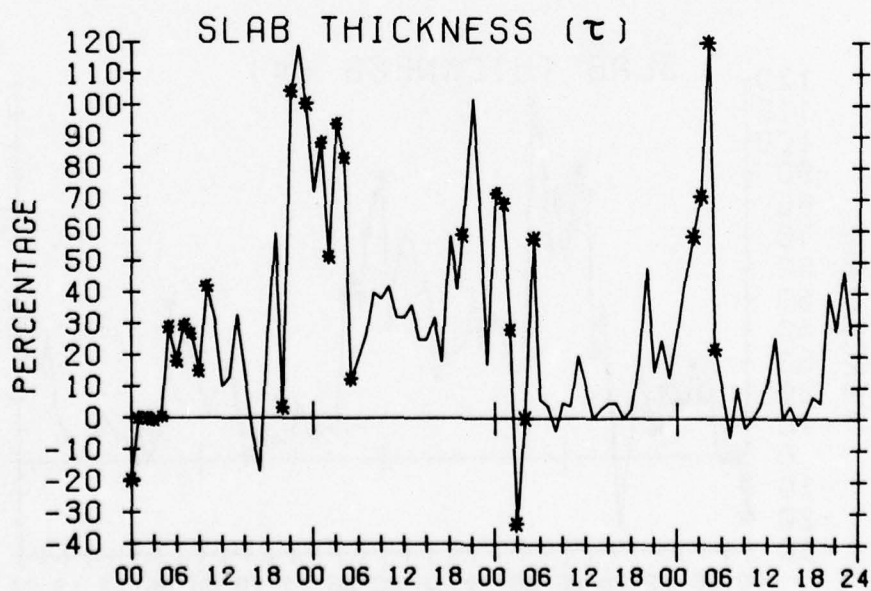
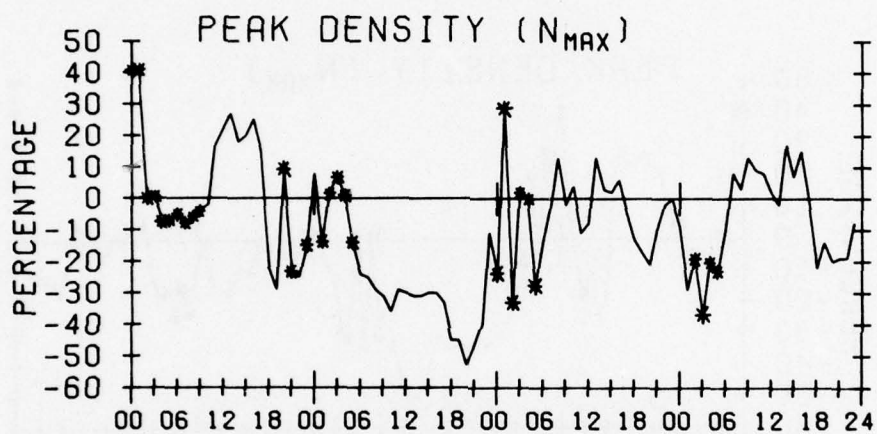
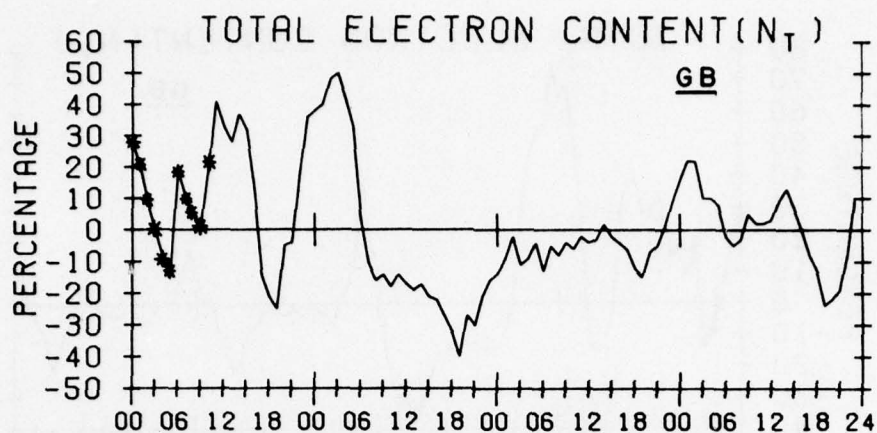


FIGURE 9c.



LOCAL TIME  
SD1 SD2 SD3 SD4  
AVERAGE DISTURBED DAILY VARIATIONS  
SD FOR FALL STORMS

FIGURE 9d.

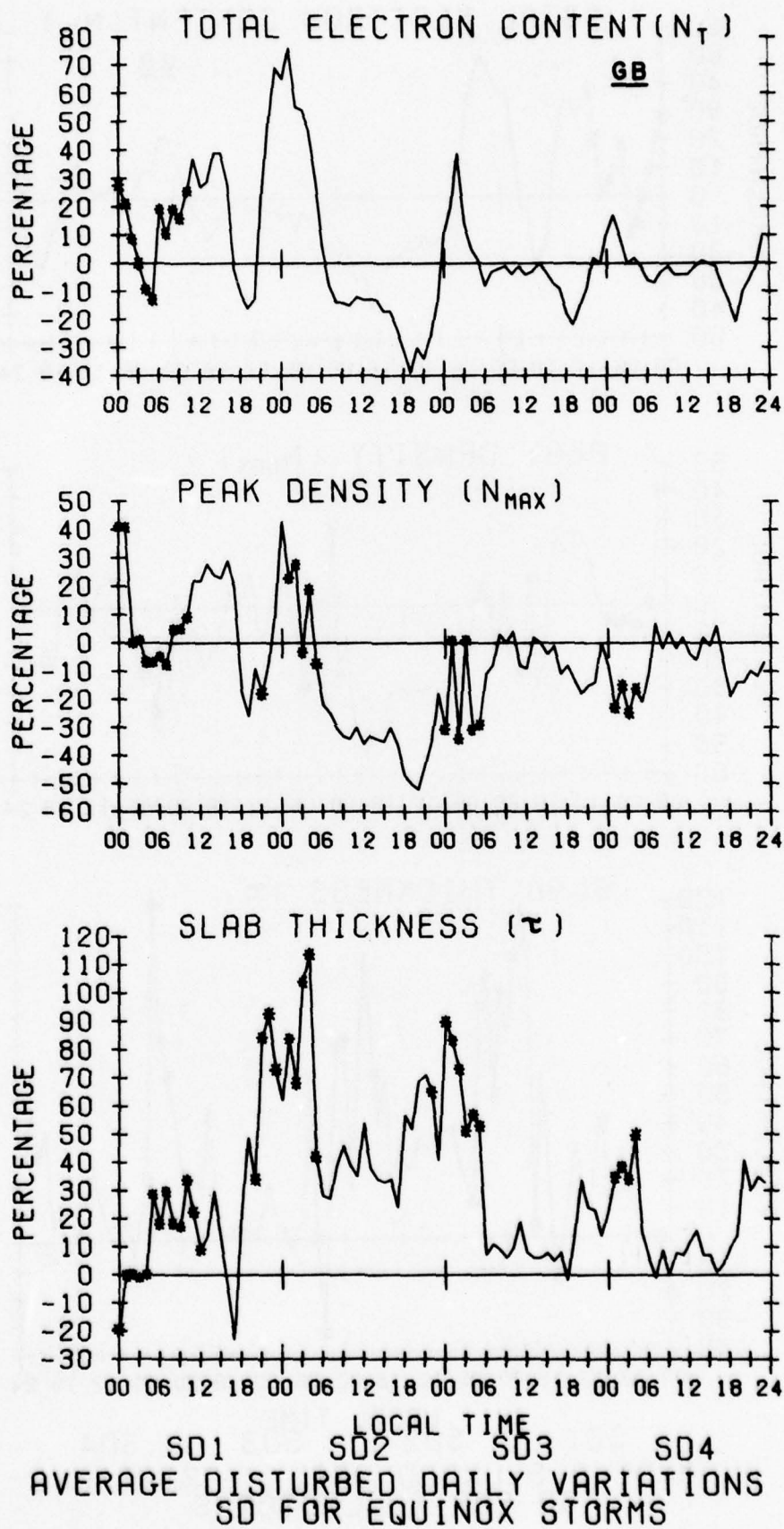


FIGURE 9e.

Table XI. Seasonal Characteristics of the TEC Afternoon  
Increase at Goose Bay ( $L \approx 4$ )

Season (with # of storms)	( $\Delta$ TEC)max in %	Time of ( $\Delta$ TEC)max LT
Winter (22)	$42 \pm 28$	13:00
Spring (13)	$49 \pm 35$	15-16:00
Summer (21)	$25 \pm 28$	16:00
Fall (11)	$37 \pm 51$	14:00
All (67)	$29 \pm 33$	13-14:00

Table XII. Seasonal Characteristics of the TEC Nighttime  
Increase on Day 2 at Goose Bay ( $L \approx 4$ )

Season (# of storms)	( $\Delta$ TEC)max in %	Time of ( $\Delta$ TEC)max LT
Winter (22)	$128 \pm 121$	00
Spring (13)	$109 \pm 163$	01
Summer (21)	$56 \pm 65$	02
Fall (11)	$50 \pm 69$	03
All (67)	$80 \pm 107$	00

TEC enhancement is considerably smaller than the TEC enhancements found during Winter storms (when the F-region daytime content is high). The local time of the  $\Delta$ TEC peak is also later in Summer than in Winter. Both aspects point to a solar production mechanism modulated by seasonally varying O/N<sub>2</sub> abundance to yield total plasma enhancements in phase with the seasonal anomaly. This trend of smaller and later  $\Delta$ TEC enhancements in Summer, larger and earlier in Winter, fits nicely into a latitude pattern for the L = 2 to 5 range, full discussion of which will be postponed until a later chapter.

In Table XII, the TEC auroral enhancement feature is summarized. This "midnight" enhancement also shows a well-defined seasonal trend with  $\Delta$ TEC during winter storms more than a factor of two higher than during summer storms. Since the nighttime TEC median behavior does not exhibit a seasonal anomaly, any auroral particle induced TEC enhancement would result in approximately twice as high a percentage increase in Winter than in Summer (see median curves in Figure 7). Thus, in the average, we see no significant difference between the amounts of auroral plasma produced under Summer and Winter conditions, though the standard deviations argue for a more consistent occurrence pattern in Winter.

The Spring and Fall results presented in Figure 5, 9 (b and d) and in Tables XI and XII do not describe a pattern equal and intermediate between the Summer and Winter curves. This suggests that an "Equinox season" is not a very meaningful concept for

storm analyses at  $L = 4$ . The results in Tables XI and XII for positive phase variations, coupled to the daytime negative phase segments in Figures 9b and 9d, point to the notion of Spring storms being "Winter-like" and Fall storms being "Summer-like". Any further comparisons of detailed pattern differences seem inappropriate given the relatively small sample size (13 and 11 storms, respectively) in comparison to Winter and Summer storms (22 and 21, respectively).

Considerable seasonal variation may also be seen in the  $N_{\max}$  and  $\tau$  patterns in Figures 9 (a-e). The large number of asterisks arise from the severe ionogram degradation which occurs during storms, and thus these average patterns are somewhat less reliable. For the  $\Delta N_{\max}$  patterns, the Summer results show mostly negative values -- historically the first general conclusion to come from early storm studies. Similarly, the general absence of a negative phase during Winter storms is once again seen. The dominant feature to emerge from the Winter storms is the large  $N_{\max}$  enhancements which occur each night. Since the St. John's ionosonde typically monitors a  $\approx 2\text{MHz}$  (trough) F-region during winter nights, the persistence of these enhancements dramatically illustrates the long recovery time of the  $L = 4$  ionosphere to strong storms.

In contrast to the TEC nighttime enhancements, the  $N_{\max}$  increases are basically limited to the Winter season. Consequently, the slab thickness parameter shows enhanced nighttime values on virtually every night of a storm, except during Winter. Again,

it should be emphasized that relatively strong geomagnetic storm periods have been selected, ones in which auroral precipitation patterns routinely move to  $L \leq 4$ . During isolated substorm events, the winter nighttime behavior at  $L = 4$  is quite different, as discussed in detail in an earlier report (Mendillo et al., 1977).

### 3.3. Average Storm Patterns -- Sagamore Hill ( $L \approx 3$ ).

The TEC observing station at Sagamore Hill (Hamilton, MA) has been used to study F-region storm effects since 1965. Most of our early studies were carried out using solar maximum data obtained from November, 1967, through December, 1969 (Mendillo et al., 1969, 1970, 1972; Mendillo, 1971 a,b, 1973). The AFCRL ATLAS of storm effects documented five years of continuous data (1968-72), covering 75 specific storms which occurred during high to medium solar flux years (Mendillo and Klobuchar, 1974, 1975). Both of these previous studies considered three parameters (TEC,  $N_{\max}$  and  $\tau$ ) and furnished most of the guidelines underwhich the present studies were carried out. As pointed out in Table VIII, however, the network of stations used in the present study provides data for medium to low solar flux years ( $\approx 1972-1975$ ). Thus, we felt that it would be inappropriate to compare our new results for  $L \neq 3$  with  $L \approx 3$  data taken during a somewhat more active epoch. Consequently we defined a new Sagamore Hill (Hamilton) data base spanning the years 1971-1975 in order to carry out an independent  $L = 3$  analysis consistent in solar flux characteristics with those done for the other sites. We call this new analysis Hamilton (A),

# MONTHLY MEDIAN TOTAL ELECTRON CONTENT

----- GOOSE BAY, LABRADOR  
 \_\_\_\_\_ HAMILTON, MASS.

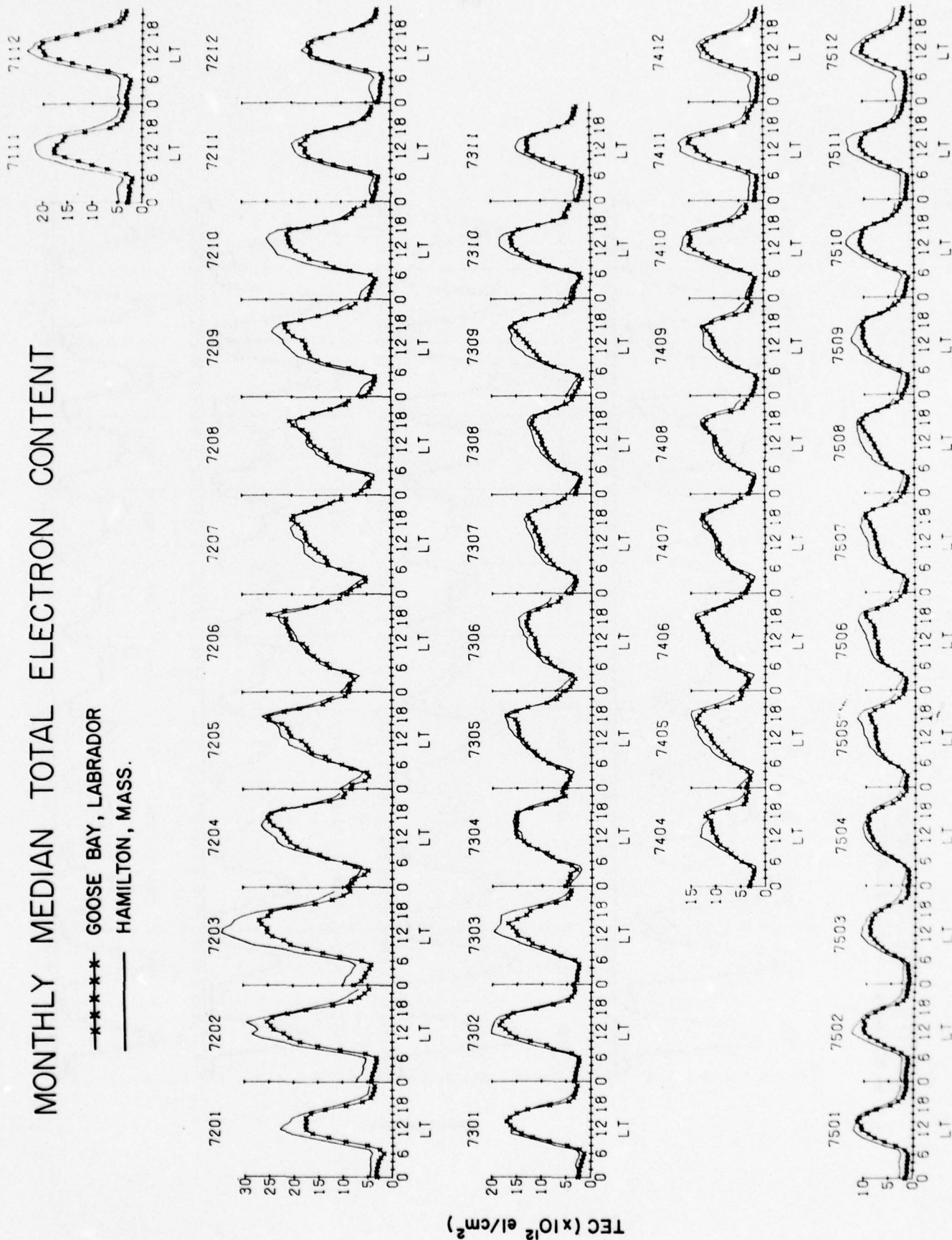


FIGURE 10a.

MONTHLY MEDIAN Nmax  
 x- ST. JOHN'S —WALLOPS ISLAND

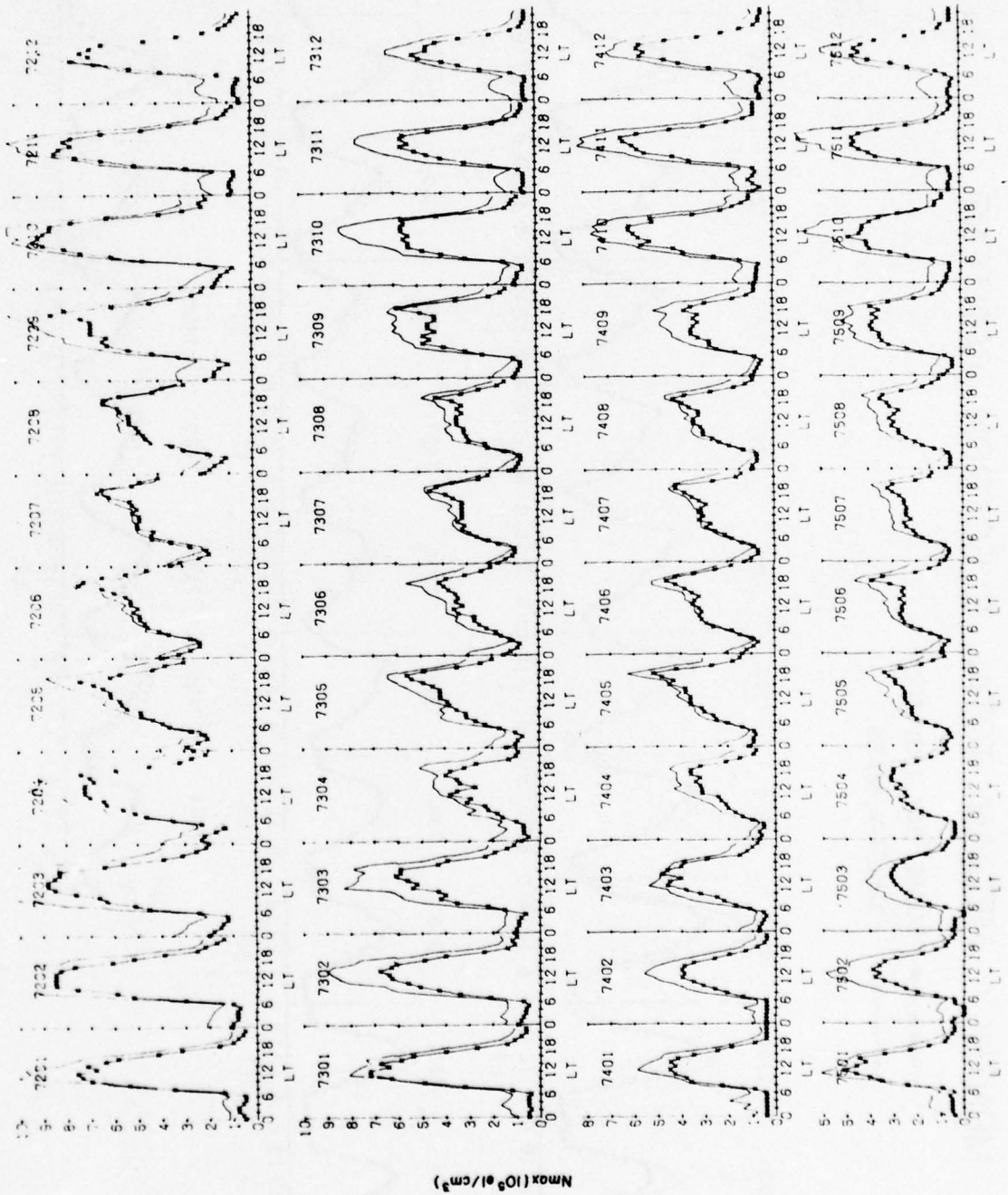


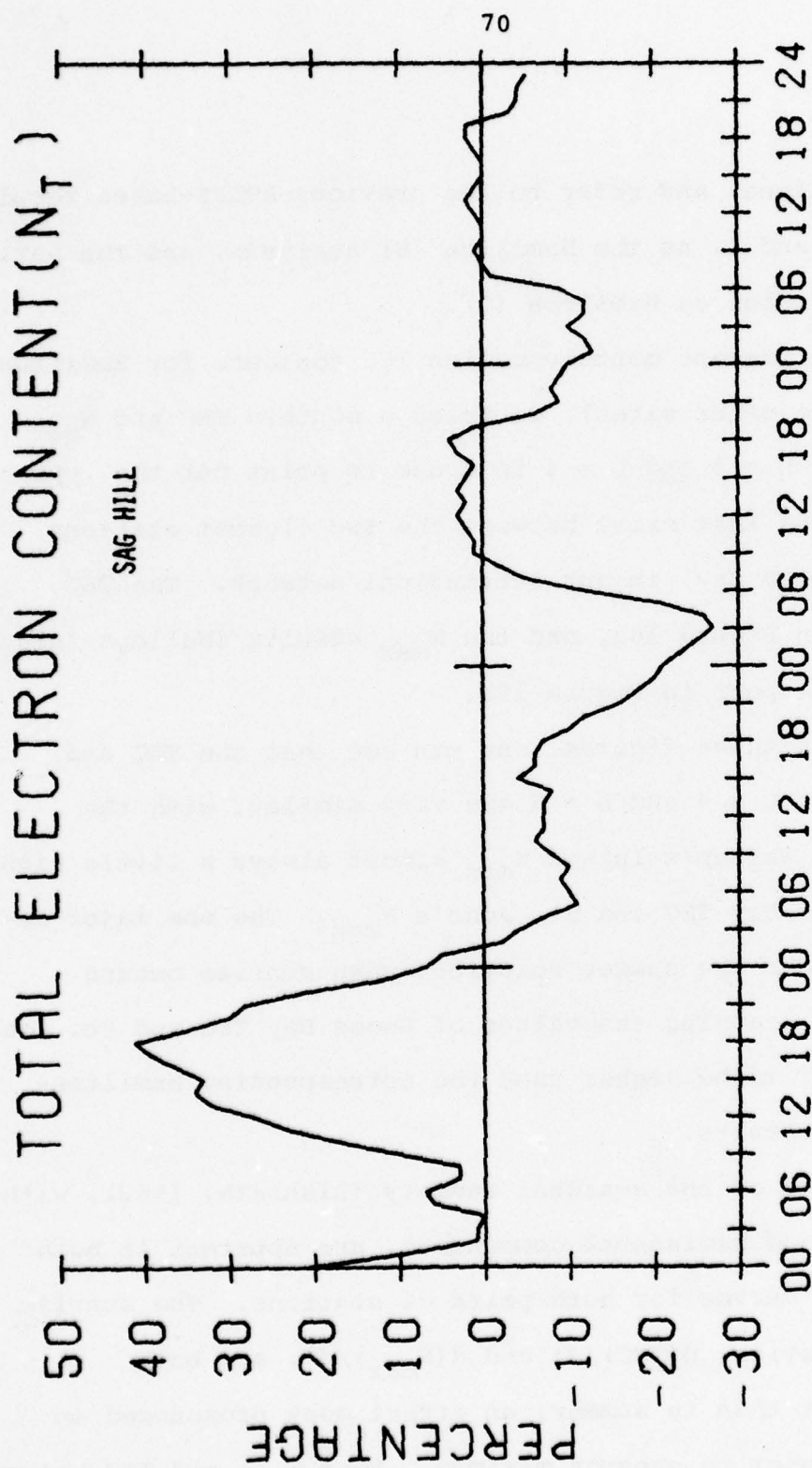
FIGURE 10b.

using TEC data alone, and refer to the previous ATLAS-based results, using TEC,  $N_{\max}$  and  $\tau$ , as the Hamilton (B) analysis, and the early solar maximum studies as Hamilton (C).

Rather than present monthly median TEC contours for Hamilton (as done with the other sites), we tried a monthly TEC and  $N_{\max}$  vs. LT format at  $L \approx 3$  and  $L \approx 4$  in order to point out the type of latitude gradients that exist between the two closest stations (Hamilton and Goose Bay) in our latitudinal network. The TEC results appear in Figure 10a, and the  $N_{\max}$  results (Wallops Island and St. John's) appear in Figure 10b.

In examining these figures, one can see that the TEC and  $N_{\max}$  behavior for  $L \approx 4$  and  $L \approx 3$  are very similar. with the Hamilton TEC and Wallop's Island  $N_{\max}$  almost always a little higher than the Goose Bay TEC and St. John's  $N_{\max}$ . The one major exception occurs near the summer solstice, when sunrise occurs earlier at  $L \approx 4$ , causing the values of Goose Bay TEC and St. John's  $N_{\max}$  near 0600 LT to be higher than the corresponding Hamilton-Wallop's Island results.

Most features of the seasonal anomaly (Rishbeth, 1968), with both its annual and semiannual components, are apparent in both the TEC and  $N_{\max}$  curves for both pairs of stations. The sunrise slope characteristics,  $d(\text{TEC})/dt$  and  $d(N_{\max})/dt$ , are both greater in winter than in summer, an effect most pronounced in  $N_{\max}$  in years closer to sunspot maximum. Noon  $N_{\max}$  and TEC values are also greater in winter than in summer; this effect is especially pronounced in  $N_{\max}$  nearer sunspot maximum. At night the seasonal



AVERAGE DISTURBED DAILY VARIATIONS  
SD FOR ALL STORMS

FIGURE 11

anomaly tends to disappear, especially at  $L \approx 4$ , i.e.,  $N_{\max}$  and TEC are larger in summer than in winter at night. In general, the seasonal anomaly in TEC is smaller than that in  $N_{\max}$ , an effect also seen in the lower daytime  $\tau$  in winter than in summer. In terms of the relative importance of the annual and semi-annual components of the seasonal anomaly, Figures 10a and 10b show that for both stations the semi-annual component dominates the TEC and  $N_{\max}$  behavior nearer sunspot maximum. The annual component becomes more important near solar minimum.

The average disturbed daily variations for the entire Sagamore Hill (A) TEC data set (109 solar minimum storms) are presented in Figure 11. The SD(TEC, LT) pattern depicted here includes all of the "characteristic features" found in earlier data sets (Sagamore Hill B and C data). These include:

- (1) A positive phase on Day 1 showing large TEC enhancements confined to the afternoon period (the "dusk effect" terminating abruptly after 1800 LT).

- (2) A negative phase on Day 2, with recovery patterns on Days 3 and 4.

- (3) Strong nighttime depletions, especially during the midnight to dawn period on Day 3.

An appreciation for the consistency of these features may be gained by examining Figure 12. Here we reproduced the SD(TEC,  $N_{\max}$ ,  $\tau$ ) patterns obtained from the earliest, solar-maximum data set (1968-69) and the expanded AFCRL ATLAS study (1968-1972).

There are several variations in the TEC "characteristic features"

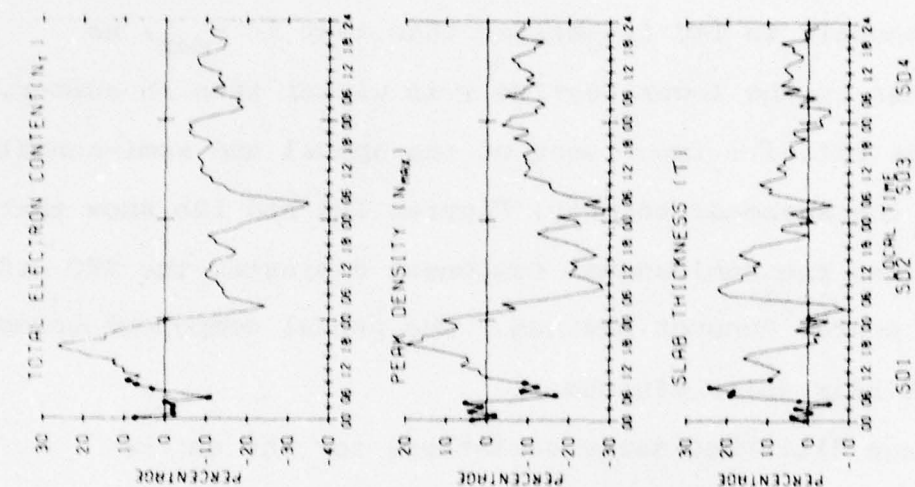


FIGURE 12b.

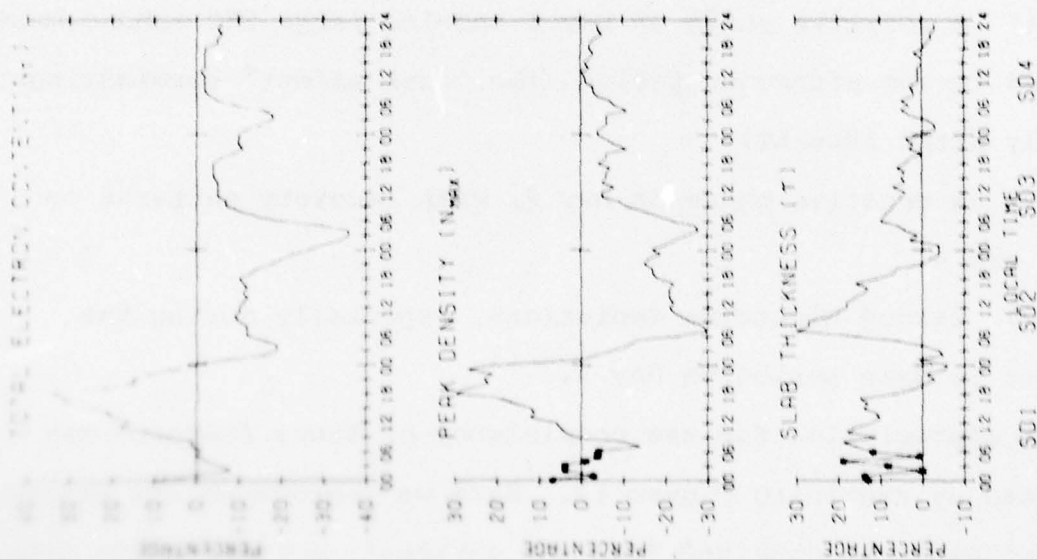


FIGURE 12a.

depicted in Figure 12. While features (1) and (3) listed above will be discussed within the context of the seasonal analysis (see below), there is one major, obvious difference that should be discussed -- namely the changing character of the daytime negative phase. It seems clear that the daytime negative phase (i.e., on Days 2, 3 and 4) is deeper and longer-lived during solar maximum years in comparison to solar minimum years. Thus, SD(TEC) in Figure 11 points to only a 2-day storm in daytime  $\Delta$ TEC, Figure 12a a day to a 4-day storm and Figure 12b to at least a 5-day storm. The SD( $N_{\max}$  and  $\tau$ ) patterns in Figure 12 (a and b) confirm the trend of a progressively quicker recovery of the Ne(h) profile as solar minimum approaches. This trend had not been fully appreciated before, and its implications with respect to physical processes are not obvious. If one assumes that the absolute intensity of geomagnetic storms does not change over the course of a solar cycle (e.g., say, an  $A_p = 45$  storm in 1968 has the same energy input as an  $A_p = 45$  storm in 1975), then the long recovery time in solar maximum years might be due to several possibilities:

- (1) perturbations upon the neutral atmosphere (i.e., decreases in  $O/N_2$ ) may be long in dissipating when the O and  $N_2$  concentrations at F-region heights are already at their solar cycle maxima.

- (2) storm-time heating effects enhancing the reaction rates for F-region loss chemistry may inherently be more sensitive to a given  $\Delta T$  when T itself is high.

- (3) ionospheric replenishment of depleted protonospheric tubes of force causes a greater drain on the F-region during high

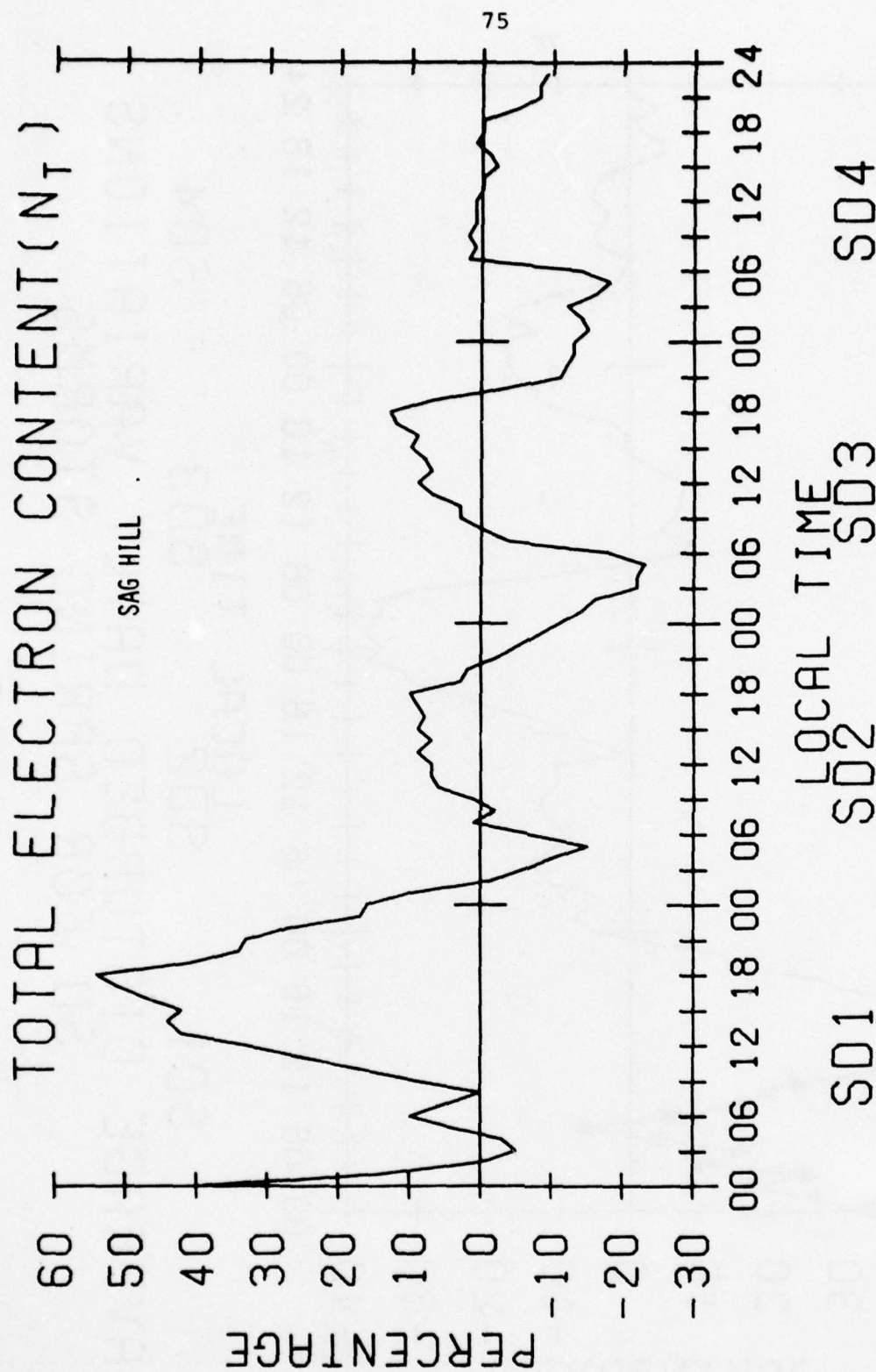
sunspot years -- when tube contents are high.

These are interesting questions which seem beyond most theoretical modelling capabilities as of the present time.

The seasonal analyses for SD(TEC) using the new Sagamore Hill (A) data set are presented in Figures 13 (a through e). As mentioned above, the greatest positive and negative  $\Delta\text{TEC}(\%)$  effects occur on Day-1 (the "dusk effect") and on Day-3 (the "trough effect" near 0300 LT). In Tables XIII and XIV we summarize these effects over an entire solar cycle by using the Sagamore Hill A, B and C data sets. We quote peak percentage variations (with standard deviations for the new A-data set) for the feature in question and its local time of occurrence. Both tables point to a remarkable consistency in the effects observed. We will comment on the seasonal results first and then on solar cycle effects (when appropriate):

(1) The  $\text{SD}_1(\text{TEC})$  results for the afternoon increase (Table XIII) show that  $\Delta\text{TEC}(\%)$  is always larger in Winter than in Summer. It also peaks 3-4 hours later in Summer than in Winter. The overall (ALL-STORMS) pattern shows the increase to be larger during solar minimum years. Spring and Fall results are not easily classified as "Summer-like" or "Winter-like" (see A and B data sets, in particular, when the numbers of events are relatively high and therefore the derived patterns more significant than with the C-data set).

(2) The  $\text{SD}_3(\text{TEC})$  results for the trough-associated minimum (Table XIV) show the effect to be deeper in Summer than in Winter,



AVERAGE DISTURBED DAILY VARIATIONS  
SD FOR WINTER STORMS

FIGURE 13a.

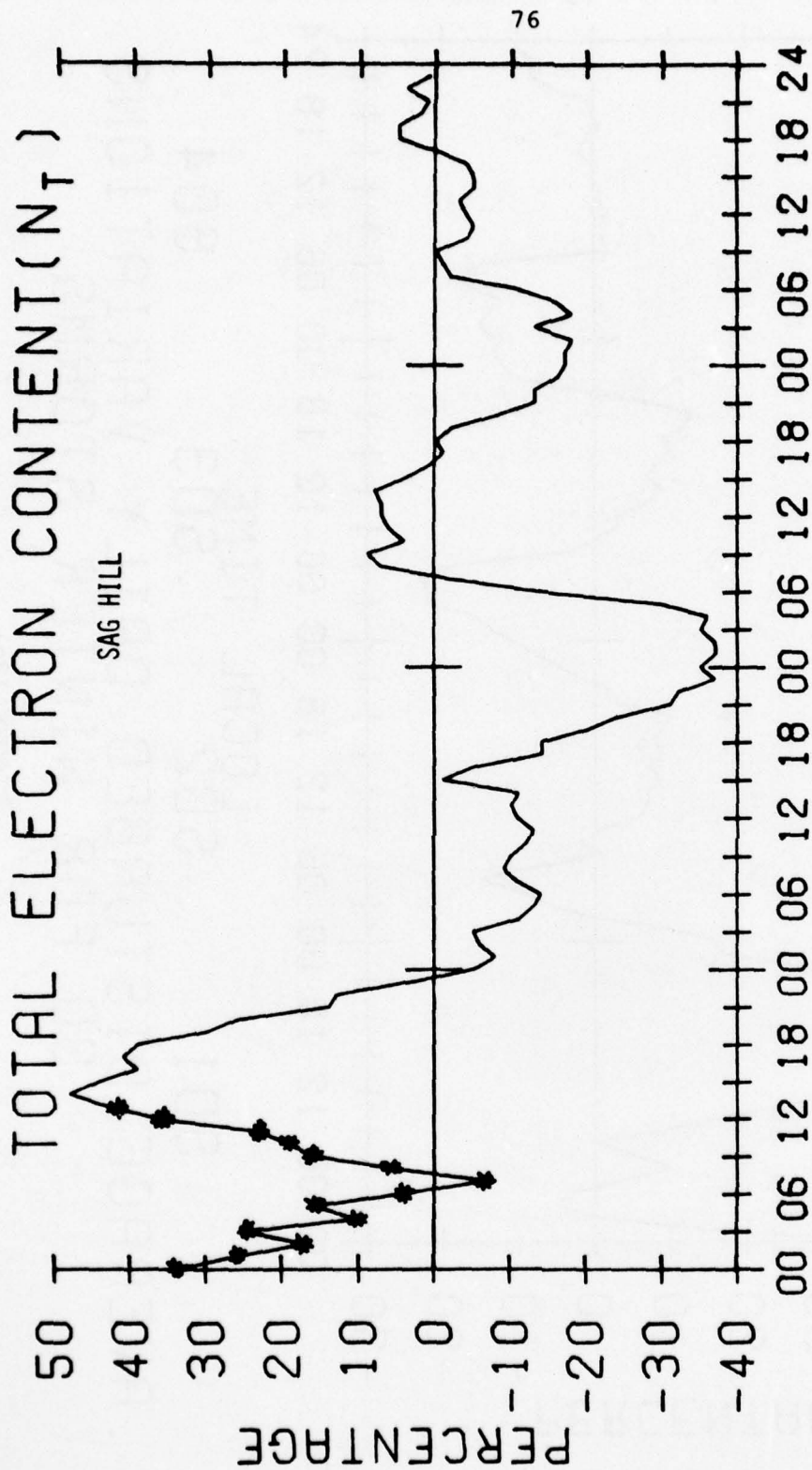


FIGURE 13b.

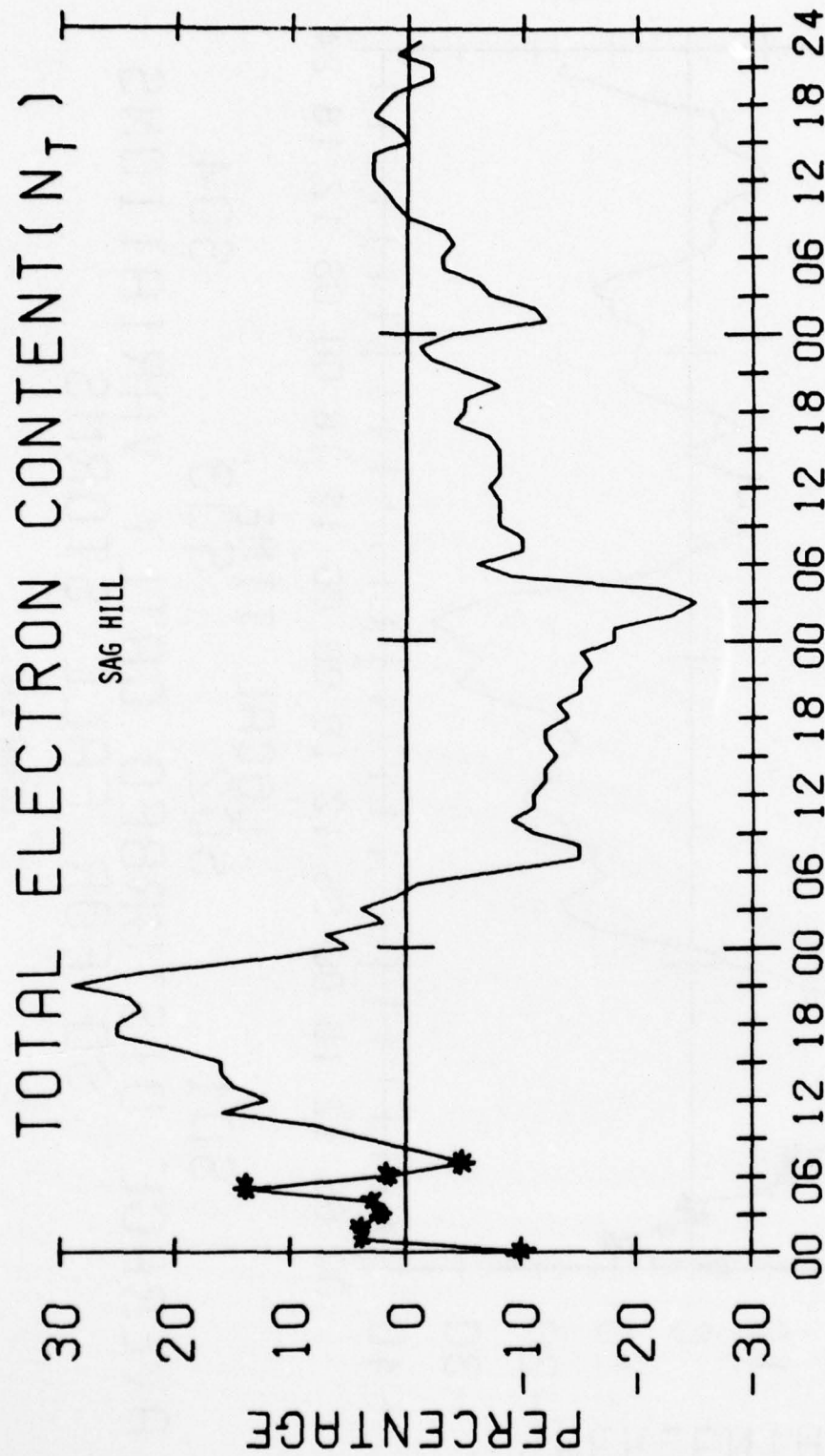


FIGURE 13c.

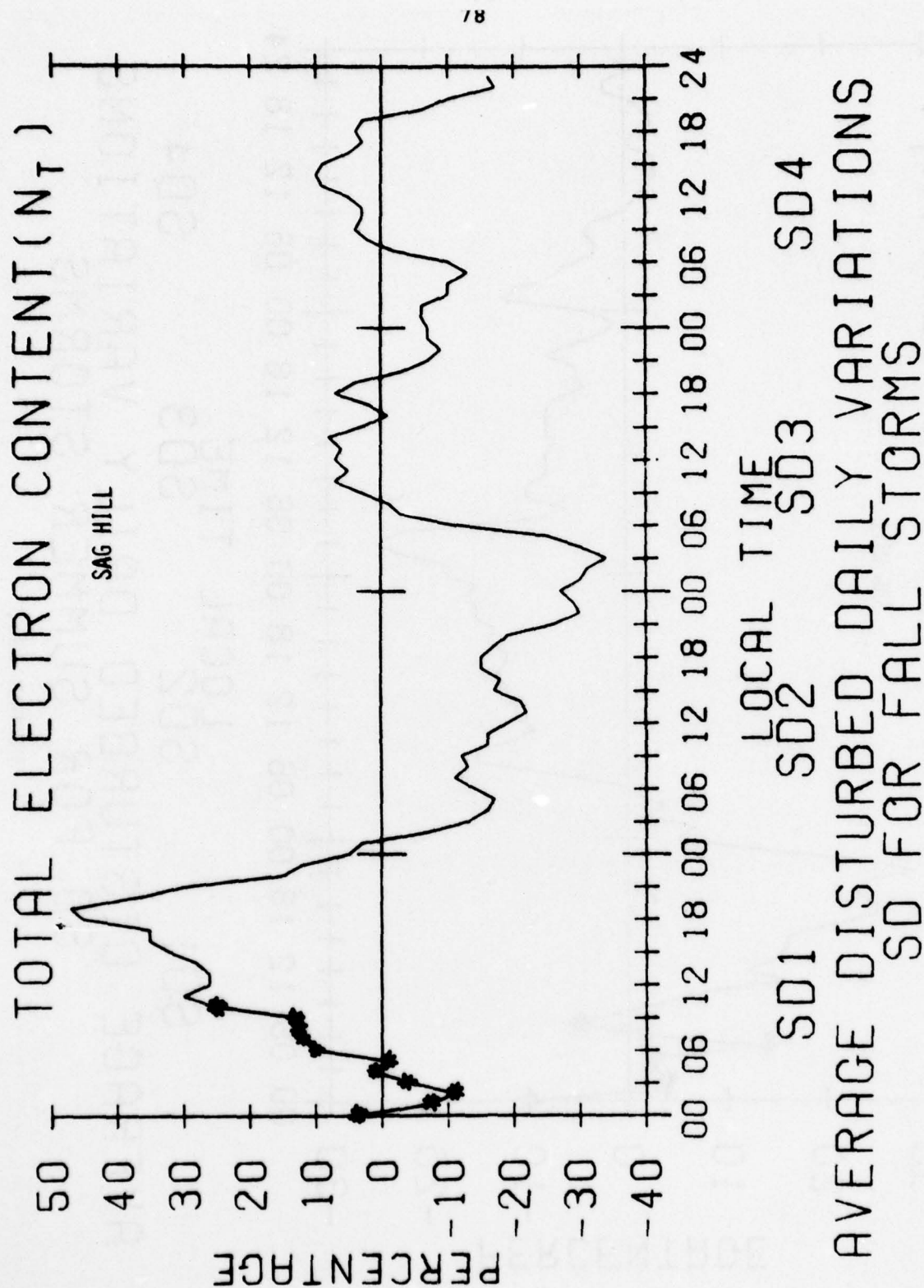


FIGURE 13d.

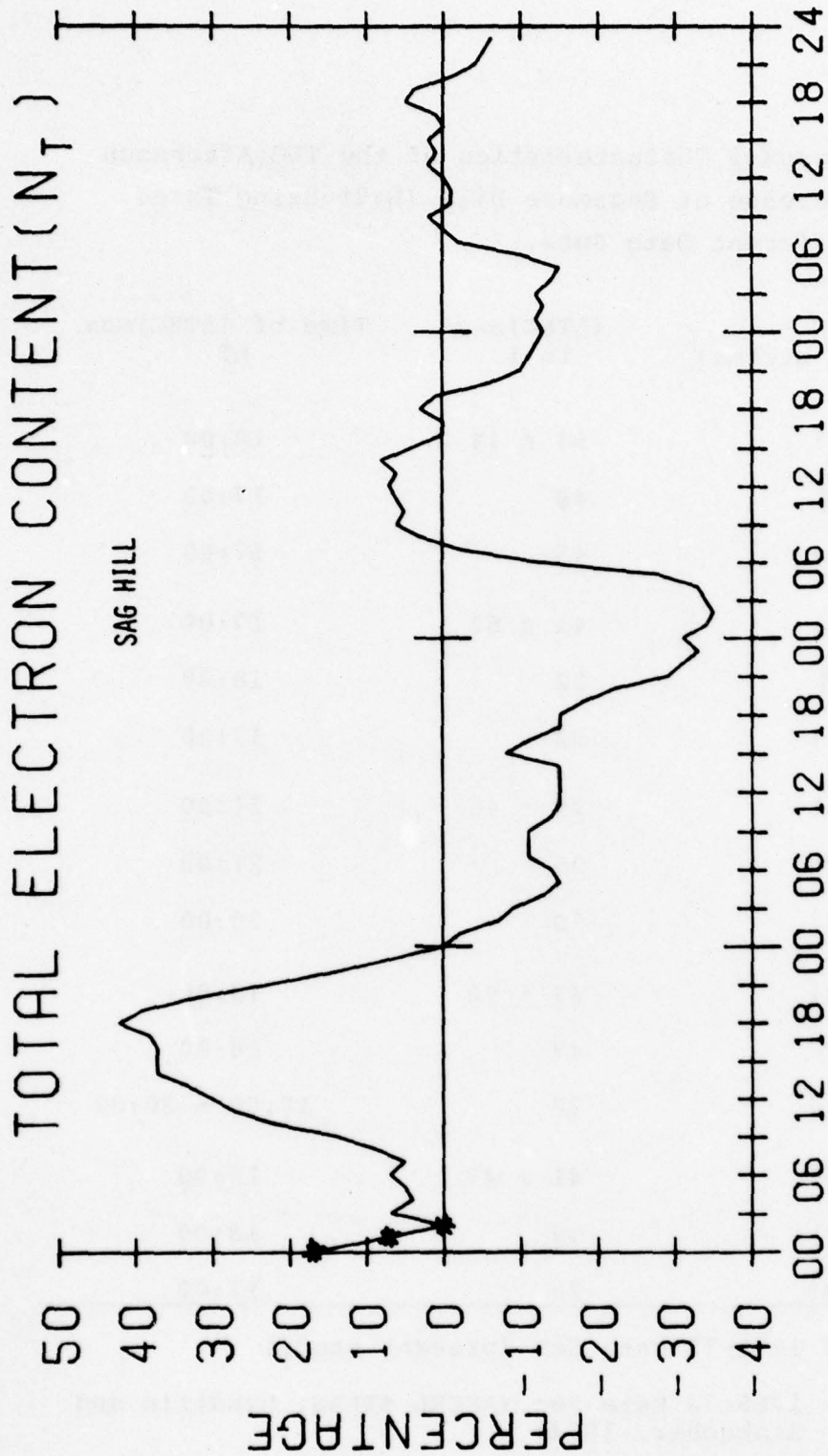


FIGURE 13e.

Table XIII. Seasonal Characteristics of the TEC Afternoon Increase at Sagamore Hill ( $L=3$ ) Using Three Different Data Sets.

SEASON (with # of storms)	( $\Delta$ TEC)max in %	Time of ( $\Delta$ TEC)max LT
Winter (34)	54 $\pm$ 49	18:00
[21]	48	17:00
{ 6 }	45	17:00
Spring (21)	41 $\pm$ 52	17:00
[14]	22	18:00
{ 5 }	32	17:00
Summer (35)	29 $\pm$ 46	21:00
[27]	25	21:00
{11}	30	20:00
Fall (19)	47 $\pm$ 50	19:00
[13]	47	18:00
{ 6 }	20	17:00 - 20:00
All (109)	41 $\pm$ 47	18:00
[75]	34	18:00
{28}	26	17:00

A. ( ) = 1971-75 Data Set (present study)

B. [ ] = 1968-72 Data Set (AFCRL ATLAS, Mendillo and Klobuchar, 1974)

C. { } = 1968-69 Data Set (Mendillo, 1971a)

Table XIV. Seasonal Characteristics of the TEC Nighttime Depletion at Sagamore Hill ( $L \approx 3$ ) Using Three Different Data Sets

SEASON (# of storms)	( $\Delta$ TEC)min in %	Time of ( $\Delta$ TEC)min LT
Winter (34)	$-22 \pm 33$	03-05
[21]	-29	03
{ 6 }	-45	02-04
Spring (21)	$-37 \pm 17$	02
[14]	-35	04
{ 5 }	-28	04
Summer (35)	$-25 \pm 27$	03
[27]	-38	03
{11}	-28	03-04
Fall (19)	$-34 \pm 30$	03
[13]	-50	04
{ 6 }	-48	04
All (109)	$-27 \pm 29$	03
[75]	-37	03
{28}	-36	04

A. ( ) = 1971-1975 Data Set (present study)

B. [ ] = 1968-1972 Data Set (AFCRL ATLAS Mendillo and Klobuchar, 1974)

C. { } = 1968-1969 Data Set (Mendillo 1971a)

but with the largest effects occurring during Spring and Fall events. If the minima are indeed due to a significant shift in the normal latitude gradients (i.e., the trough normally near  $L \approx 4$  is now near  $L \approx 3$ , as the Goose Bay results of the previous section suggests), then the F-region under equinoctal conditions must be singled out as being particularly sensitive to latitudinal motions. Finally, a trend does appear for the minima to be deeper during more active solar flux periods.

Perhaps the most unsettling results to come from our long-term studies of ionospheric storms is the lack of an understanding of the equinoctal storm morphologies, and perhaps the Spring storms most of all. The storm-time coupling of the ionosphere to semi-annual neutral atmosphere effects perhaps holds the answer -- and this should be addressed within the context of the day-to-day variability question as well.

#### 3.4. Average Storm Patterns Near $L \approx 2$ .

Since most of the ionospheric perturbing processes associated with geomagnetic storms have their origin at high magnetic latitudes ( $L \geq 3$ ), the AFGL ionospheric stations at Narssarssuaq, Goose Bay and Sagamore Hill were the initial sites examined in the search for storm morphologies. The  $L = 3$  to 5 range thus considered might be broadly classified as describing effects from upper midlatitudes to auroral zone locations. It is expected that effects of magnetospheric origin dominate at these sites and thus similar effects should occur where similar magnetic coordinates occur -- regardless

of longitude. The sparcity of long-term TEC data in the  $L = 3-5$  range from non-Atlantic coast regions makes this notion somewhat difficult to test. The only station near  $L \approx 3$  where storm-time TEC data simultaneous with Sagamore Hill data exists is Edmonton, Canada (daRosa, 1972). The April 14-15, 1971, period has been examined in detail and a great deal of similarity was found at both  $L \approx 3$  sites, in particular with reference to the time of the  $SD_1$  afternoon increase, its rapid termination, and the subsequent post-midnight depletions (Mendillo et al., 1974).

At lower midlatitude sites ( $L \leq 2$ ), the character of F-region disturbance effects traditionally pointed to less well defined phases (Matsushita, 1959; Obayashi, 1964). The initial positive phase seemed to last longer than the high latitude case, though in both the positive and negative variations, the average patterns rarely exceeded  $\pm 10\%$  effects. We have used our own averaging techniques in the hope of obtaining average local time patterns which more realistically relate to actual individual storm morphologies. Realizing that neutral atmosphere composition changes probably dominate storm processes at low latitudes, we investigated the  $L \approx 2$  ionosphere at three widely spaced longitudes where the differences between geographic and geomagnetic coordinates might significantly impact the resulted storm-induced effects. In this chapter, we examine two sets of  $L \approx 2$  storm patterns in the context of the latitude chain previously described. Longitudinal differences are treated in the following chapter.

### 3.4.1. Rosman Storm Patterns ( $L \approx 2.2$ )

As described in Table VIII, the Rosman TEC data base is limited to the year 1972, a year of intermediate solar flux ( $S_{10.7} \approx 160$  for 1970,  $\approx 120$  for 1972 and  $\approx 80$  for 1975). The data were taken by Stanford University and reduced at AFGL using 1-hr time resolution in LMT. In Figure 14 we present the set of TEC contours which summarize the monthly median conditions. Perhaps the most obvious feature is the strong semi-annual component in the day-time values--with a pronounced absolute maximum in Spring. Table III shows that 15 storm periods were identified for 1972, but data loss during 2 events limits the total sample to 13 storm periods. A seasonal breakdown for such a small data base would be ill-advised, so we limit our discussion to the  $SD(TEC,LT)$  curve for all storms (Figure 15).

The SD features in Figure 15 may be systematically related to those seen at  $L \approx 3$  (Figures 11 and 12):

- (1) The TEC enhancement on Day 1 is significantly stronger and occurs later than the "Dusk Effect" at Sagamore Hill. During the 1800 - 2000 LT period,  $\Delta TEC(\%) \approx 70-75\%$ , followed by a local minimum of  $\approx 40\%$  near 2200 LT, and a mid-night maximum near  $+50\%$ .
- (2) The negative phase on Day 2 is comparable at  $\sim -10\%$  to  $L \approx 3$  results.
- (3) The largest negative excursions occur during the 0300 - 0600 LT period on Day 3--indicating that trough-associated disturbed latitude gradients extend equatorward of  $L \approx 3$

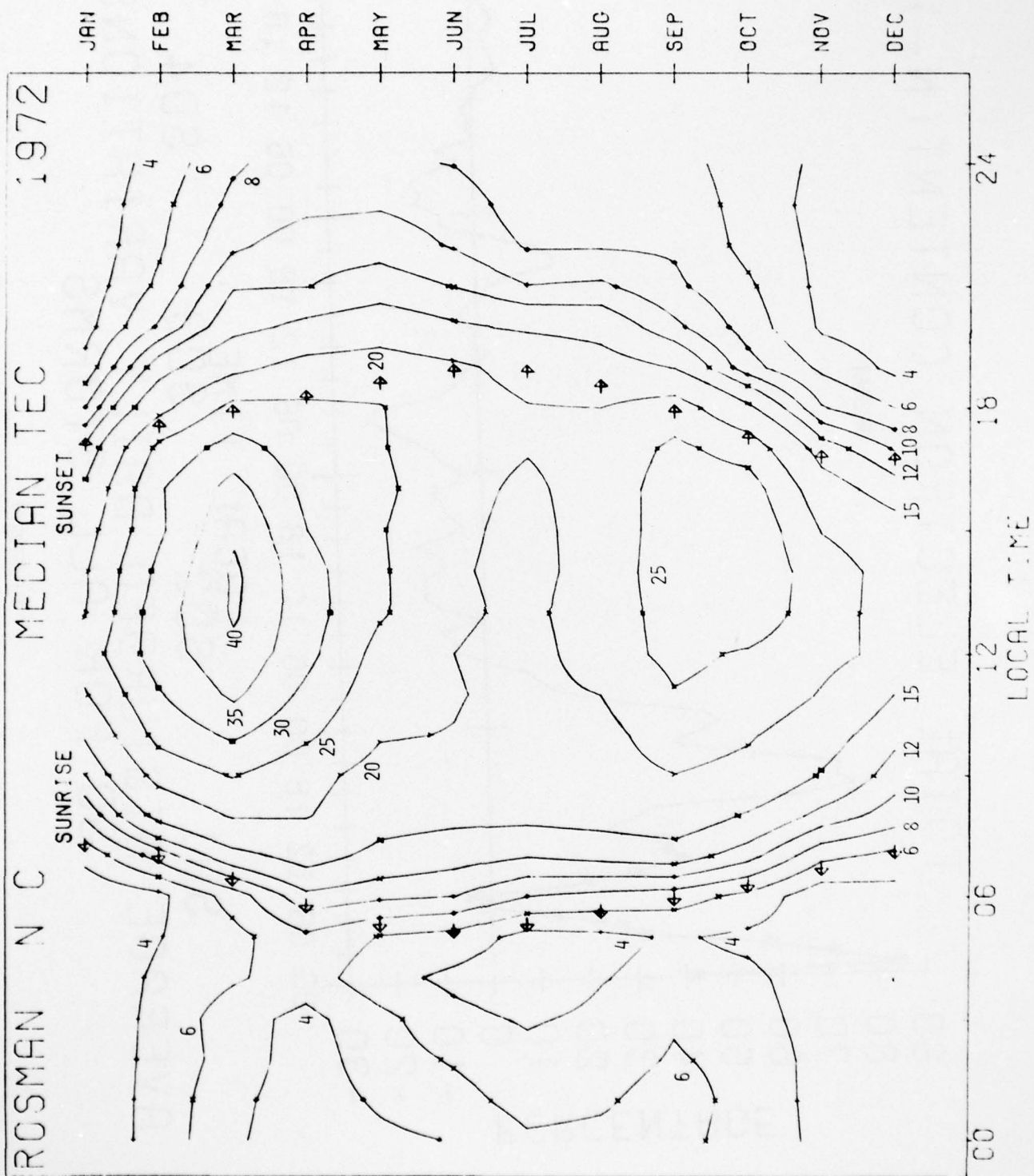


FIGURE 14

AD-A056 978

BOSTON UNIV MASS DEPT OF ASTRONOMY

BEHAVIOR OF THE IONOSPHERIC F-REGION DURING GEOMAGNETIC STORMS (U)

MAR 78 M MENDILLO

F19628-75-C-0044

UNCLASSIFIED

ACBU-SER-III-NO-6

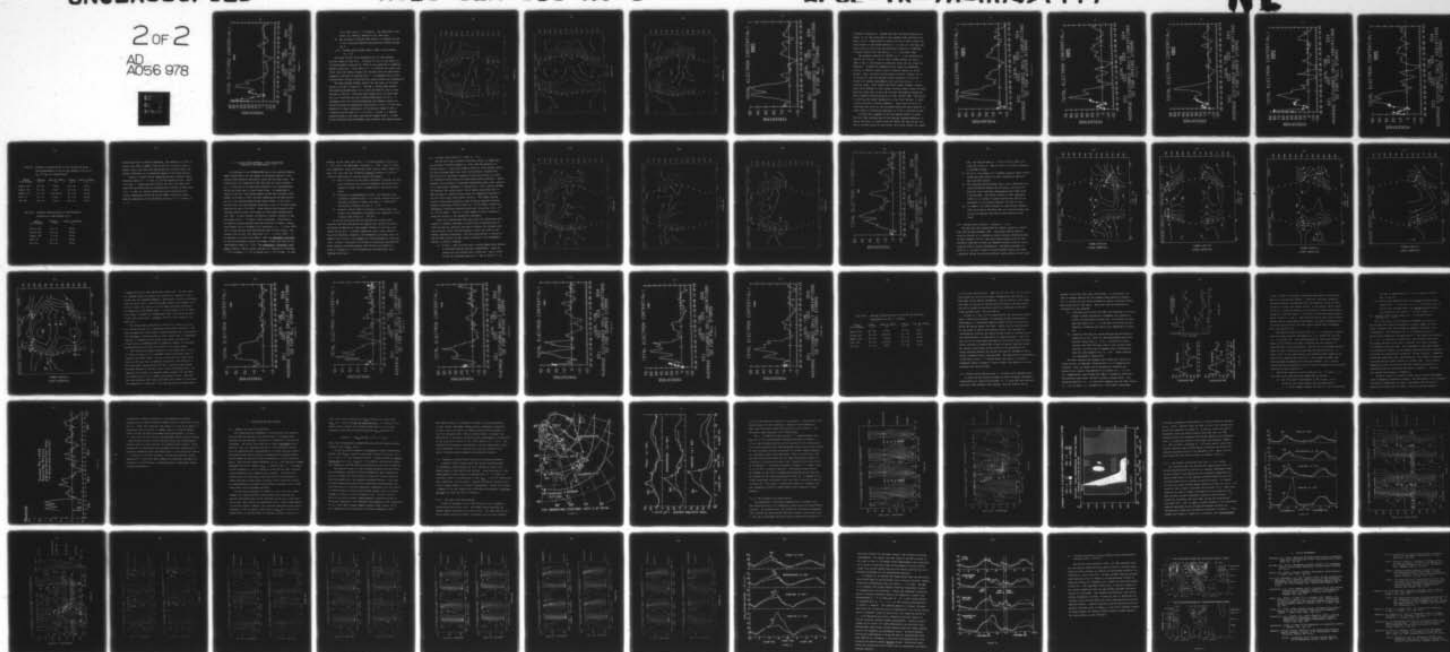
AFGL-TR-78-0092 (11)

FIG 4/1

NL

2 OF 2

AD  
A056 978



END

DATE  
FILMED

9-78

DDC

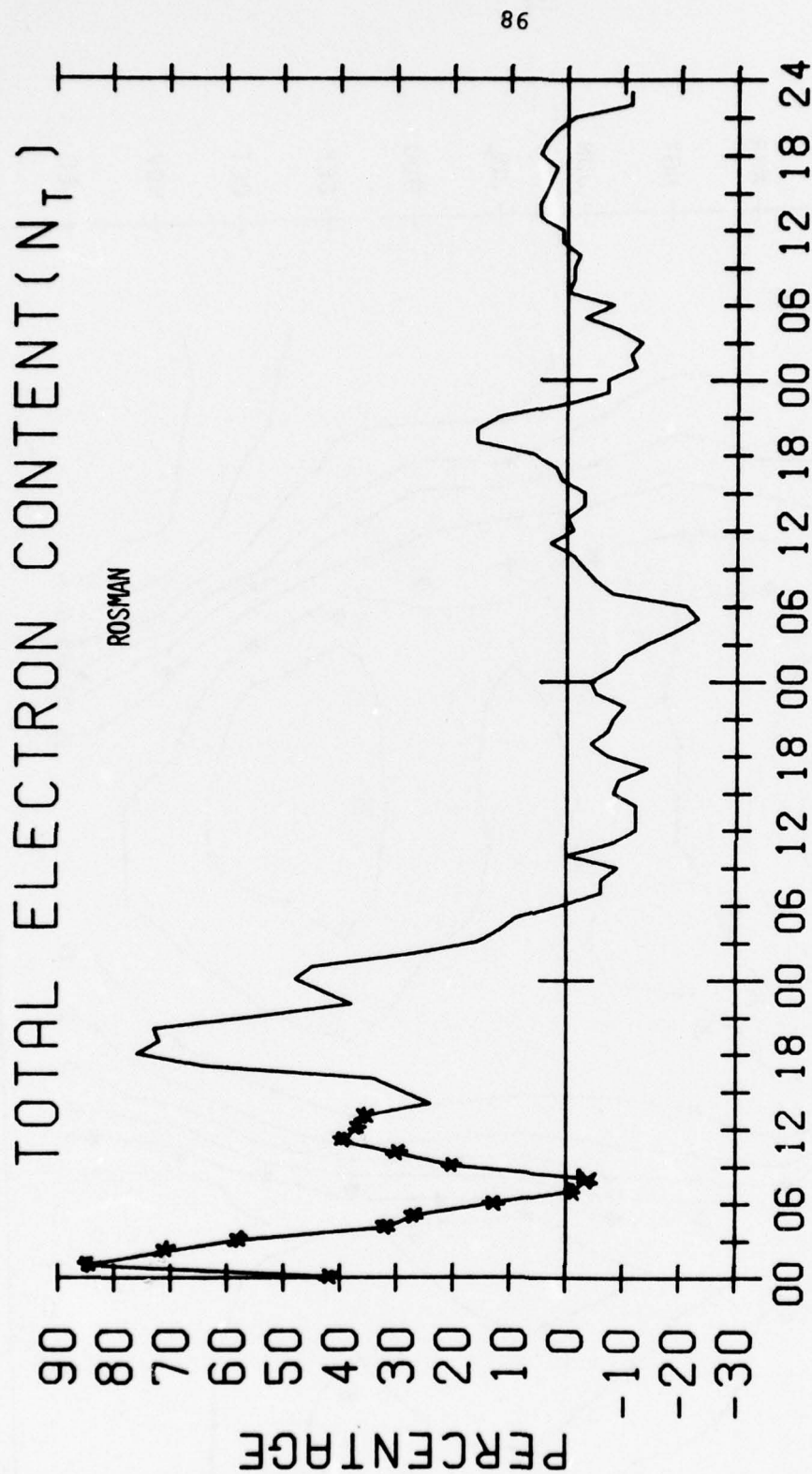


FIGURE 15.

to at least the  $L \approx 2.2$  location. The magnitude of the effect is, however, reduced at the lower site.

- (4) The recovery of daytime  $\Delta\text{TEC}$  effects is complete by Day 3, but lingering nighttime perturbations extend through Day 4.

#### 3.4.2. Kennedy Space Flight Center (KFSC) Storm Patterns ( $L \approx 1.8$ )

Data from the Air Force sponsored site at Cape Kennedy, Florida, began in late 1973. In Figure 16 (a,b,c) the annual set of monthly median contours for 1974-5-6 are presented to summarize ambient conditions. These data at  $L \approx 1.8$  confirm the single year (1972) data from Rosman (Figure 14) and show that the semi-annual component continues to dominate the  $L \approx 2$  ionosphere during solar minimum years--though the Spring-time annual maxima has dissappeared.

The Cape Kennedy SD(TEC) pattern for the total of 70 storm periods is given in Figure 17. The Day 1 results show daytime and nighttime maxima near 50 % at 1500 and 2200 LT, with a local minimum at 1700 LT. Given the large sample size, we would take this as a statistically more reliable description of the  $L \approx 2$  ionosphere than the 13-storm morphology from Rosman (Figure 14). The main feature to appreciate from Figures 14 and 17 is the clear absence of a rapid termination of the positive phase on Day 1--a feature clearly seen at  $L \approx 3, 4$  and 5. On Day 2, a daytime negative phase is not seen, and thus we suggest that  $L \approx 2$  must be the dividing location between clear positive and negative phase

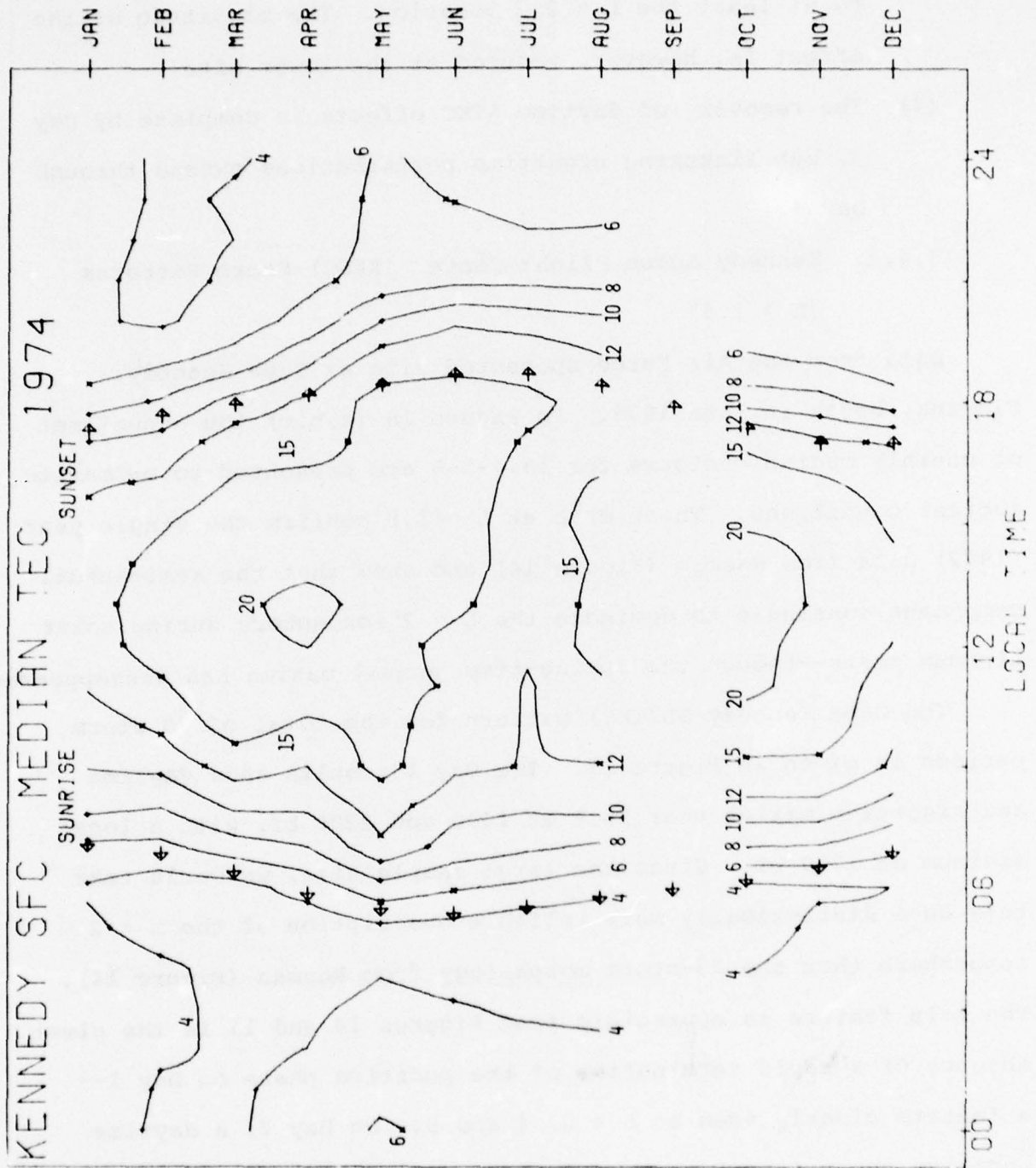


FIGURE 16a.

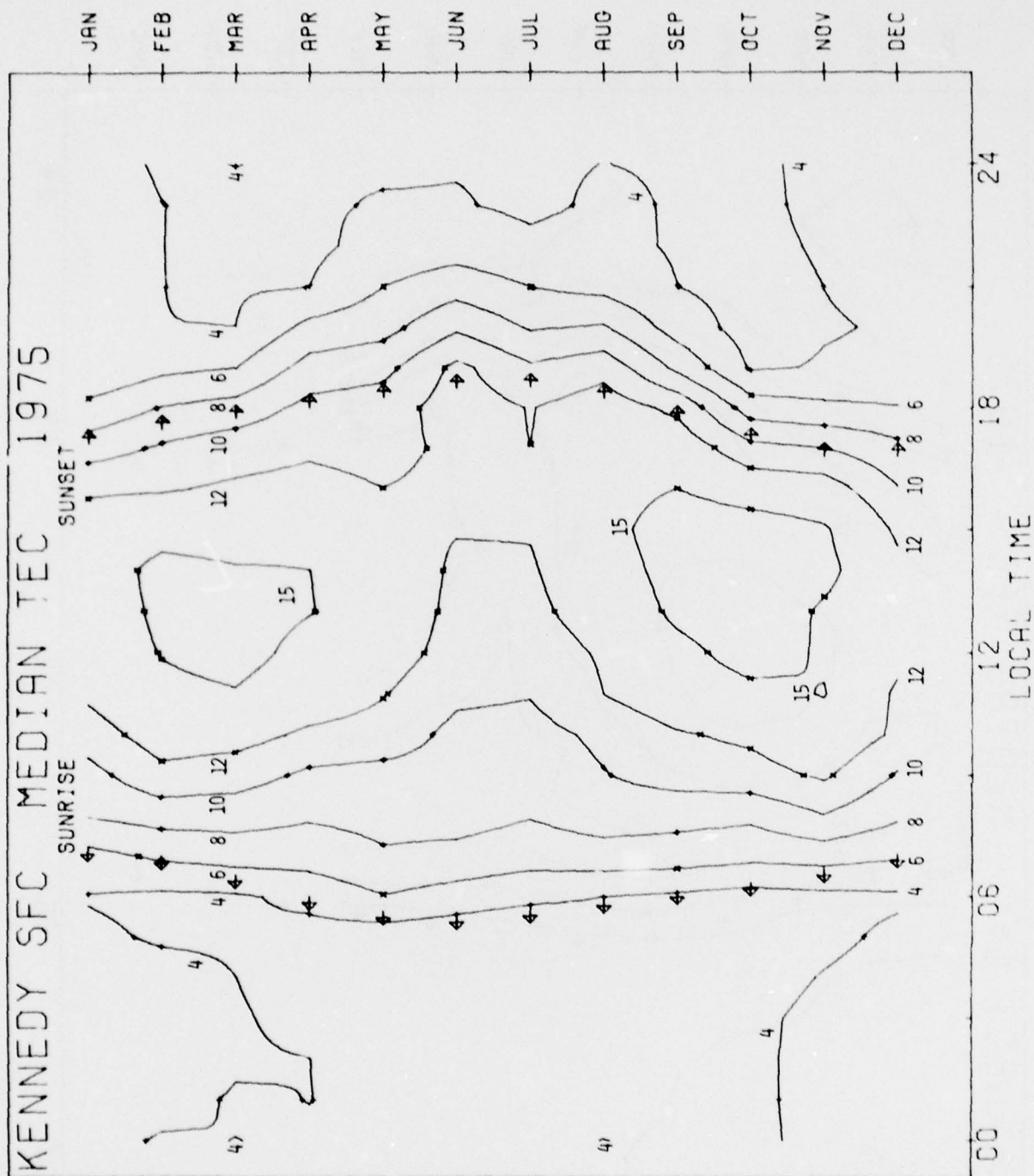


FIGURE 16b.

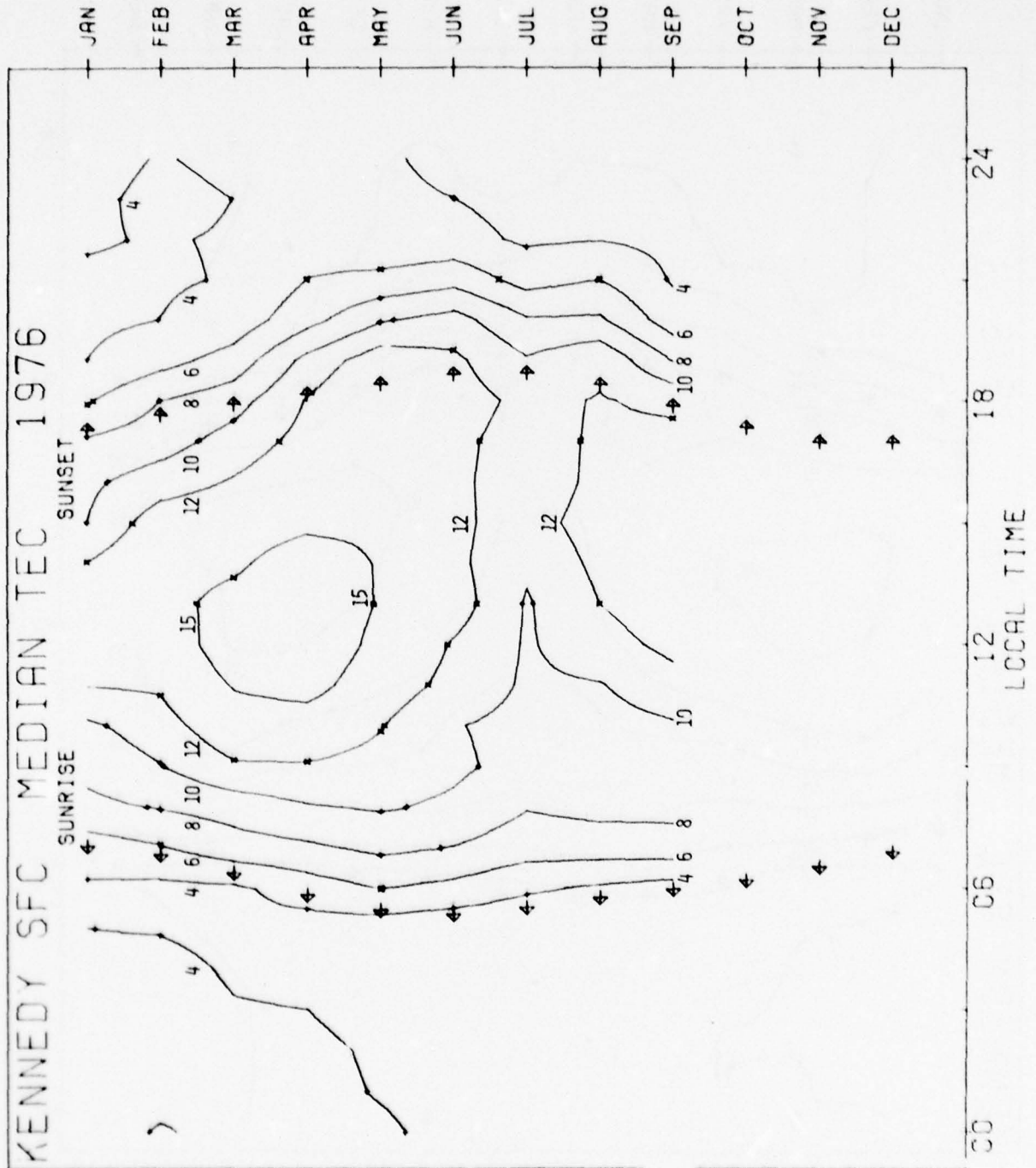
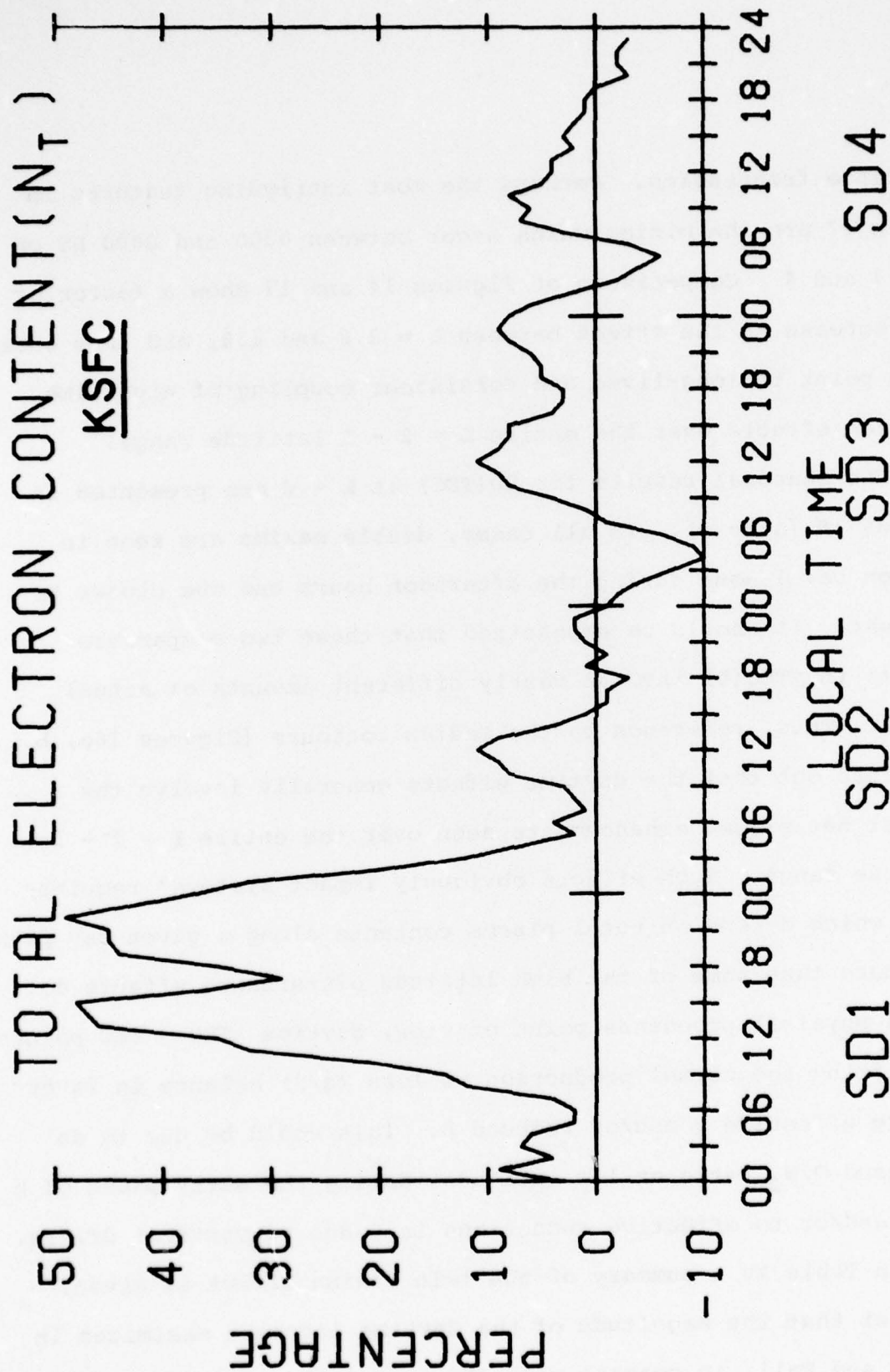


FIGURE 16c.



AVERAGE DISTURBED DAILY VARIATIONS  
SD FOR ALL STORMS

FIGURE 17

occurrence frequencies. Perhaps the most intriguing features in Figure 17 are the minima which occur between 0300 and 0600 LT on Days 3 and 4. Comparisons of Figures 14 and 17 show a factor of two decrease in the effect between  $L = 2.2$  and  $1.8$ , and thus once again point to long-lived and consistent coupling of nighttime F-region effects over the entire  $L \approx 2 - 5$  latitude range.

The seasonal results for  $SD(TEC)$  at  $L \approx 2$  are presented in Figures 18 (a to e). In all cases, double maxima are seen in  $\Delta TEC$  on Day 1--one during the afternoon hours and one closer to midnight. It should be emphasized that these two comparable effects in  $\Delta TEC(\%)$  involve vastly different amounts of actual plasma. Thus, reference to the median contours (Figures 16a, b, c) points out that the daytime effects generally involve the largest net plasma enhancements seen over the entire  $L \approx 2 - 5$  latitude range. Such effects obviously impact systems' requirements which depend on total plasma contents along a given ray path much more than some of the high latitude disturbance effects do. From a physical processes point of view, daytime  $\Delta TEC \propto TEC$  points to shifting the normal production vs loss ( $q/\beta$ ) balance in favor of more effective  $q$  and/or reduced  $\beta$ . This could be due to an increased  $O/N_2$  ratio at low latitudes during the early phase of a storm and/or to effective reductions in  $\beta$  due to vertical drifts.

In Table XV a summary of the twin maxima effect is given. The fact that the magnitude of the daytime increase maximizes in Spring and Fall, in concert with the normal TEC semi-annual variation, further points to the concept that storm effects are simple

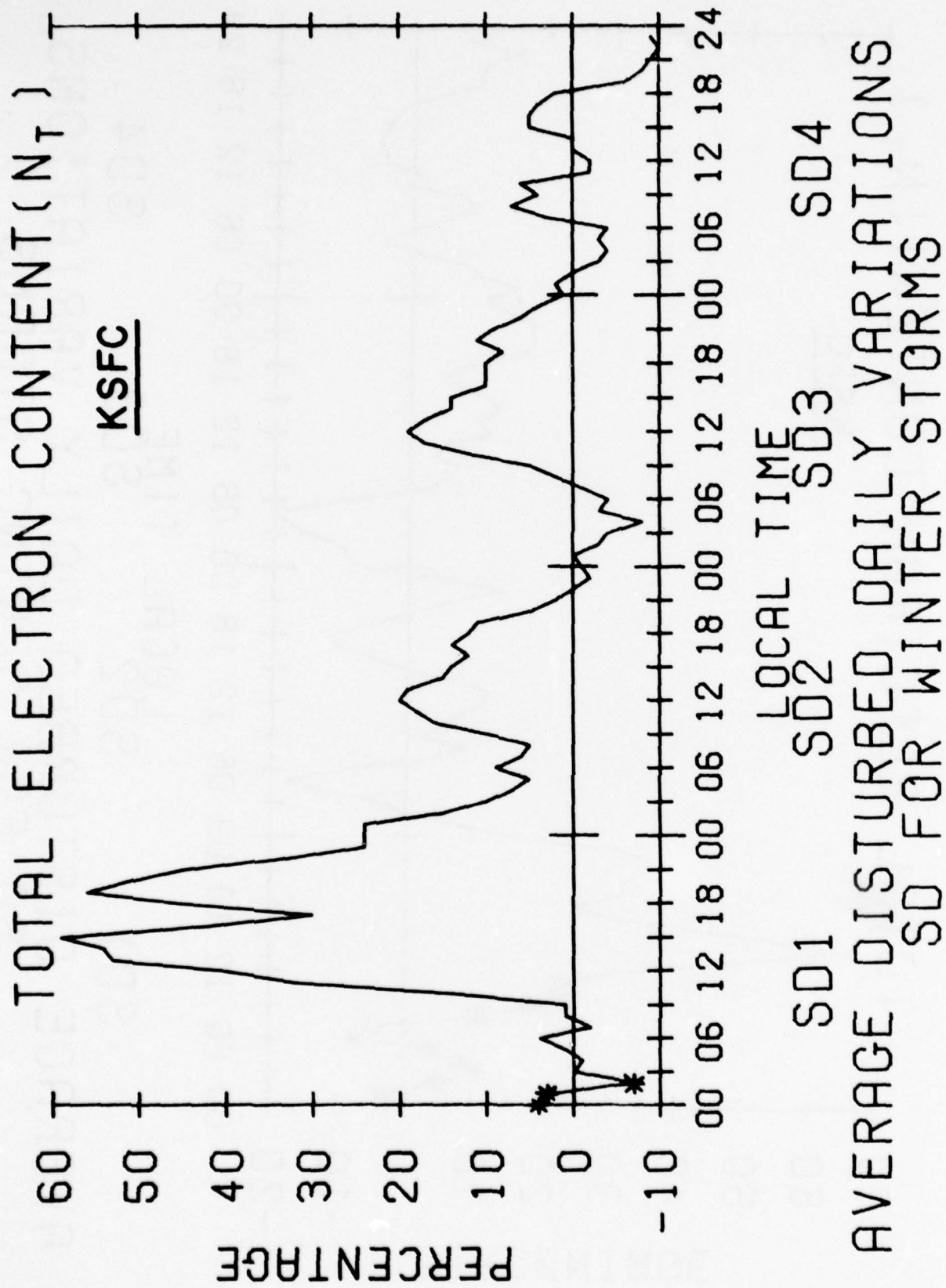
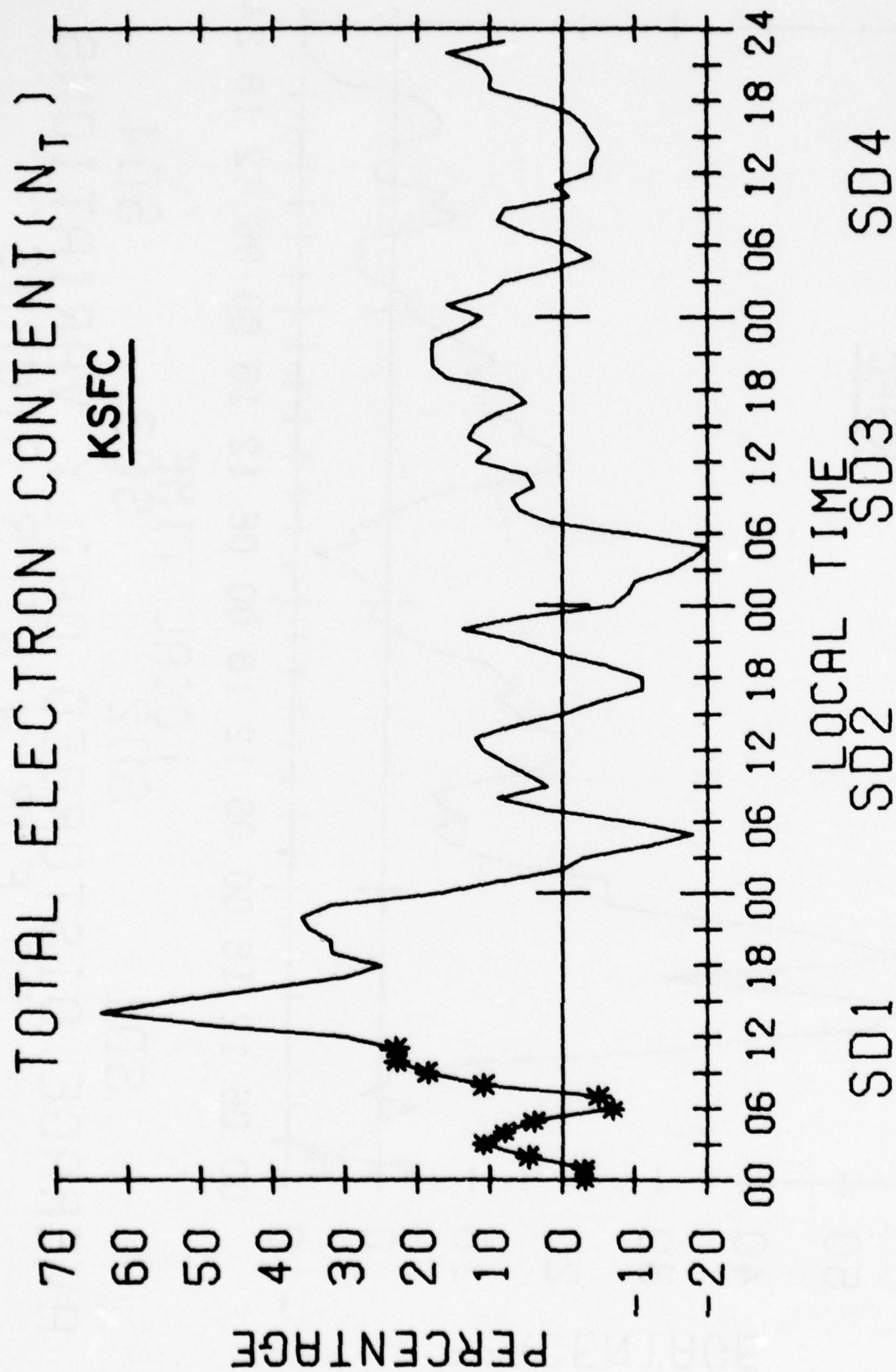
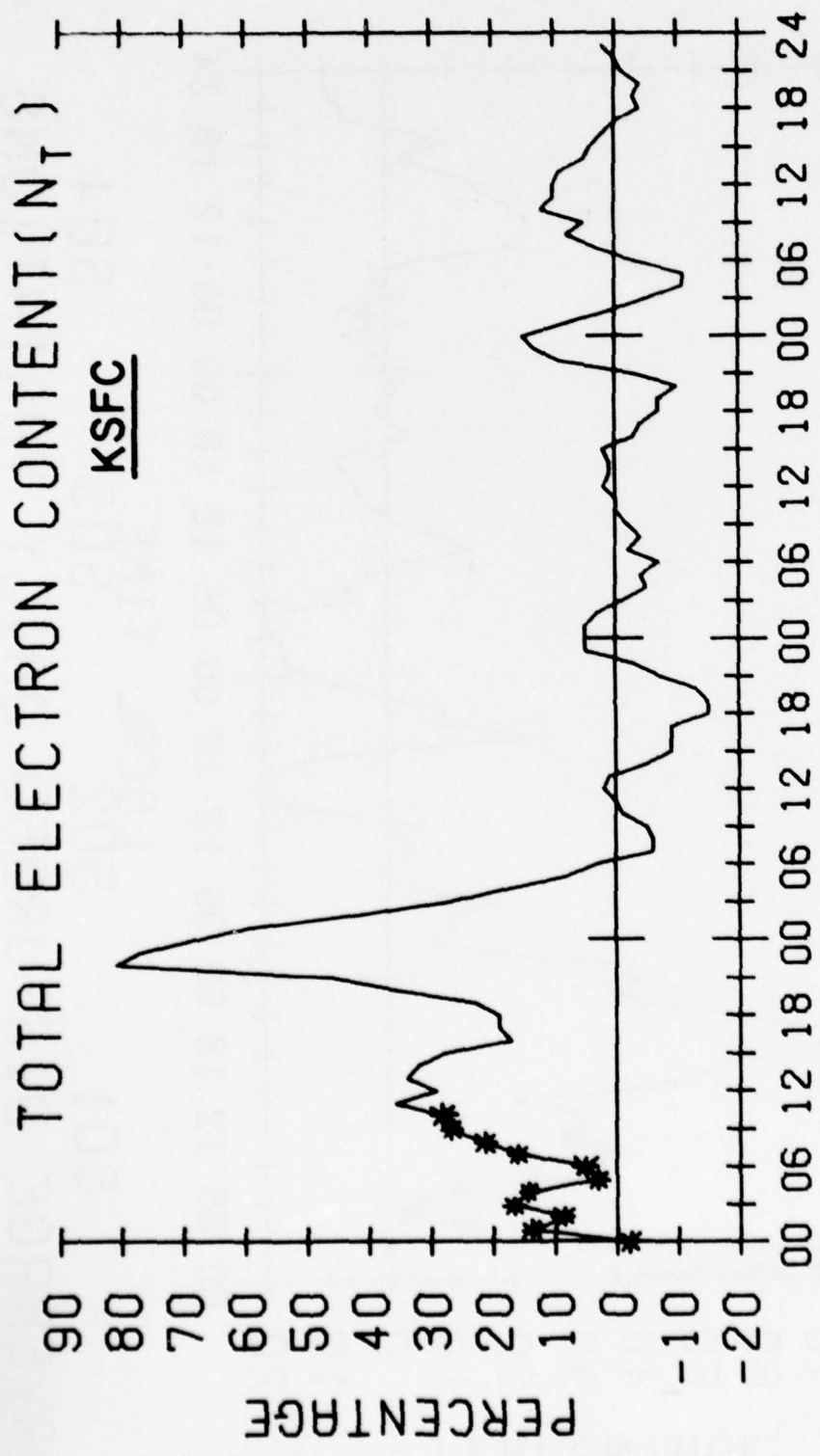


FIGURE 18a.



AVERAGE DISTURBED DAILY VARIATIONS  
SD FOR SPRING STORMS

FIGURE 18b.



SD1      SD2      SD3      SD4

AVERAGE DISTURBED DAILY VARIATIONS  
SD FOR SUMMER STORMS

FIGURE 18c.

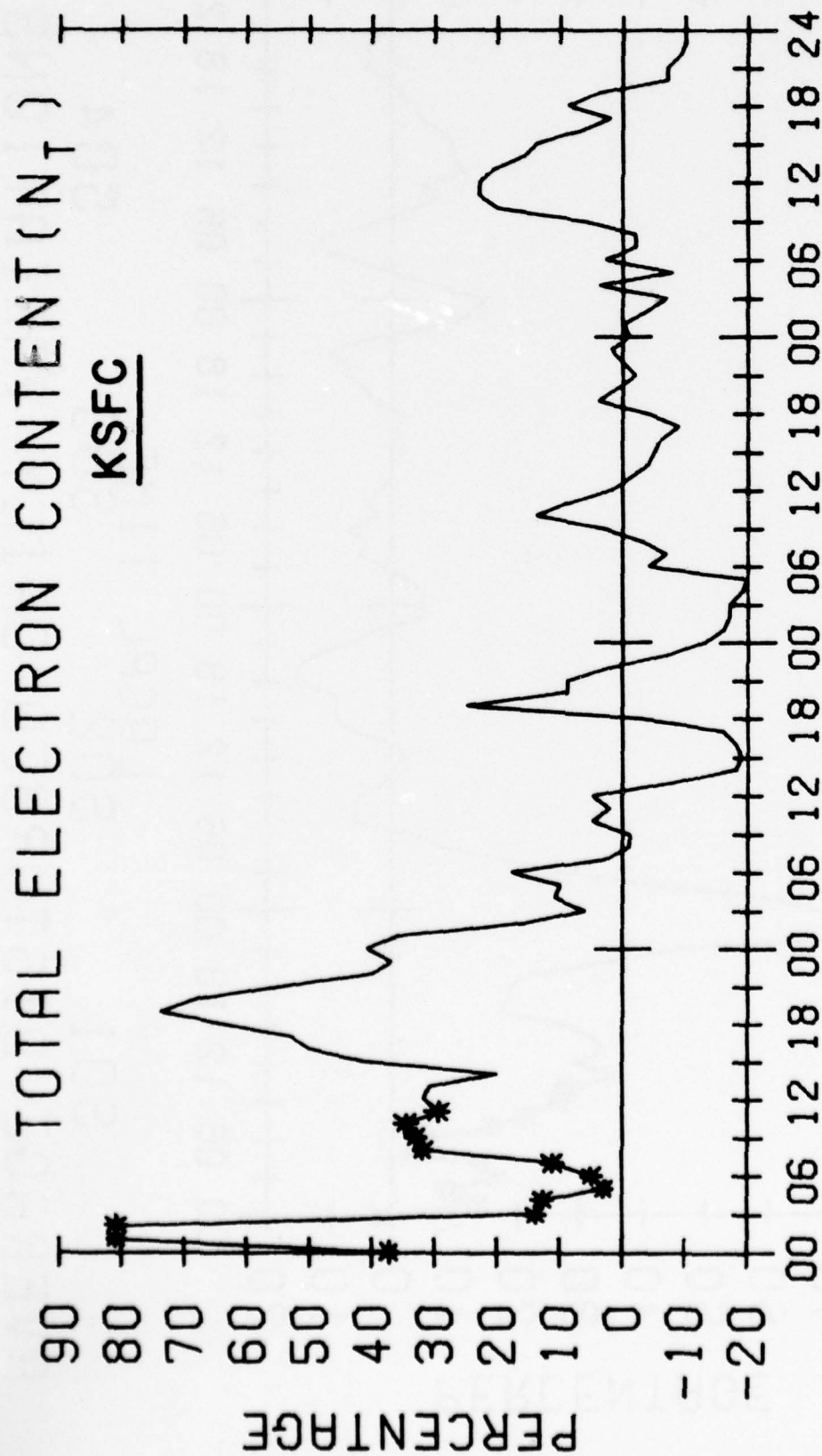
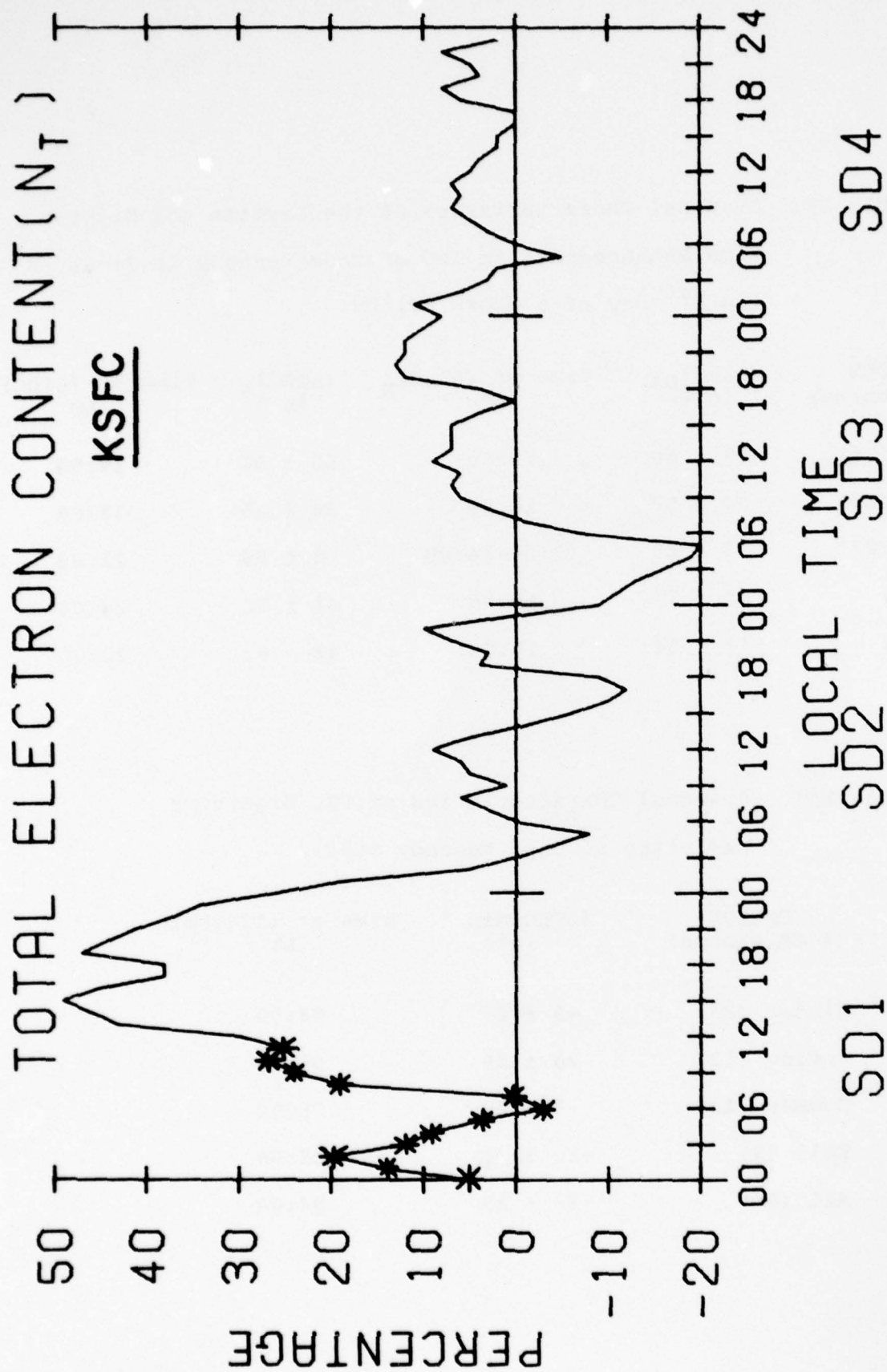


FIGURE 18d.



AVERAGE DISTURBED DAILY VARIATIONS  
SD FOR EQUINOX STORMS

Table XV. Seasonal Characteristics of the Daytime and Night-time Enhancements in TEC at Cape Kennedy ( $L \approx 2$ ) as on the 1<sup>st</sup> Day of a Storm Period.

SEASON (# of storms)	$(\Delta\text{TEC})_{\text{DAY}}$ in %	Time of $(\Delta\text{TEC})_{\text{N}}$ LT	$(\Delta\text{TEC})_{\text{N}}$ in %	Time of $(\Delta\text{TEC})_{\text{N}}$ LT
Winter (26)	$59 \pm 66$	15:00	$56 \pm 56$	19:00
Spring (15)	$64 \pm 52$	14:00	$34 \pm 35$	22:00
Summer (22)	$33 \pm 29$	13:00-14:00	$80 \pm 90$	22:00
Fall (7)	$74 \pm 77$	19:00	$41 \pm 52$	24:00
All (70)	$49 \pm 54$	15:00	$48 \pm 62$	22:00

Table XVI. Seasonal Characteristics of TEC Nighttime Depletion at Cape Kennedy ( $L \approx 2$ ).

SEASON (# of storms)	$(\Delta\text{TEC})_{\text{min}}$ in %	Time of $(\Delta\text{TEC})_{\text{min}}$ LT
Winter (26)	$-8 \pm 27$	04:00
Spring (15)	$-20 \pm 26$	05:00
Summer (22)	$-7 \pm 20$	06:00
Fall (7)	$-20 \pm 31$	05:00
All (70)	$-10 \pm 25$	04:00

intensifications of ambient processes. The dominance of  $\Delta\text{TEC}$  in Winter over  $\Delta\text{TEC}$  in Summer, with an earlier occurrence time in Winter, again indicates that day-length and therefore solar production efficiency is an important aspect of the storm picture.

Finally, in Table XVI we summarize the major negative phase depletion seen at  $L \approx 2$ , that is, the TEC minima from 04 - 06:00 LT on Day 3. Comparisons with Figure 13b and d (or Table XIV) show that the depletions are systematically related to those seen at  $L \approx 3$ , that is, greater depletions during Spring and Fall events, comparable depletions during Summer and Winter events, with the magnitudes of the decreases factors of 2 to 3 weaker at  $L \approx 2$ .

#### 4. F-REGION STORM PATTERNS -- THE LONGITUDINAL NETWORK AT MID-LATITUDES ( $L \approx 2$ ).

As discussed in the INTRODUCTION and in the previous Chapter, ample reasons exist for the search of longitude effects in the average storm patterns obtained at lower mid-latitude sites. The construction of a substantial TEC data base for storm analyses at  $L \approx 2$  was one of the more major aspects of our investigations during the final year of this 3-year study. As summarized in Tables I and VIII, the limited amount of TEC data available from Rosman (13 storms in 1972) has been augmented by the AFGL station set up at the Kennedy Space Flight Center (KSFC) in late 1973. The TEC data from Cape Kennedy contained a total of 70 storm events spanning the years 1973-1976. These results were treated in the previous Chapter within the context of latitudinal morphologies near  $70^{\circ}\text{W}$ . In this Chapter, we perform a similar analysis on TEC data bases from  $L \approx 2$  sites at other longitudes. Specifically, we examine 63 storm periods from data obtained in Athens, Greece, from October 1972 to December 1976 (pertinent to  $L \approx 1.4$  near  $28^{\circ}\text{E}$ ) and 31 storm periods from observations made in Osan, Korea, from January 1974 to June 1976 (pertinent to  $L \approx 1.3$  near  $137^{\circ}\text{E}$ ). It is important to notice from Table 1 that the geographic latitudes of the sub-ionospheric points for Rosman, Athens and Osan are all approximately equal at  $\approx 33^{\circ}\text{N}$ . The geomagnetic (invariant) latitudes, however, exhibit quite a spread as a function of longitude:  $\Lambda \approx 47^{\circ}$  at Rosman,  $\Lambda = 31^{\circ}$  at Athens and  $\Lambda = 27^{\circ}$  at Osan. At Cape

Kennedy, on the other hand, the  $L \approx 1.8$  sub-ionospheric point has  $\Lambda \approx 41^\circ$ , with a low geographic latitude of  $\approx 26^\circ\text{N}$ . Thus, at these four comparable, lower mid-latitude sites (Rosman, KSFC, Athens and Osan) one could make the following a priori estimates of the anticipated importance of various physical processes:

- (1) KSFC is clearly at the lowest geographic latitude and thus solar production and neutral atmosphere dominated effects should be larger there in comparison to the other three sites.
- (2) Processes of magnetospheric origin, and therefore ones presumably dependent upon  $L$  or  $\Lambda$  values, should have their greatest influence at Rosman and KSFC ( $\Lambda \approx 47^\circ$  and  $41^\circ$ ) and minimum influence at Osan ( $\Lambda \approx 27^\circ$ ).
- (3) Seasonal effects might be greatest at Athens where geographic and geomagnetic coordinates are comparable at the relative high values of  $\approx 31^\circ$ - $34^\circ$ .

In the following sections we describe the average storm patterns from Osan and Athens and compare the results with those previously documented at Cape Kennedy (Figures 17 and 18a,e and Tables XV and XVI). A further comparison with a small amount of data from Salisbury, Rhodesia, the geomagnetic conjugate point for Athens, will provide a few comments on inter-hemispheric consistencies. Finally, reference will be made to previously published TEC storm studies using measurements from Arecibo and Stanford in order to comment on  $L = 1\frac{1}{2}$ -2 morphologies obtained under solar maximum conditions.

#### 4.1. Average Storm Patterns -- Osan ( $L \approx 1.3$ ).

The TEC data base available from Osan, Korea, is summarized via contours of monthly median vs. local time TEC behavior in Figures 19a,b,c. The period covered (1974-76) falls wholly within the solar minimum epoch and, quite unfortunately, missing data during the Fall and Winter seasons of each year result in a lack of information about annual and semi-annual median patterns. Nevertheless, the 20 months of available observations show clear evidence for a semi-annual component in daytime TEC -- with a Spring maximum and absolute TEC values about 5 units higher than those seen at Cape Kennedy; at nighttime both sites are comparable with TEC in the 4-6 units range (see Figures 16a,b,c). The higher daytime values at Osan seem contrary to what would be expected from geographic coordinates ( $33^{\circ}\text{N}$  at Osan vs.  $26^{\circ}\text{N}$  for KSFC), though the geomagnetic coordinate gradient definitely favors Osan (i.e.,  $27^{\circ}$  vs.  $47^{\circ}$  for KSFC). This is a clear example of what is meant by longitude effects in the background ionosphere.

Given the 20-month Osan data base (with its limitations with respect to seasonal coverage), we were able to identify only 31 storm periods for analysis, and thus we present the average local time patterns,  $SD(\%)$ , for ALL storms in Figure 20, with no subsequent seasonal break-down. The Osan storm pattern in Figure 20 and the KSFC pattern for ALL storms in Figure 17 are remarkably similar in several respects:

- (1) On Day 1, both stations show a double-peaked  $SD(\%)$  pattern of afternoon and pre-midnight enhancements. Table XV showed that the daytime peak at KSFC was  $\approx 48\%$  at 15:00 LT and the nighttime peak to be  $\approx 48\%$  at 22:00 LT. At

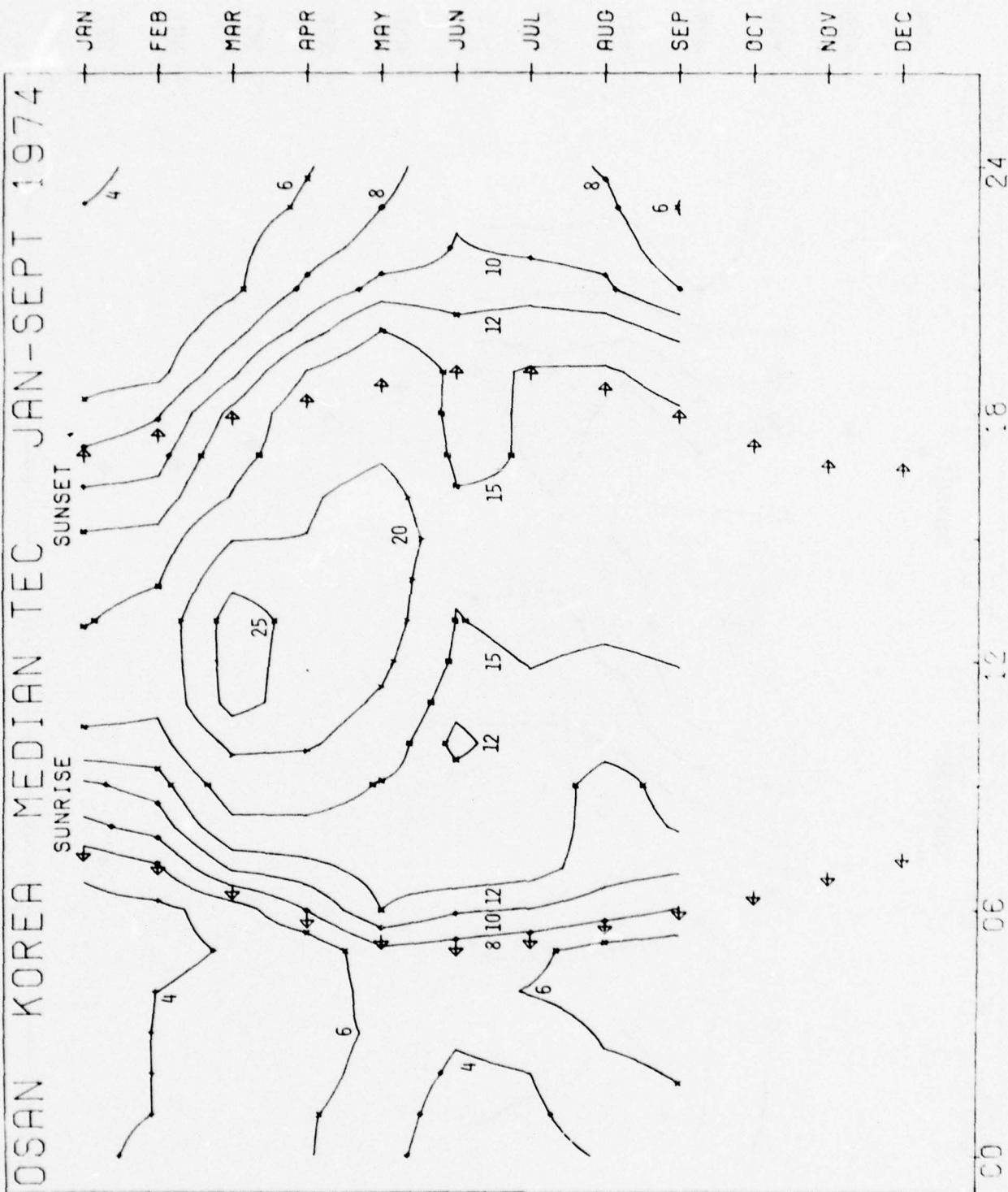


FIGURE 19a.

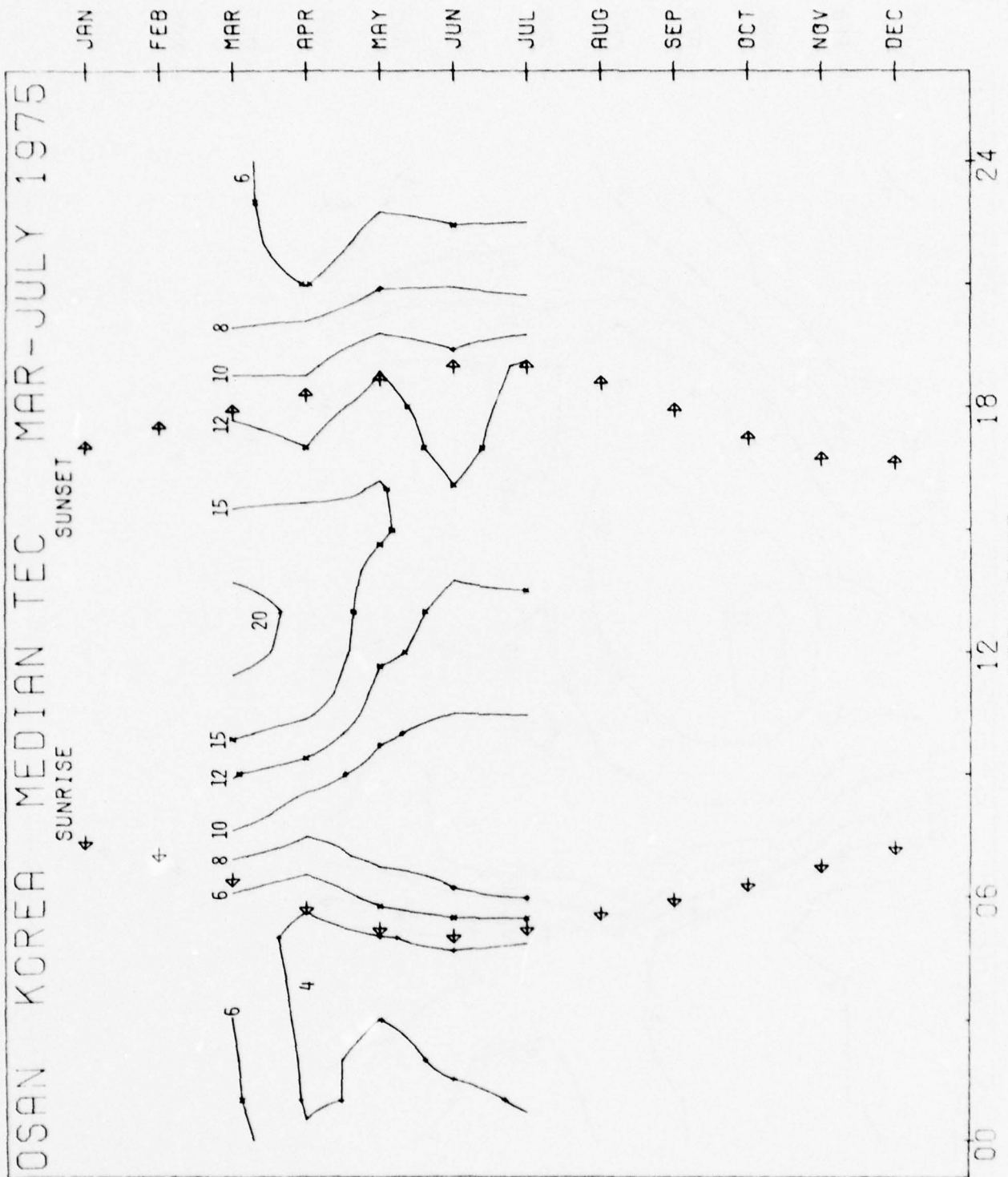


FIGURE 19b.

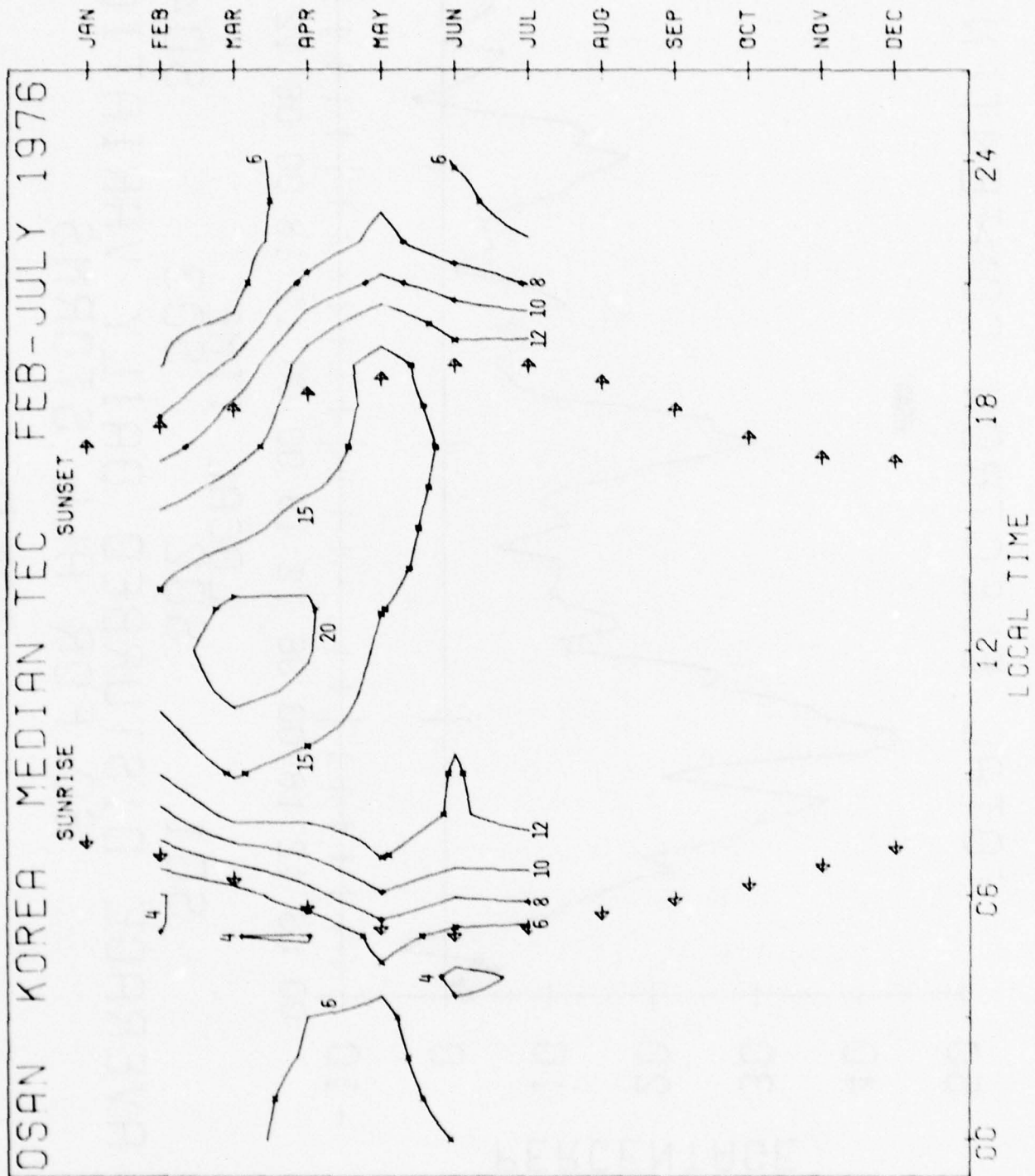


FIGURE 19c.

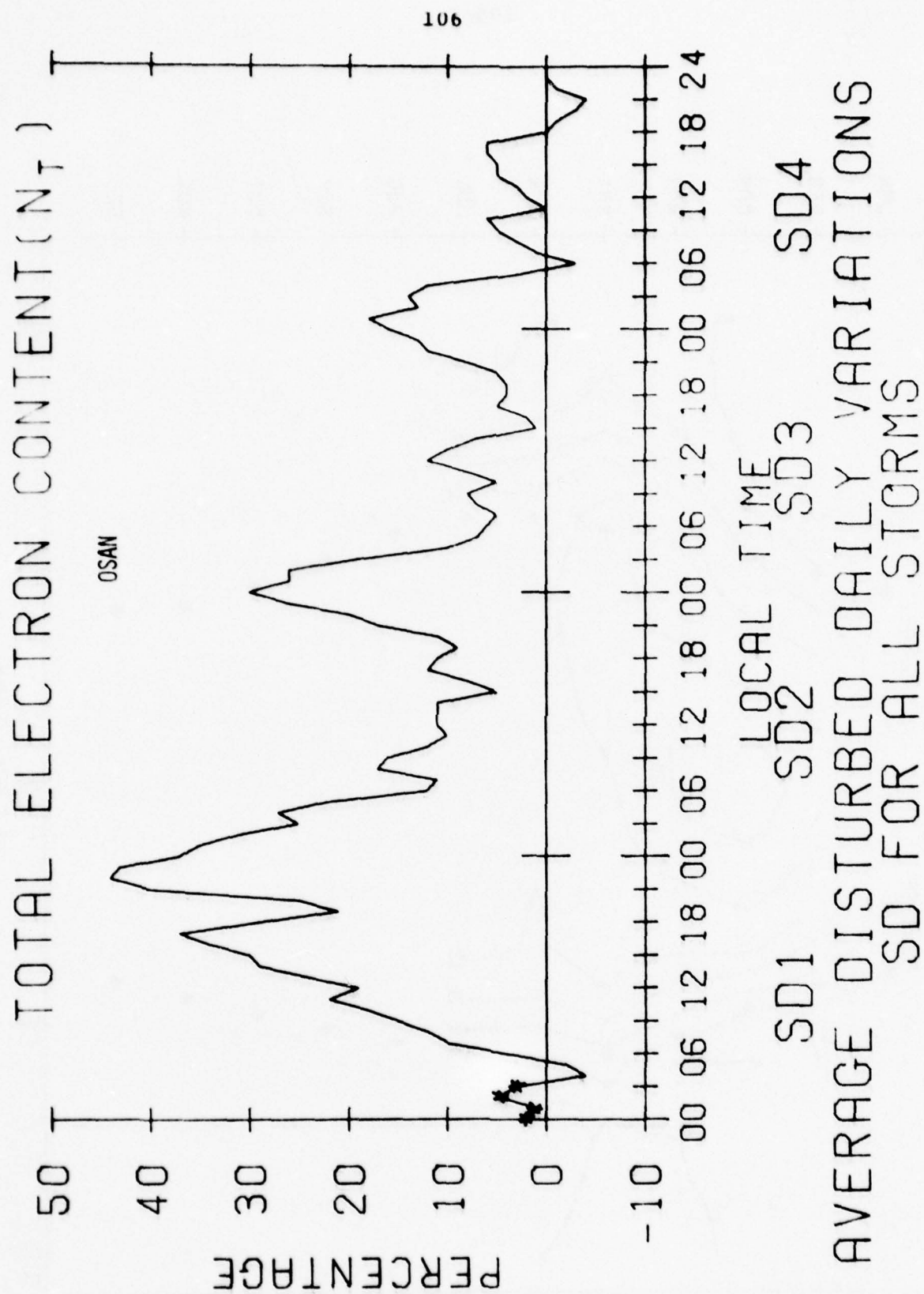


FIGURE 20.

Osan, the daytime peak is  $\approx 37\%$  at 17:00 LT while the nighttime effect of  $\approx 44\%$  at 22:00 LT is nearly identical to the KSFC values.

- (2) On Day 2, no evidence for a daytime negative phase exists -- though the Osan pattern is more consistently positive than the KSFC results.
- (3) The nighttime period between Days 2 and 3 shows the only clear difference between the two sites, with Osan exhibiting large nighttime enhancements while KSFC shows a TEC minimum. The higher L-value at KSFC apparently results in a linkage to upper mid-latitude effects (as discussed in the previous Chapter) not seen at Osan.
- (4) In summary, an overall pattern of semi-diurnal enhancements (with early afternoon and late evening maxima) may be seen to dominate the entire storm period at both sites.

#### 4.2. Average Storm Patterns -- Athens ( $L \approx 1.4$ ).

The TEC data base established for Athens spanned the period June 1972 through December 1976. The monthly median behavior given in Figures 21 (a through e) reveal several extended periods of data outages; the Fall and early Winter months have the most extensive coverage and thus the seasonal analysis might be influenced by such an uneven distribution. The median patterns for 1972 (i.e., the year closest to solar maximum, Figure 21a) show a behavior during Fall and early Winter quite similar to that seen

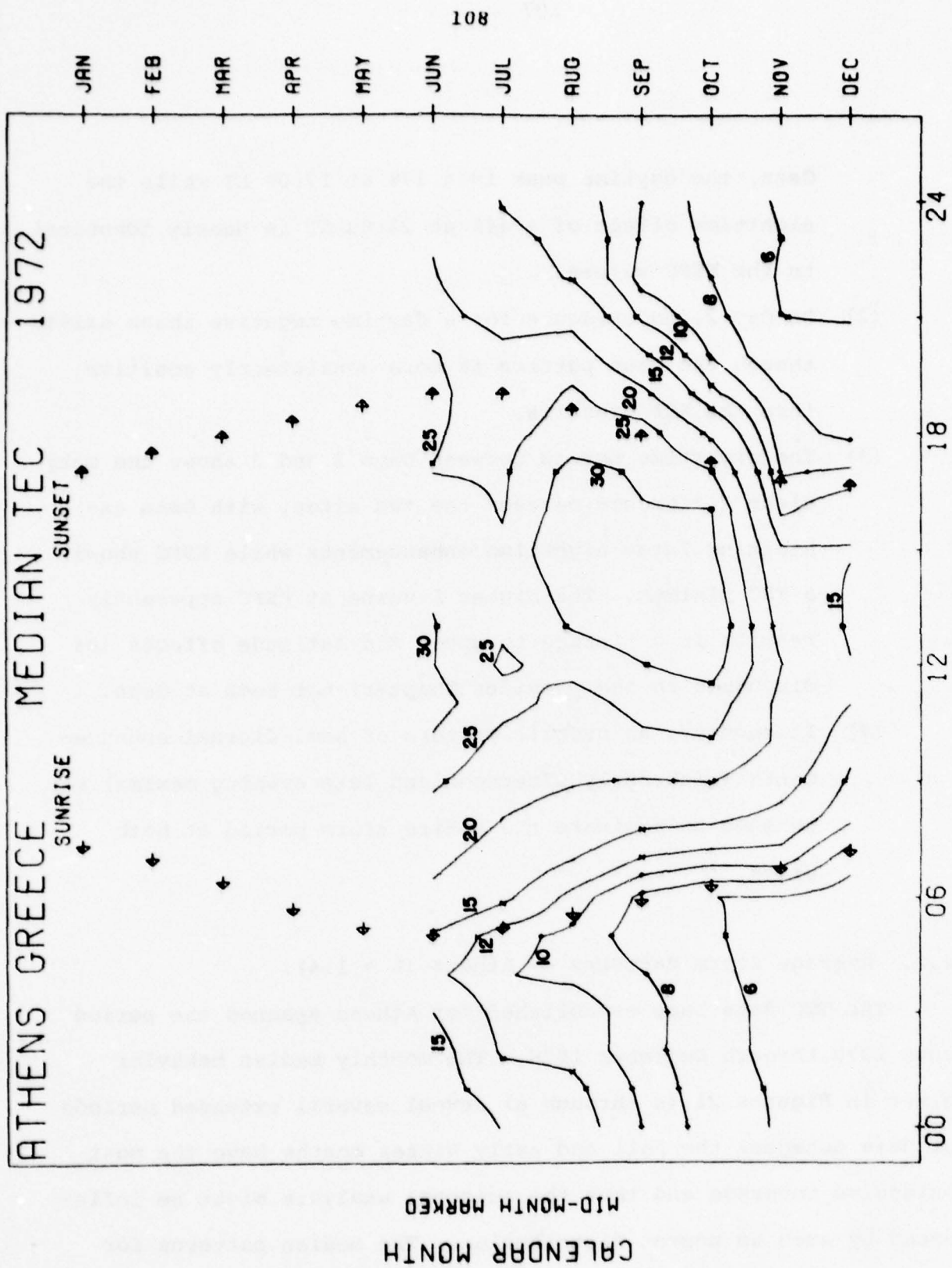


FIGURE 21a.

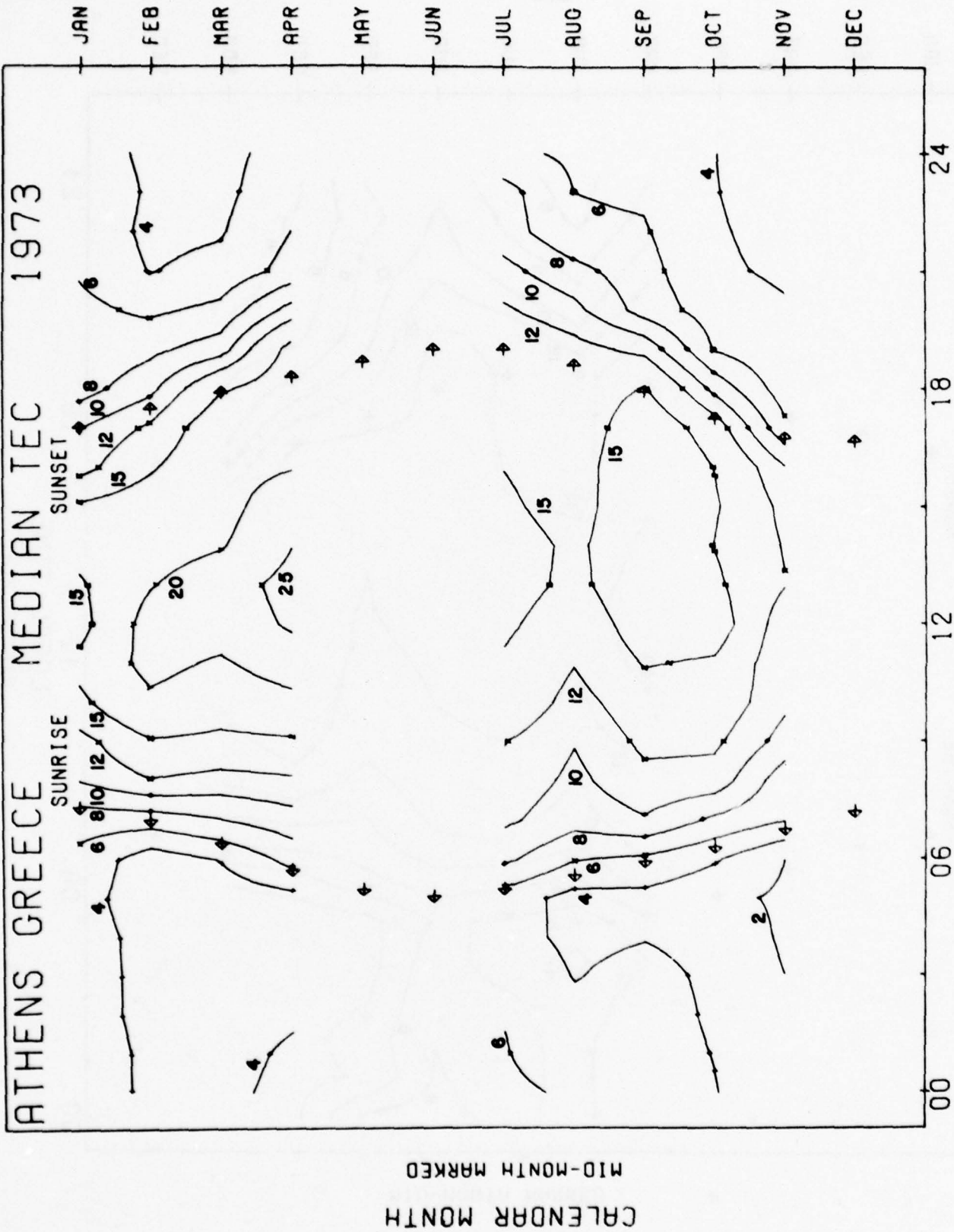


FIGURE 21b.

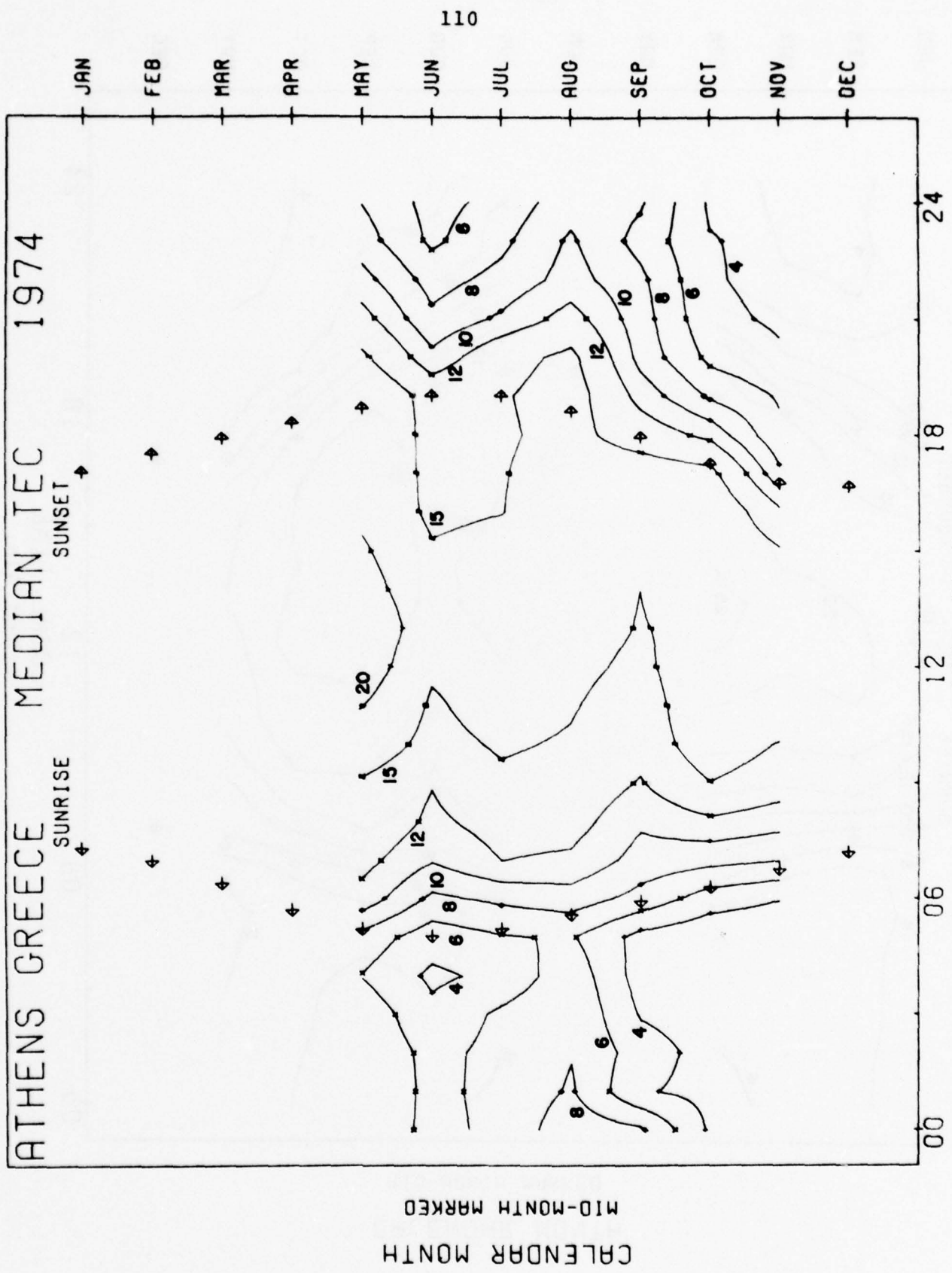


FIGURE 21c.

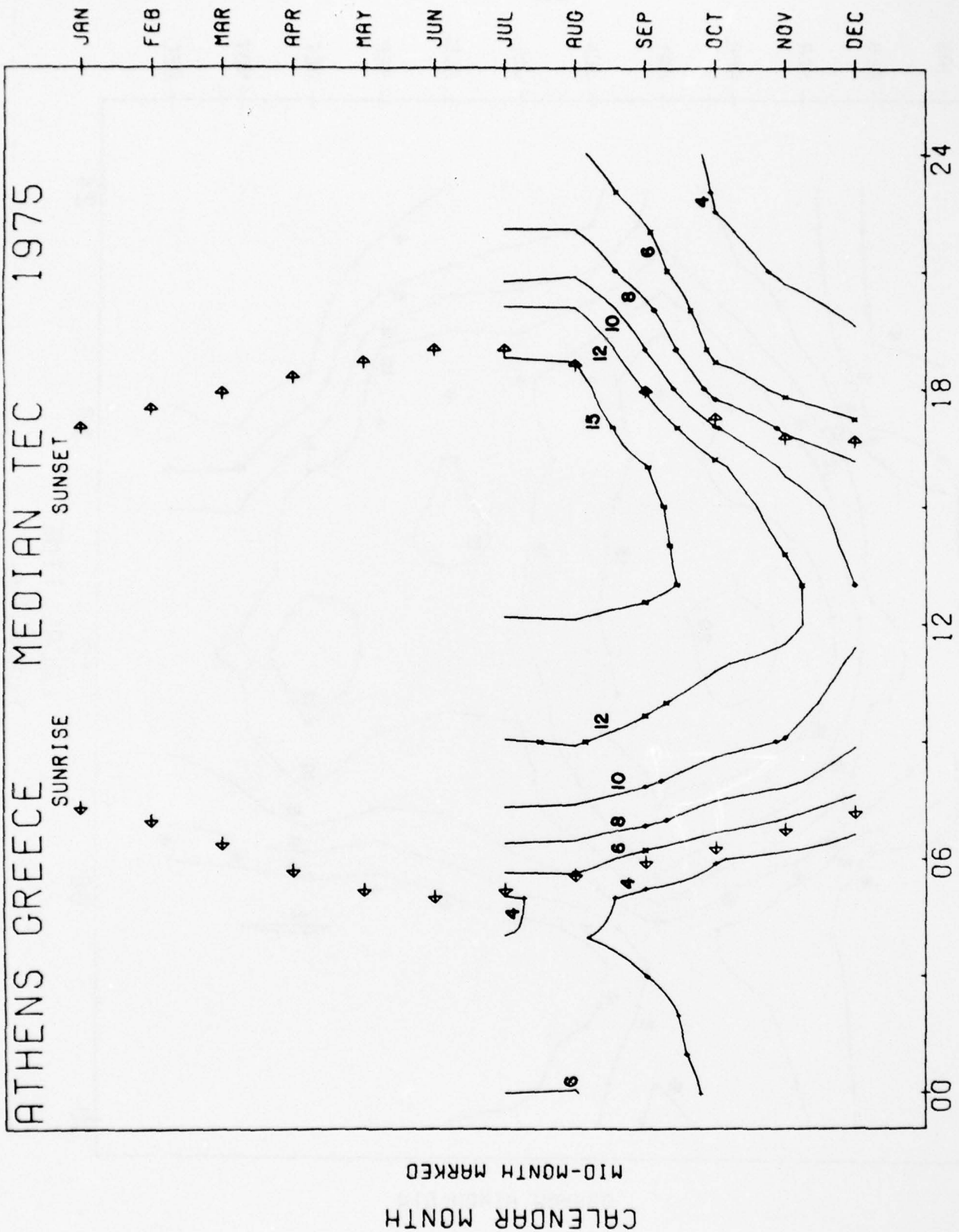


FIGURE 21d.

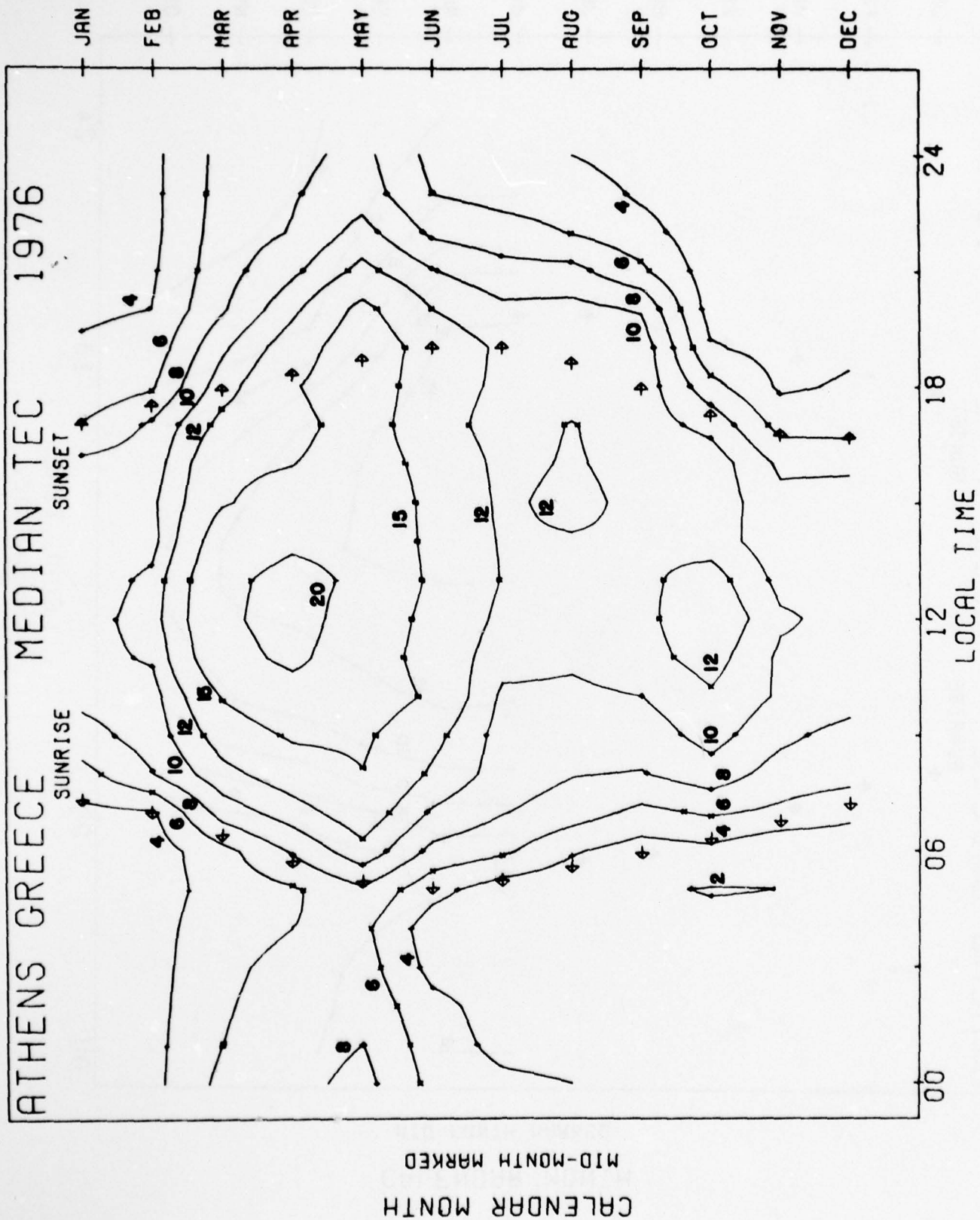


FIGURE 21e.

at Rosman during the same period (see Figure 14). The TEC levels are somewhat higher at Athens, and though only 6 months of data exists, the Fall maximum suggests a semi-annual variation consistent with the other sites. During the summer months, the diurnal variation in Figure 21a points to a very small day/night difference in comparison to the Rosman data. It would appear that the nighttime values at Athens are "anomalously high" and thus we decided to omit the period June - September from our storm analysis (see Table VIII).

The Athens median patterns for 1974-75-76 (Figures 21c,d,e) give little evidence for a pronounced semi-annual variation. The solar minimum year 1976 reveals a Spring maximum with a much weaker Fall secondary. The Osan data for 1976 (Figure 19c) is remarkably similar in documenting this Spring peak, while the KSFC data (Figure 16c) are somewhat lower in absolute values; the secondary maxima during Fall at KSFC are evident in all three years.

The average disturbance pattern for the Athens TEC is given in Figure 22, where all 63 available storm periods were used to construct the SD(%) curve. On Day 1 large positive phase excursions in  $\Delta$ TEC are seen to dominate the pattern from 09:00 LT on. The "twin peak" characteristic for Day 1 found at Cape Kennedy and Osan (Figures 17 and 20) is not so well pronounced here. In examining the storms on a seasonal basis, however, we find that the feature does occur at Athens (see Figures 23a,e). The daytime and nighttime  $\Delta$ TEC values and their local times of occurrence are summarized in Table XVII. One can see that the daytime peak

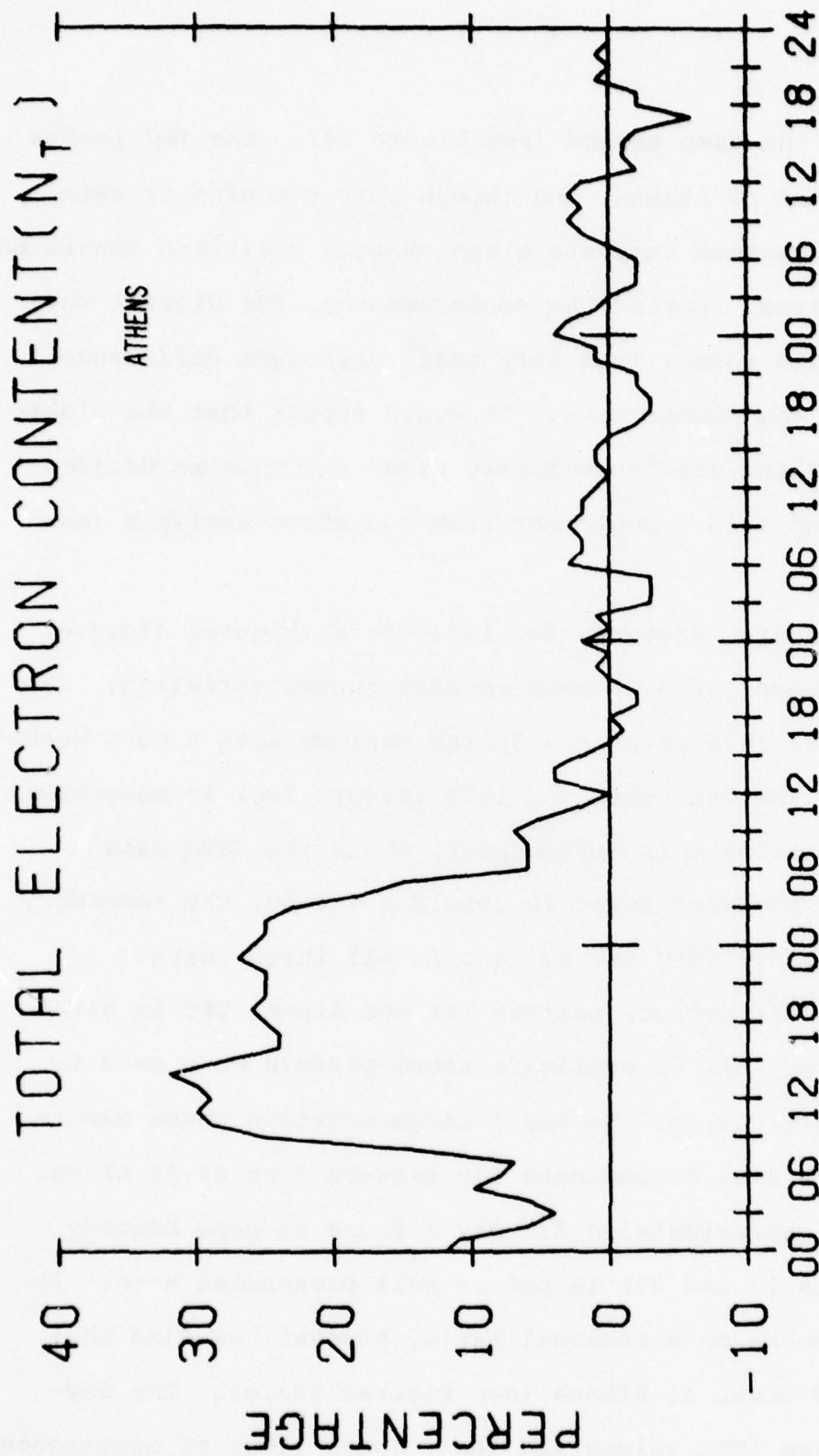
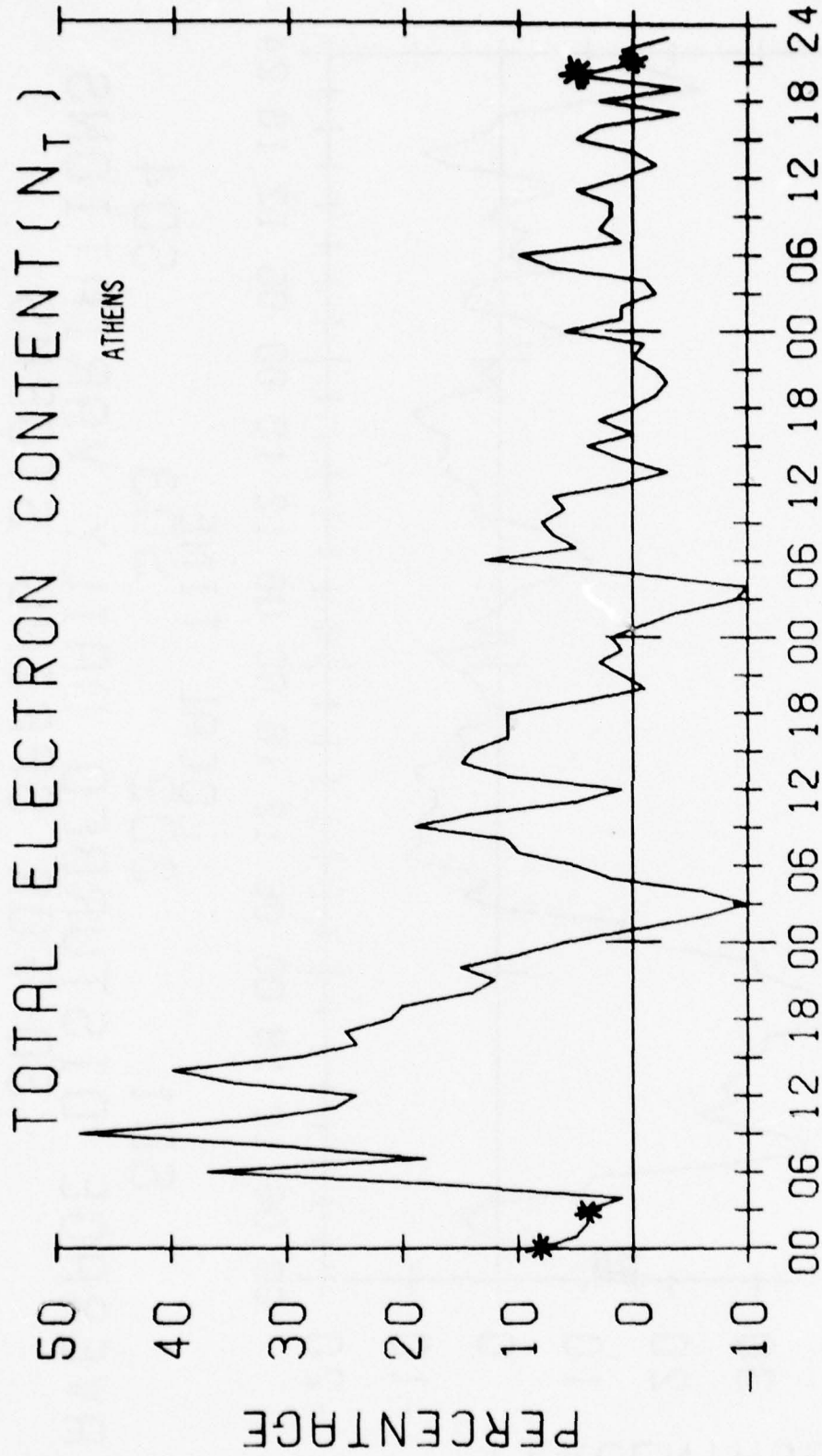
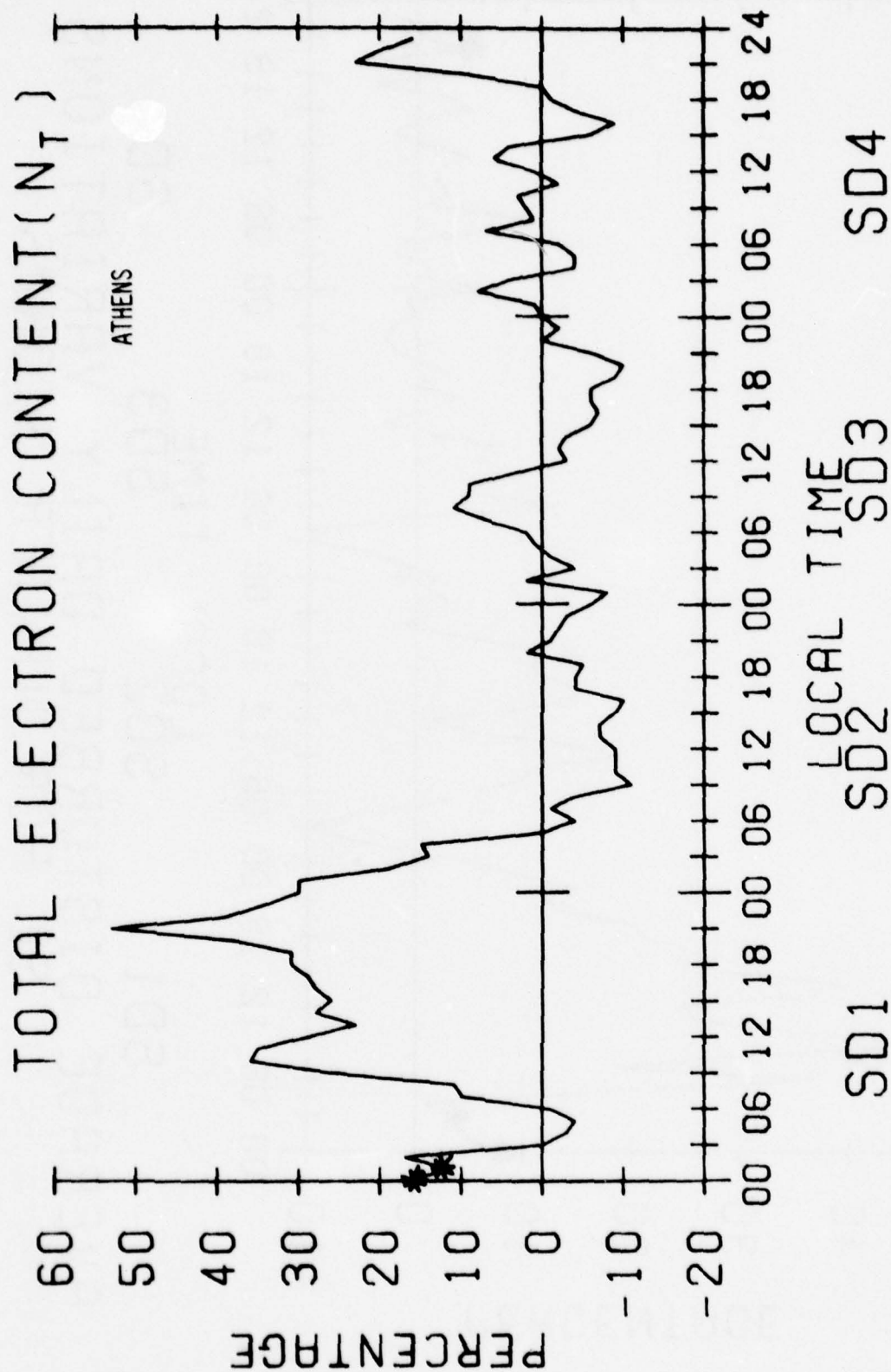


FIGURE 22.



AVERAGE DISTURBED DAILY VARIATIONS  
SD FOR WINTER STORMS

FIGURE 23a.



AVERAGE DISTURBED DAILY VARIATIONS  
SD FOR SPRING STORMS

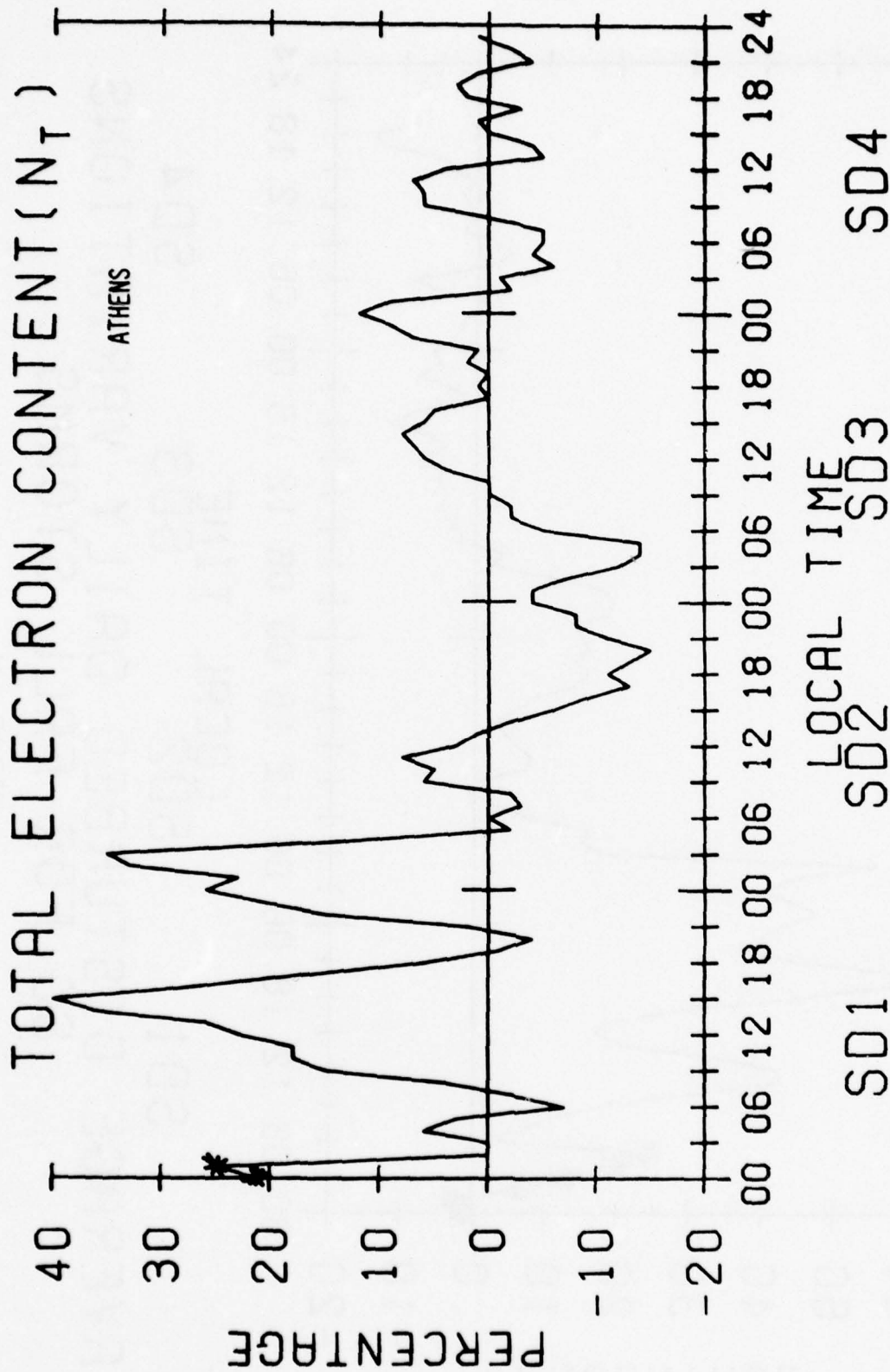


FIGURE 23c.

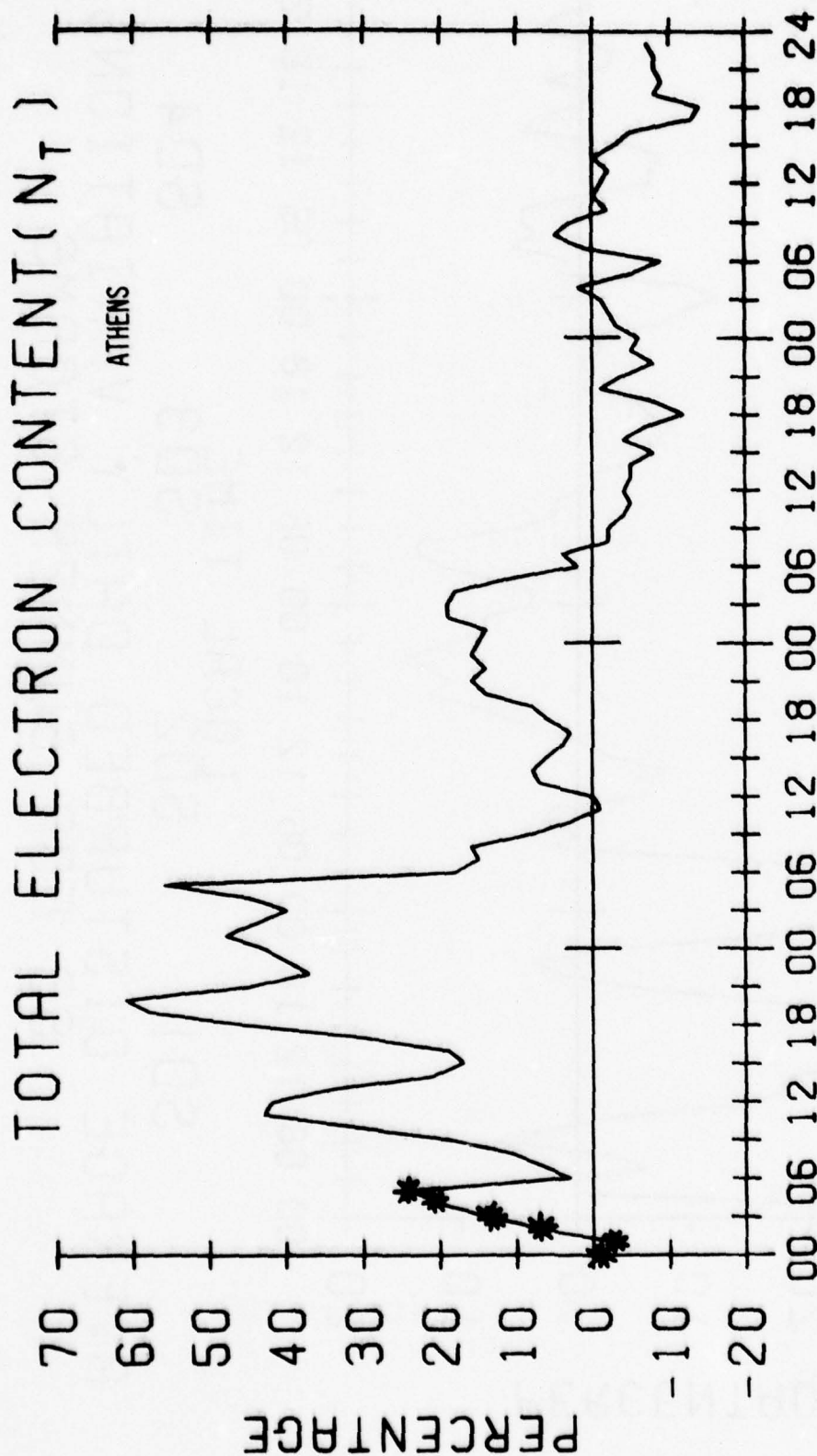
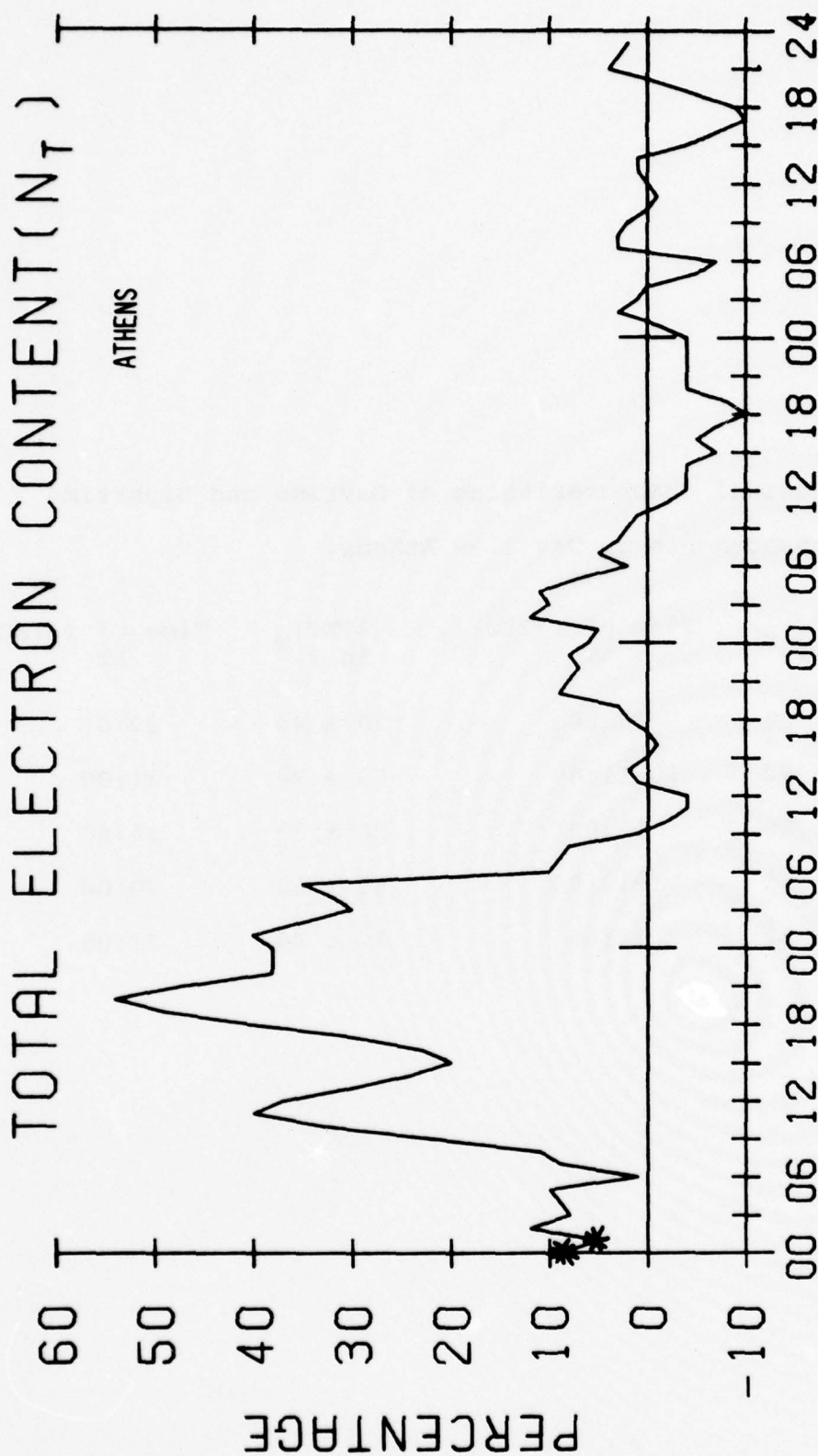


FIGURE 23d.



AVERAGE DISTURBED DAILY VARIATIONS  
SD FOR EQUINOX STORMS

FIGURE 23e.

Table XVII. Seasonal Characteristics of Daytime and Nighttime Enhancements on Day 1 -- Athens.

Season (# of storms)	$(\Delta\text{TEC})_{\text{D}}$ in %	Time of $(\Delta\text{TEC})_{\text{D}}$ LT	$(\Delta\text{TEC})_{\text{N}}$ in %	Time of $(\Delta\text{TEC})_{\text{N}}$ LT
Winter (16)	48 $\pm$ 84	17:00	20 $\pm$ 44	22:00
Spring (10)	36 $\pm$ 42	10-11:00	53 $\pm$ 74	21:00
Summer (20)	40 $\pm$ 26	15:00	26 $\pm$ 33	24:00
Fall (17)	42 $\pm$ 55	11-12:00	61 $\pm$ 69	20:00
All (63)	32 $\pm$ 52	14:00	27 $\pm$ 44	23:00

is relatively constant near  $\approx 40\%$ , but the  $\Delta LT$  range for its occurrence spans the 10-17:00 LT range; consequently, the feature is described in the overall average by  $\approx 32\%$  at 14:00 LT. the nighttime peak is confined to the 20-24:00 LT range, with much larger and earlier peaks during Spring and Fall, resulting in the All-storm average being  $\approx 27\%$  at 23:00 LT.

On days 2, 3 and 4 of the storm period, the All-storm average shows a semi-diurnal pattern of dawn/dusk minima and day/night enhancements. A consistent negative phase on Day 2 is seen only during the Spring season (Fig 22b). While only 10 storm periods are available to define this Spring pattern, the "strange" or "inconsistent" patterns for Spring storms found at virtually every site examined must, at some point, be taken seriously. The fact that all of the data bases presented in this report show the semi-annual variation in median TEC to peak in Spring (and thus become the overall yearly peak) surely points to the possibility of a unique coupling between the neutral and ionized atmospheres being further stressed during storm periods. The semi-diurnal perturbation in TEC seen in the  $L \approx 2$  studies might also point to a neutral atmosphere effect, perhaps of tidal origin, that emerges in a more prominent way during storms.

#### 4.3. Average Storm Patterns Near $L \approx 2$ During Solar Maximum Years.

In this and the previous Chapter we have discussed ionospheric storm effects at lower mid-latitudes ( $L \approx 2$ ) using TEC data obtained from four sites (Rosman, Cape Kennedy, Osan and Athens) during

medium to low solar flux years (1972-1976). In this section we wish to compare results for our average storm patterns (Figures 15, 17, 20 and 22) with those obtained at similar locations during more active solar flux years. Data sets from two stations are available for this purpose:

- (1) A 28-storm period from 1967-1969 from Stanford, California, chosen to match the period of Sagamore Hill (Hamilton) C-data, as described in Figure 12b. An analysis of these data pertinent to a  $L \approx 1.7$  site was carried out earlier (Mendillo, 1976a) and the results are reproduced in Figure 24a.
- (2) A smaller data base for storm analysis was described by Lanzerotti et al. (1975) for TEC measurements made from Arecibo, Puerto Rico ( $L \approx 1.4$ ). A total of 12 storm periods from 1968-1970 were used to form average storm patterns, and the results compared with a simultaneous data set from Sagamore Hill ( $L \approx 2.8$ ). These patterns are reproduced in Figure 24b.

The SD(%) patterns for Sagamore Hill (Hamilton) depicted in Figure 24 are, as expected, characteristic of all Sagamore Hill analyses. Thus, we expect the SD patterns for Stanford and Arecibo to be equally representative of effects at  $L \approx 1.7$  and 1.4, respectively, even though the number of storms is relatively low and multi-year based (28 and 12 events, respectively). The Stanford results for  $L \approx 1.7$  should be compared with the KSFC results ( $L \approx 1.8$ ) in Figure 17. Evidence for a "twin peak" enhancement

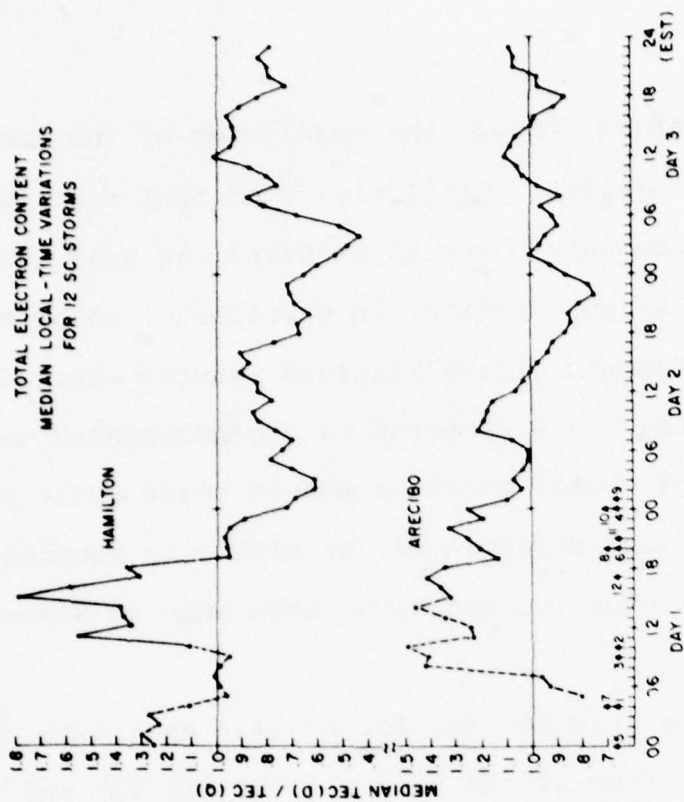


FIGURE 24b.

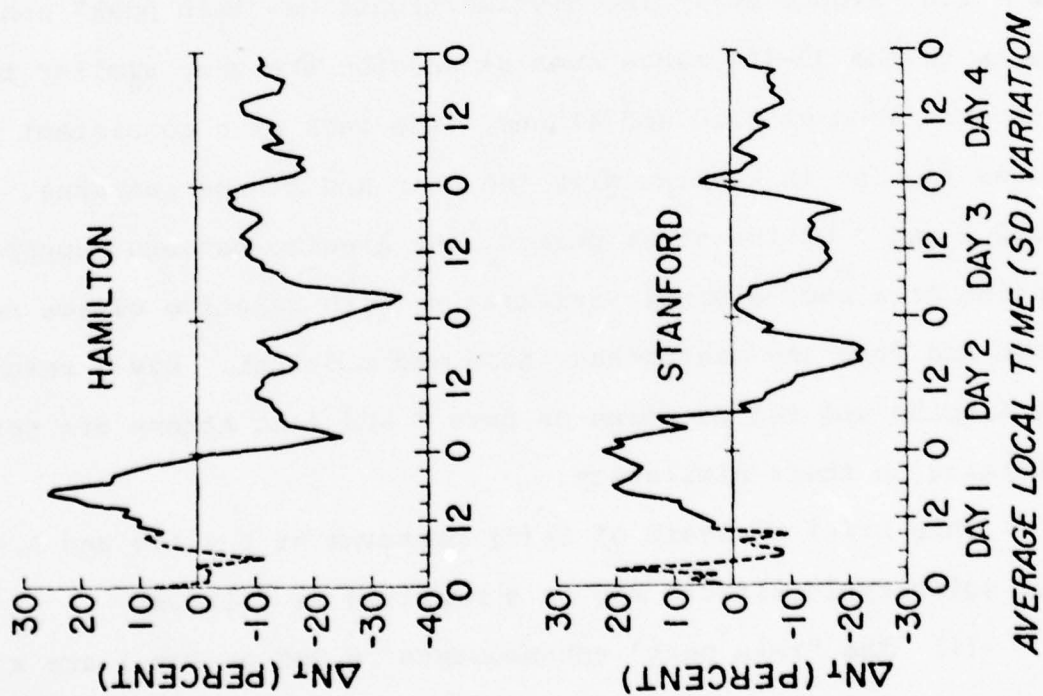


FIGURE 24a.

on Day 1 exists at Stanford, though the magnitudes of the enhancements are considerably smaller. Similarly, prominent nighttime recoveries and/or enhancements occur at Stanford, as seen at KSFC, as well as at Osan and Athens (notice, in particular, 00 LT values on Day 4). The major feature of the Stanford results which distinguishes it from the other  $L \approx 2$  patterns is the pronounced negative phase on Days 2, 3 and 4. This could be due to solar cycle effects, rather than to longitudinal differences, an effect in keeping with the solar cycle control over the negative phase seen at Sagamore Hill (see section 3.3).

The Arecibo results (Figure 24b) for  $L \approx 1.4$  should be compared with the storm patterns from Athens ( $L \approx 1.4$ , Figure 22) and Osan ( $L \approx 1.3$ , Figure 20). The daytime/nighttime "twin peak" enhancements in the 30-40% range seen at Arecibo are very similar to patterns seen at Osan and Athens. The lack of a consistent negative phase is also in keeping with the Osan and Athens patterns. On Days 2 and 3 of the storm period, the Arecibo pattern supports the notion of a semi-diurnal variation -- with relative minima near dawn and dusk and maxima near noon and midnight. Day 3 results at Arecibo and the patterns on Days 3 and 4 at Athens are particularly striking in their similarity.

This brief analysis of SD(%) patterns at  $L \approx 1.4$  and  $L \approx 1.8$  for solar cycle effects may be summarized as follows:

- (1) The "twin peak" enhancements in TEC on Day 1 are a factor of two larger during solar minimum years at  $L \approx 1.7-1.8$  (compare Figures 23a and 17), but are basically

the same in magnitude at  $L \approx 1.3-1.4$  (compare Figures 24b, 20 and 22).

- (2) During solar maximum years, the daytime negative phase extends to  $L \approx 1.7$  but not to  $L \approx 1.4$  (see Figure 24a, b). During solar minimum years, the daytime negative phase is confined to the region  $L > 1.8$  (see Figure 17).

#### 4.4. Average Storm Patterns Near an $L \approx 2$ Conjugate Point -- Salisbury ( $L \approx 1.4$ ).

As a final topic in this section, we present in Figure 25 the average storm pattern obtained for a small number of storms using a TEC data base from Salisbury, Rhodesia (courtesy of Dr. D. Matsoukas). The Salisbury site is of interest because it monitors the geomagnetic conjugate point of the Athens measurements ( $L \approx 1.4$ ). As described in Table VIII, the Salisbury data base only spans the period July 1973 to October 1973, which included 9 ionospheric storm periods. This represents a very small sample for statistical studies, so we examined each storm period separately to search for characteristic patterns. Of the 9 storms, 3 commenced during the nighttime hours (23:00-05:00 LT) and seemed to instigate prolonged positive phase results for several days. The 6 daytime commencing events (06:00-22:00 LT) were therefore selected for averaging using the procedures outlined in Chapter 2. These are the results which appear in Figure 25.

The SD-1 results in Figure 25 show a broad daytime enhancement with a subsequent nighttime increase. The magnitudes of the increases and their LT dependence are thus in agreement with the overall pattern for storms seen at Athens. Since the period examined

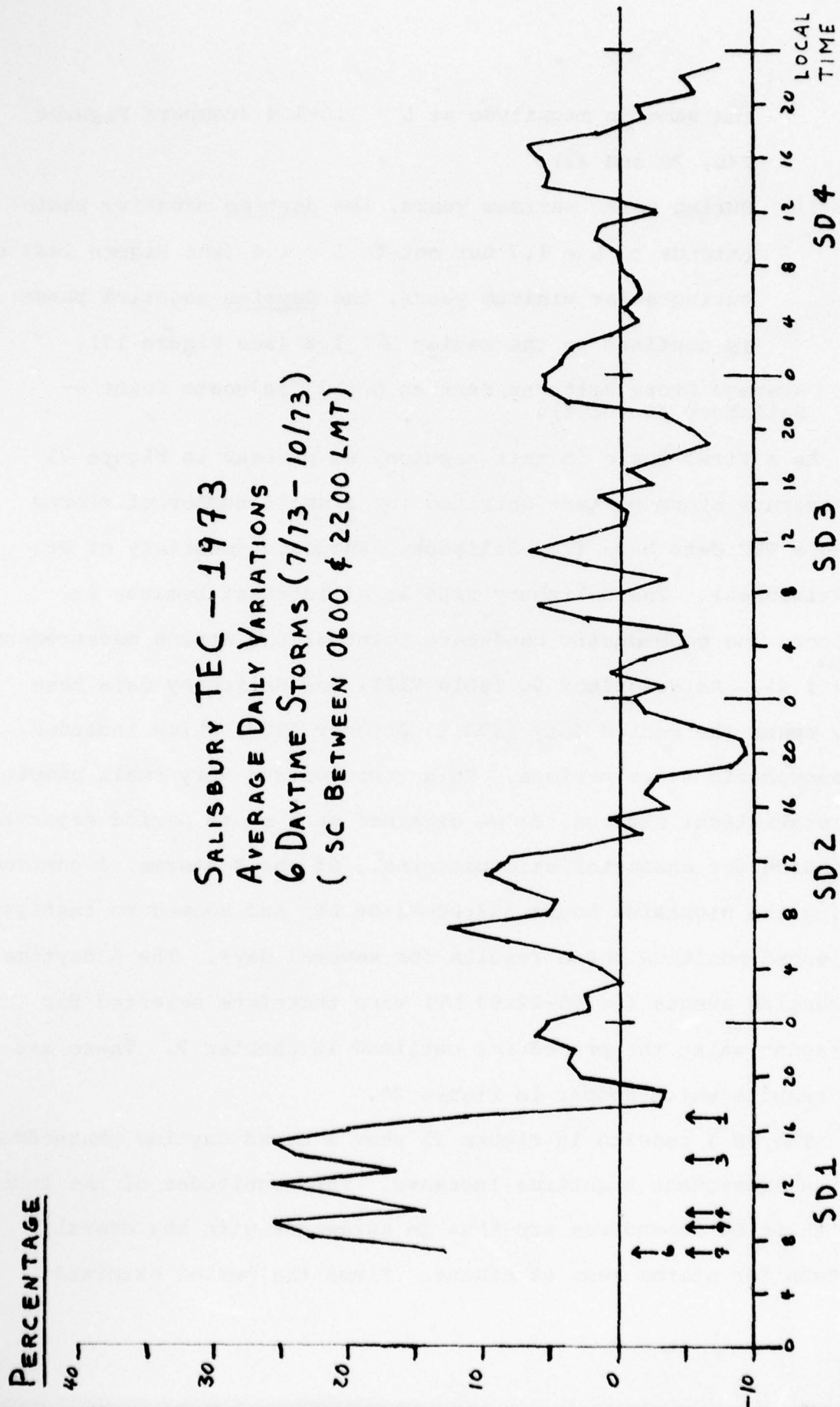


FIGURE 25.

corresponds to Winter and Spring in the Southern Hemisphere, comparisons with Athens behavior should perhaps be made with Figures 24 a, b. Then, the Salisbury "twin peaks" are seen to be smaller -- though the vast difference in sample sizes (6 versus 26 Winter/Spring events) may make such comparisons questionable. On Days 2, 3 and 4 of the storm period, the Salisbury SD(%) patterns suggest a semi-diurnal variation with dawn/dusk minima and noon/midnight maxima, with no overall positive or negative phase evident. These results are in remarkably good agreement with the "characteristic features" documented with the Athens data -- and indeed with similar  $L \approx 2$  patterns from KSFC and Osan. We conclude that the careful analysis of a relatively small number of storms has confirmed the existence of a semi-diurnal, storm-associated, long-lived, global F-region perturbation.

## 5. DISCUSSION AND CASE STUDIES

### 5.1. Summary and General Conclusions.

The investigations documented in the previous four Chapters have provided an extensive and detailed set of average storm patterns for the disturbed F-region as a function of latitude and longitude. The aim of the study was to obtain meaningful storm patterns, that is, characterizations of the disturbed F-region that are quantitatively representative of actual observed effects, and patterns that may be easily incorporated into working models which attempt to specify F-region morphology on a near real-time basis. Two previous reports (Mendillo et al., 1975; Mendillo 1976b) discussed the use of  $SD(TEC, N_{max}, \tau)$  patterns near  $L \approx 3$  to update F-region models as a way of assessing storm effects upon ionospherically-supported radio communications systems. The multi-site results given in the present study now afford the opportunity to extend such use to semi-global coverage, and to make the patterns as representative as possible by providing seasonally (and in some cases solar cycle) dependent patterns.

We have seen repeatedly in Chapters 3 and 4 that the largest changes in F-region structure associated with storms are the positive excursions seen on the afternoon of the day of the storm, and in some cases during the subsequent night. These enhancements in electron content ( $\Delta TEC(\%)$ ) are generally associated with similar increases in the F-region's peak density ( $\Delta N_{max}(\%)$ ), and thus we suggest that if only TEC data are available during a storm (or at

some site), those interested in  $\Delta N_{\max}$  effects may assume that  $\Delta N_{\max} (\%) \approx \Delta \text{TEC}(\%)$  during the positive phase. It should also be noted in this context that average storm patterns in critical frequency, foF2, may be obtained from the  $N_{\max}$  patterns via

$$\Delta \text{foF2}(\%) = \{(\Delta N_{\max}(\%)/100 + 1)^{\frac{1}{2}} - 1\} \times 100$$

where the corresponding standard deviation can be taken as approximately  $\frac{1}{2}$  the  $\sigma(N_{\max})$  value.

During the negative phase of ionospheric storms, simultaneous SD(TEC) and SD( $N_{\max}$ ) patterns have been studied at only two sites ( $L \approx 3$  and  $L = 4$ , see Figures 8 and 12). During periods of daytime depletions (e.g. SD<sub>2</sub>),  $\Delta N_{\max}(\%) \approx 2 \times \Delta \text{TEC}(\%)$ , and thus we suggest this scheme if only TEC data are available at the site of interest.

The physical causes of the F-region perturbations associated with geomagnetic storms have been discussed by many researchers; we will not make the effort here to review the various theories, but only comment on a few generally accepted notions. The large F-region enhancements which occur during the afternoon hours on the first day of a storm are generally considered to be the result of storm-induced vertical drifts moving freshly created F-region plasma to regions of reduced chemical loss. We have argued in favor of an electrodynamic, magnetospheric convection origin of the drifts (Mendillo, 1975, Mendillo and Klobuchar, 1974, Lanzerotti et al., 1975) while others suggest neutral winds (Jones, 1973), or a combination of winds and  $E \times B$  effects (Anderson, 1976).

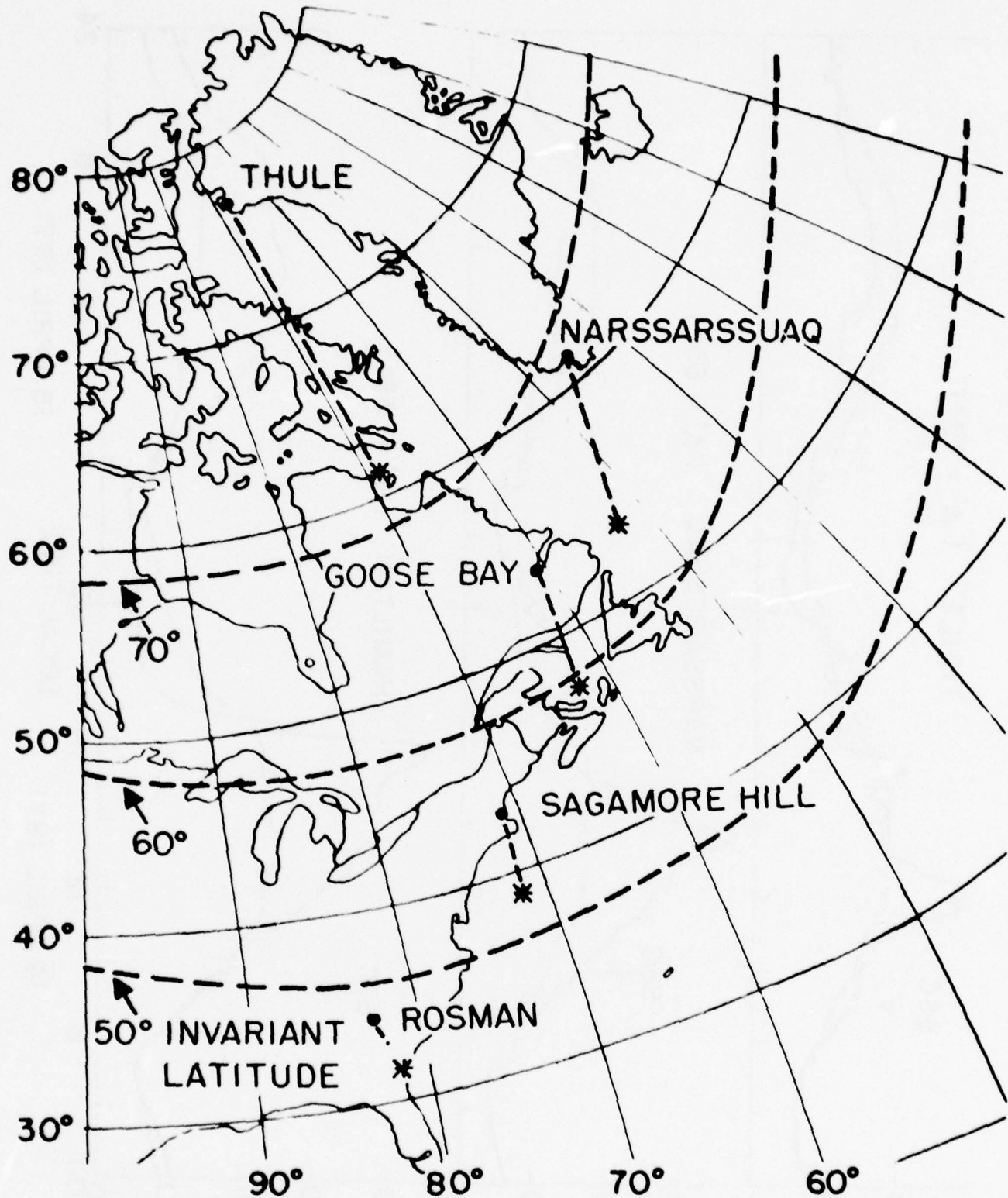
The negative phase of ionospheric storms is less controversial in that neutral atmosphere changes affect ionospheric chemistry in such a way as to upset the normal production/loss balance in favor of increased loss. Ample evidence exists to support the explanation of chemically determined loss enhancements via decreases in the  $O/N_2$  ratio (Prolss et al., 1976; Hedin et al., 1977). The longevity of ionospheric disturbances, and the semi-diurnal variations discussed in this context, have not been treated in any detail from the neutral composition aeronomic viewpoint.

## 5.2. Examples of Storm Effects Along the Latitudinal Network.

A massive report dealing with the average characteristics of ionospheric storms should, we feel, contain at least a few sample cases of individual storm periods. A mellow perusal of the AFCRL ATLAS of storm effects at Sagamore Hill ( $L \approx 3$ ) offers 75 different views of perturbations in TEC,  $N_{max}$ ,  $\tau$ ; we will concentrate here, therefore, on the overall, coupled latitudinal response seen during a small subset of "classic" disturbances. Figure 26 provides a summary of the TEC network near  $70^\circ W$  showing geomagnetic invariant latitude ( $\Lambda$ ) grids not given in Figure 1.

### 5.2.1. The April 1971 Storm Period.

Figure 27 presents a set of TEC curves for the ionospheric storm period 14-15 April 1971. The dashed curves describe the monthly median patterns at the three sites. TEC data from the Air Force Geopole station at Thule, Greenland, has not been examined



TEC OBSERVING STATIONS (ATS-3 AT 70°W)

FIGURE 26.

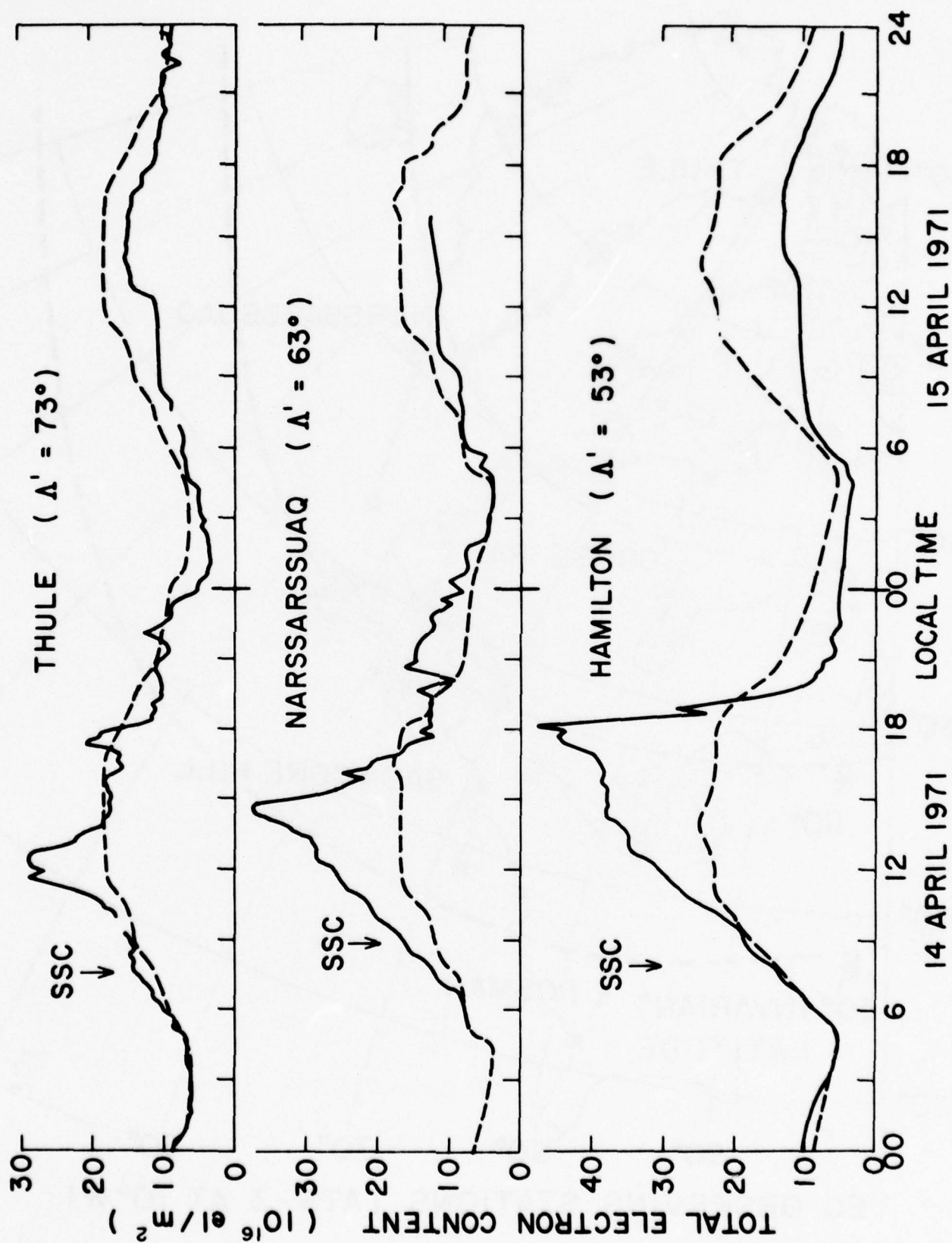


FIGURE 27.

in any of the previous sections of this report -- mainly due to the limited amount of data available. Selected station-months of Thule data have been reduced for particular case studies -- and these April data represent one of those cases.

The  $L \approx 3$  (Hamilton) data and the  $L \approx 5$  (Narssarssuaq) data show all of the characteristic features described in Chapter 3. To get a more complete picture of the severity of the distortions in F-region latitude/local time morphology which occur during storms, we plot in Figures 28 and 29 contours of iso-TEC values displayed on a latitude versus local time grid.\* Note, in particular, how the SD-1 TEC positive phase and its sharp termination changes as a function of latitude and local time. Trough effects near 03:00 LT at Hamilton -- discussed at length in Chapter 3 -- appear clearly in the SD-2 (15 April) behavior. The negative phase during the daytime on the 15th is dramatically depicted by the sparsity of contours on the right-hand-side of Figure 29. A summary of the actual percentage variations in TEC over this 2-day period appears in Figure 30. This type of presentation shows in a dramatic way how ionospheric storms so significantly alter ambient F-region behavior.

#### 5.2.2. The December 1971 Storm Period.

The geomagnetic storm which commenced on 17 December 1971 had associated with it an ionospheric storm period of extraordinary severity. At Sagamore Hill, the largest TEC afternoon enhancement ever recorded was observed and similarly drastic effects were seen

\* TEC data from Rosman have been used to extend the coverage to  $L \approx 2$ .

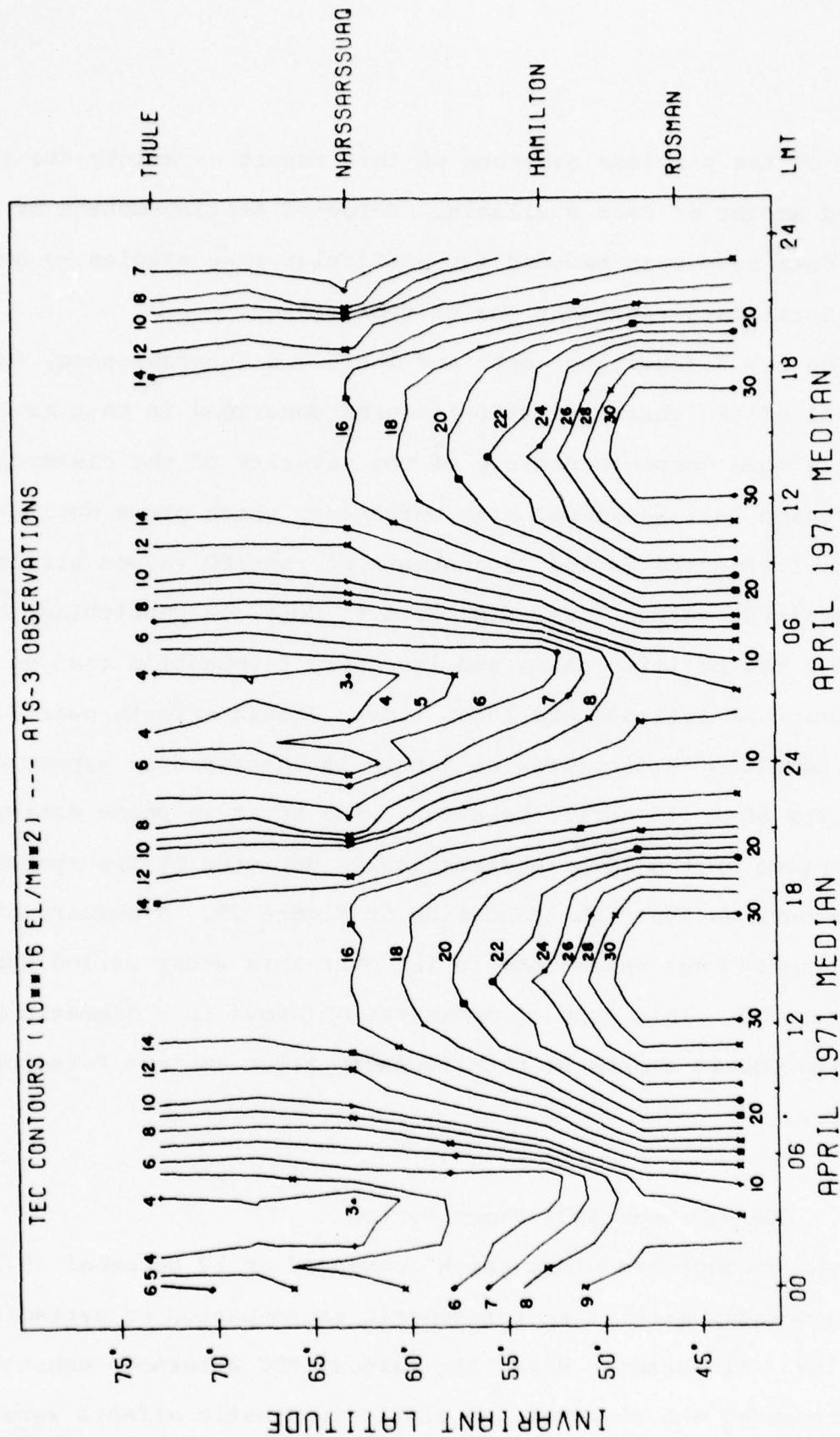


FIGURE 28.

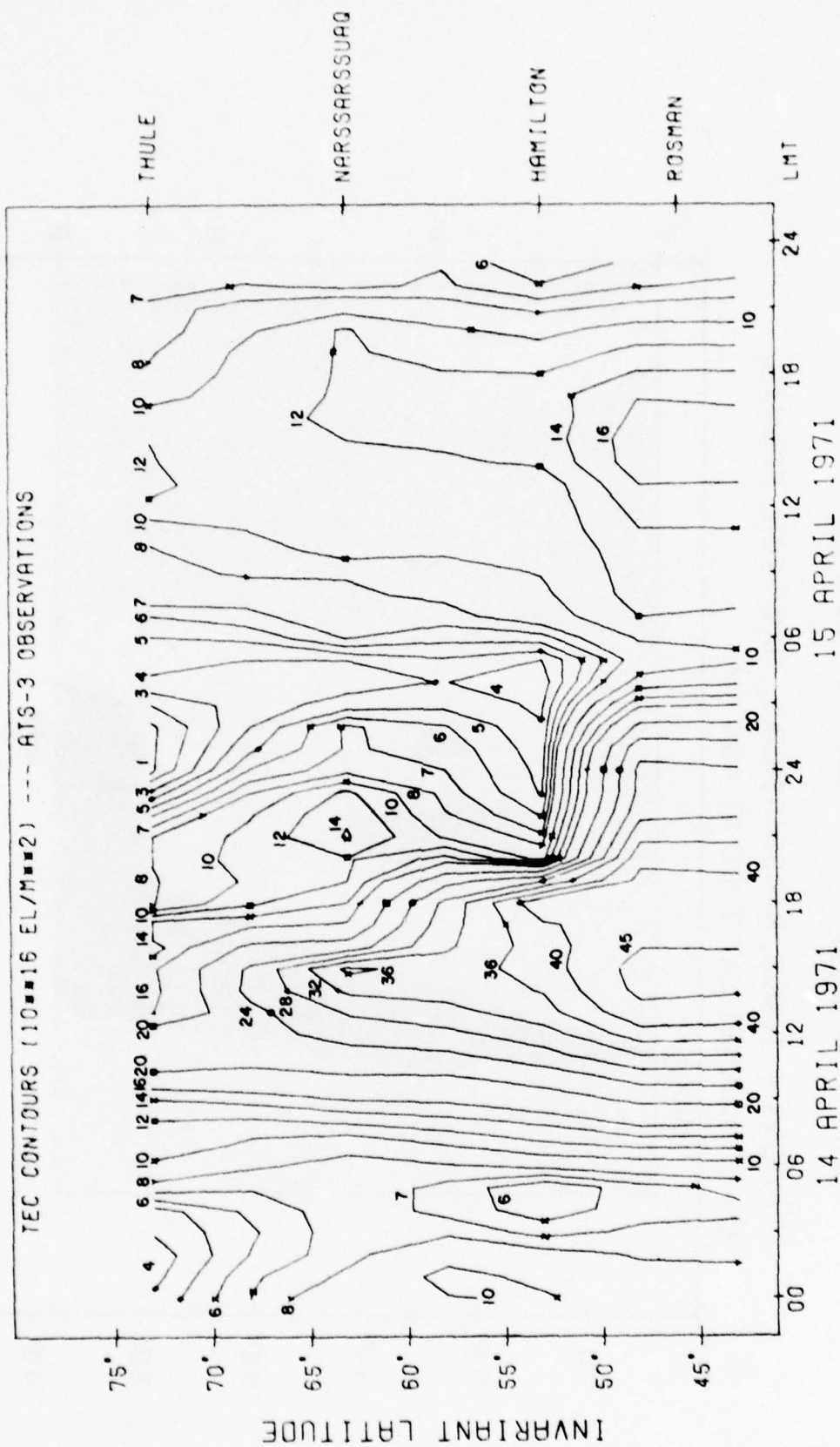


FIGURE 29.

# CHANGES IN TOTAL ELECTRON CONTENT DURING A GEOMAGNETIC STORM



STATIONS = THULE, NARSARSUAQ, HAMILTON, ROSMAN.

$\Delta'$  = INVARIANT LATITUDE AT 400 KM

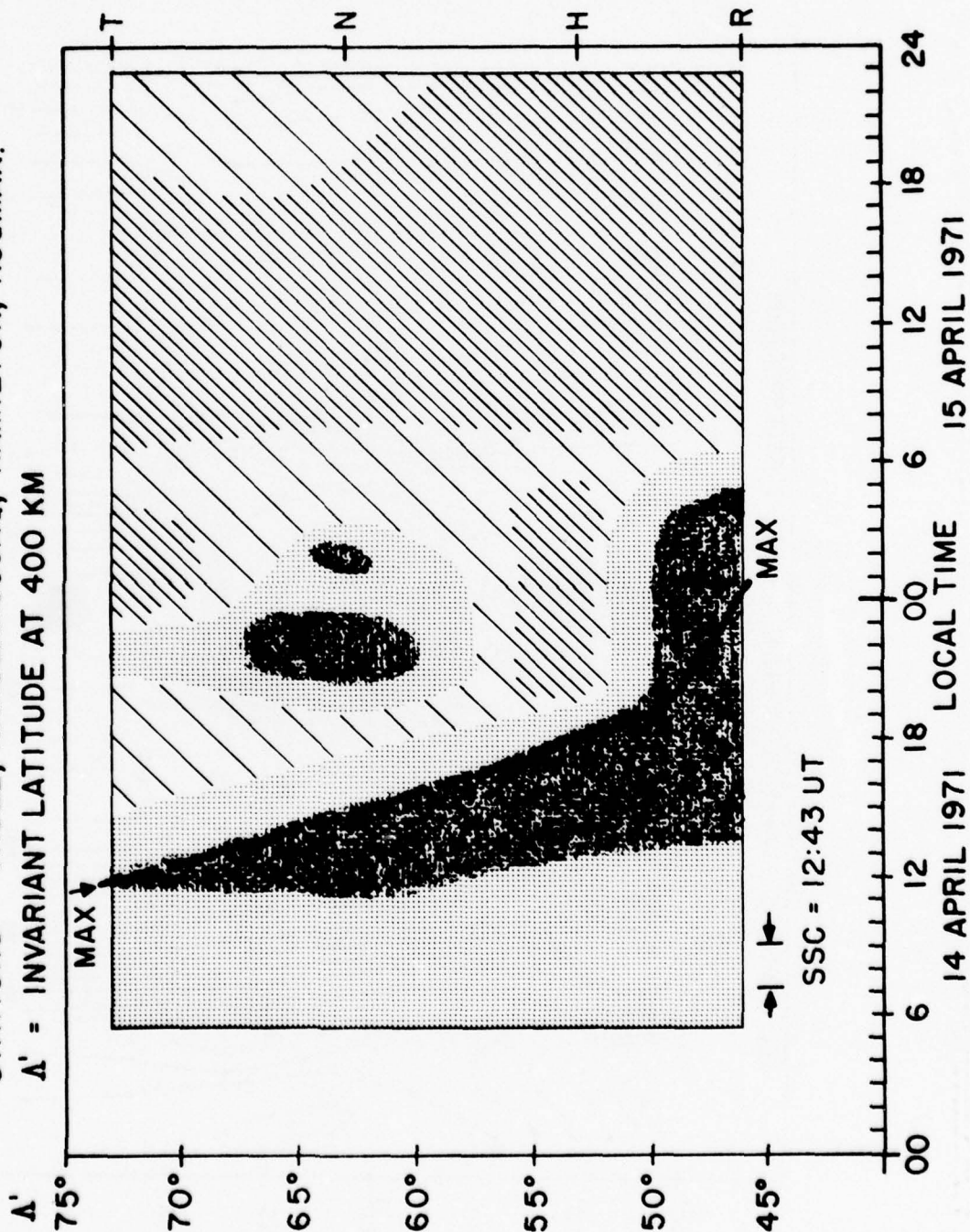


FIGURE 30.

at various ionospheric observatories in both hemispheres (Schodel et al., 1974). Results along the AFGL latitude chain during this period are presented in Figure 31. A special effort was made to coordinate satellite beacon observations made near the  $70^{\circ}\text{W}$  meridian during this December 1971 period (Mendillo and Klobuchar, 1975). A 6-station network of TEC sites from Kingston, Jamaica ( $\lambda \approx 34^{\circ}$ ), to Thule, Greenland ( $\lambda \approx 73^{\circ}$ ), were used to study latitudinal gradient under monthly median conditions and during the severely disturbed period 17-18 December, 1971. These data are given using the TEC contour format in Figures 32 and 33.

#### 5.2.3. Latitudinal Distortions Over the $L = 3$ to 5 Range.

The discovery that the TEC positive phase peak on Day 1 of a storm occurred earlier and was at a smaller enhancement level as the L-value of the observing site increased, prompted us to look in some detail at the ambient latitude gradients over this latitude range and at a series of specific events. In Figures 34 (a-f) we present monthly median behavior of TEC over the  $L \approx 3-5$  range for the 12 month period May 1972 to April 1973. These data describe the type of normal latitude/local time gradients that must be used in model simulation studies of storm effects. In Figure 35, we present TEC data taken during the storm period 15-16 May 1972. This is again a classic example of the latitudinal behavior described by the average disturbance patterns for Narssarssuaq, Goose Bay and Hamilton presented in Chapter 3. This example was chosen to support our contention that electrodynamic

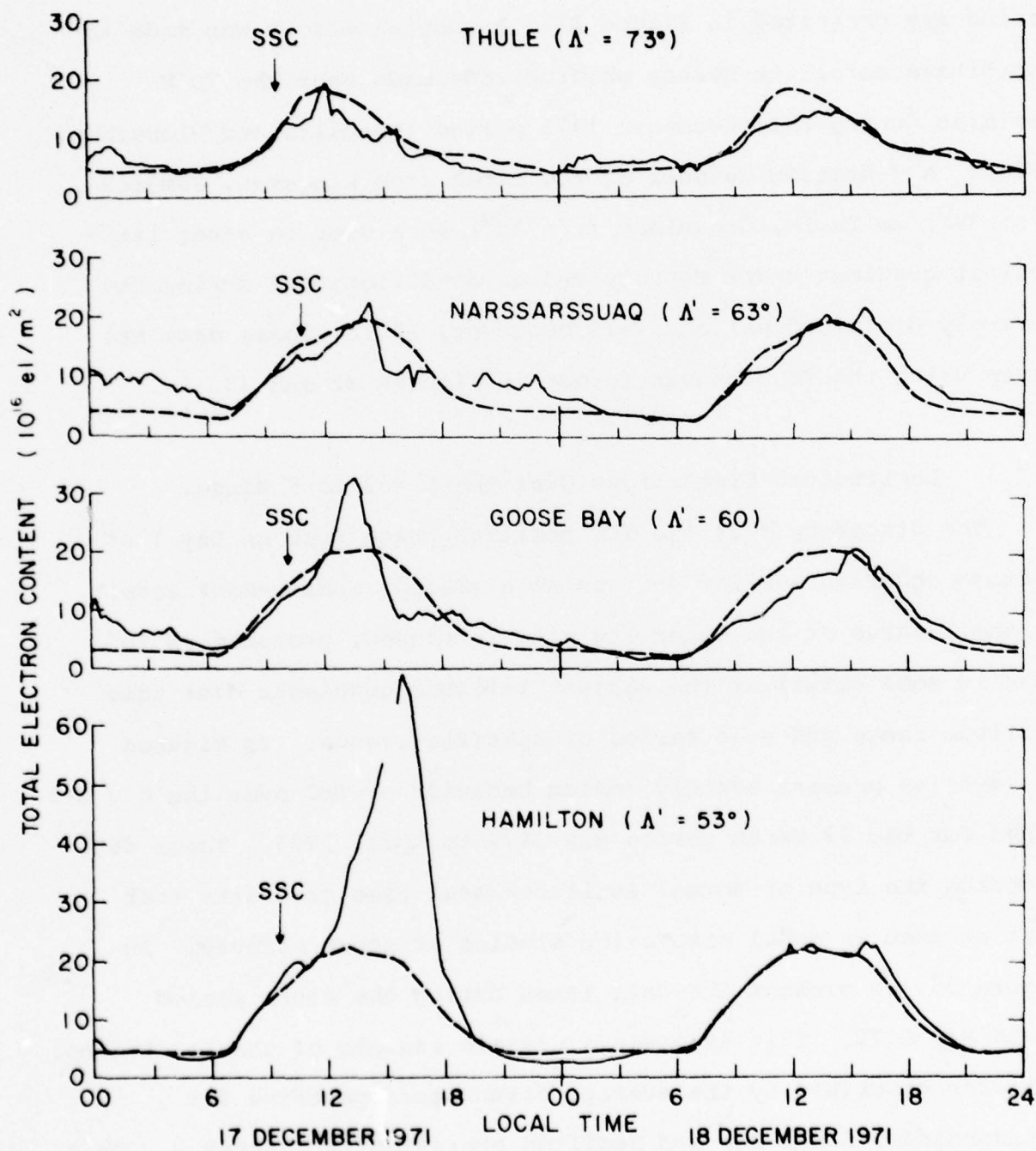


FIGURE 31.

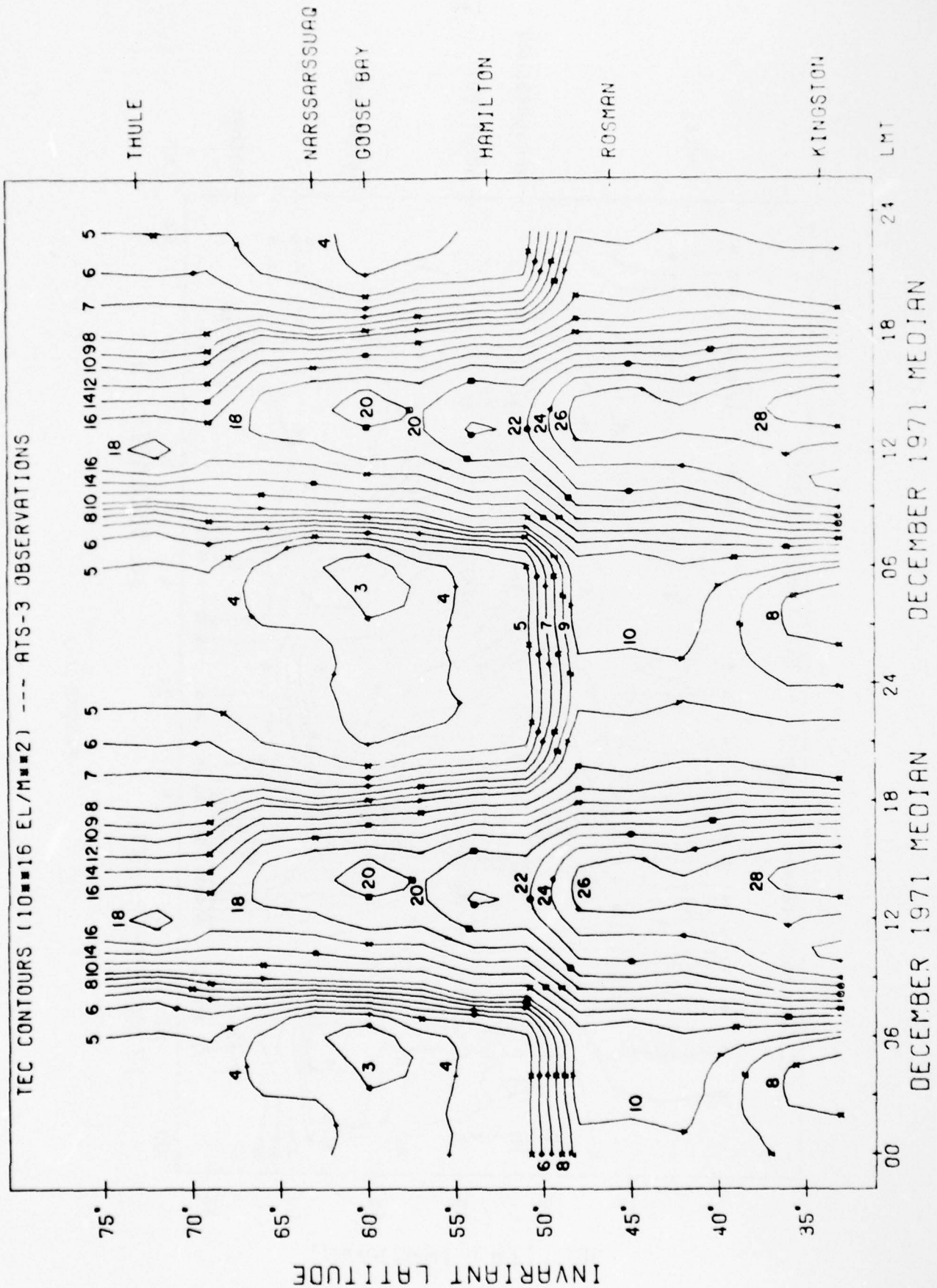


FIGURE 32.

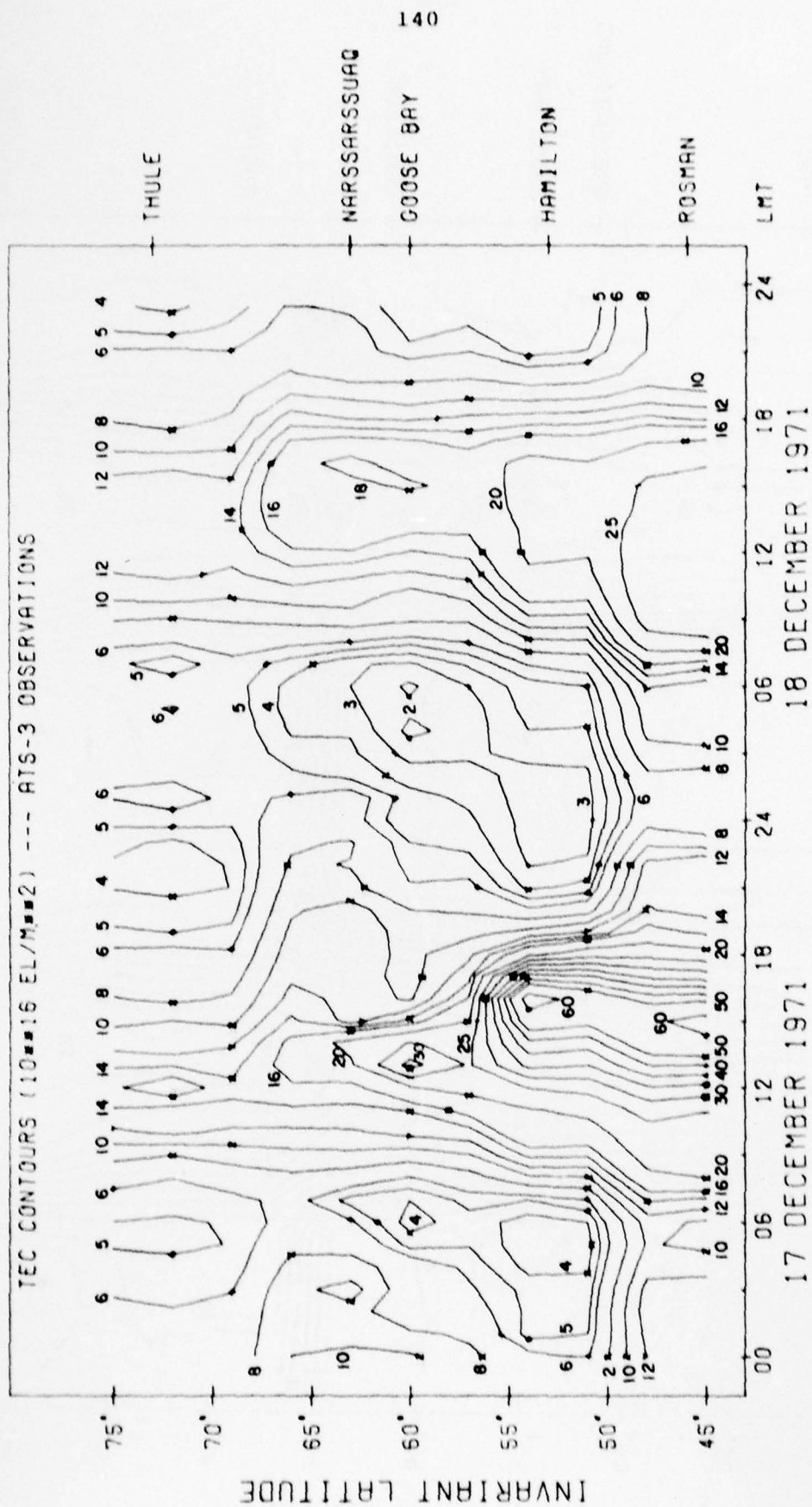


FIGURE 33.

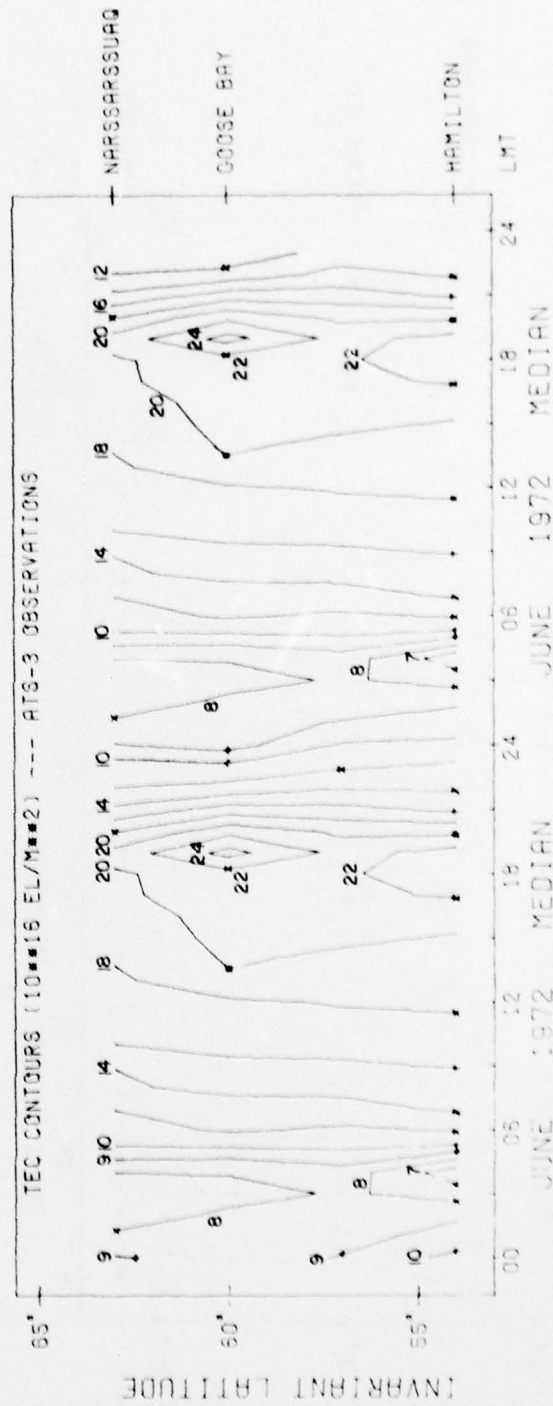
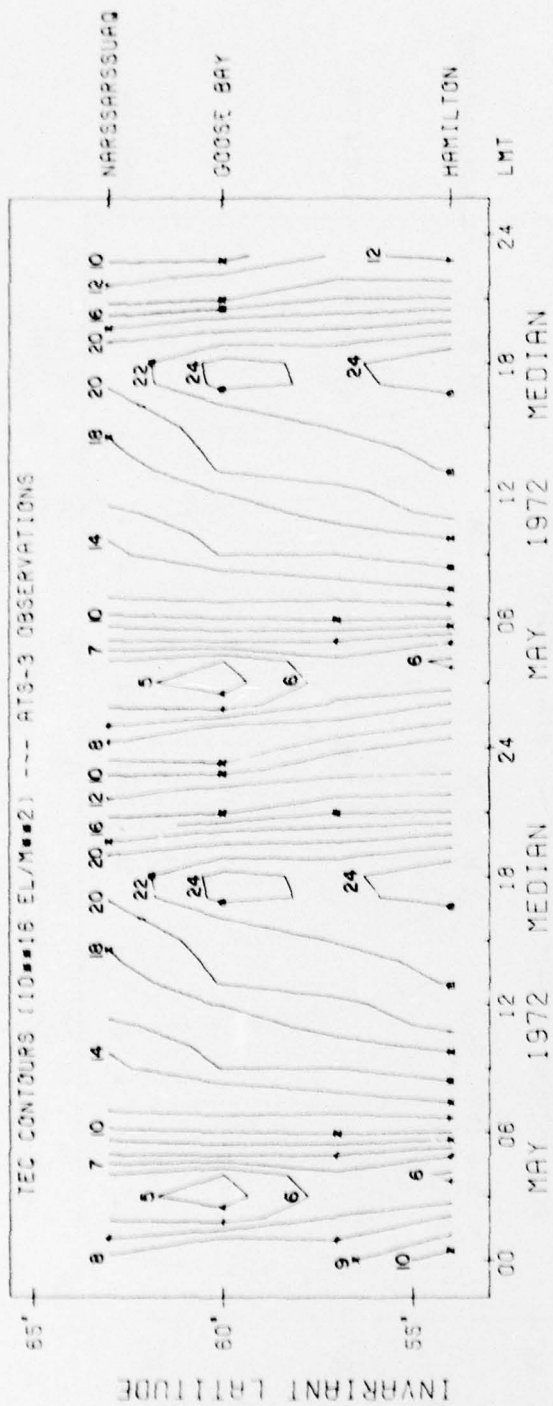


FIGURE 34a.

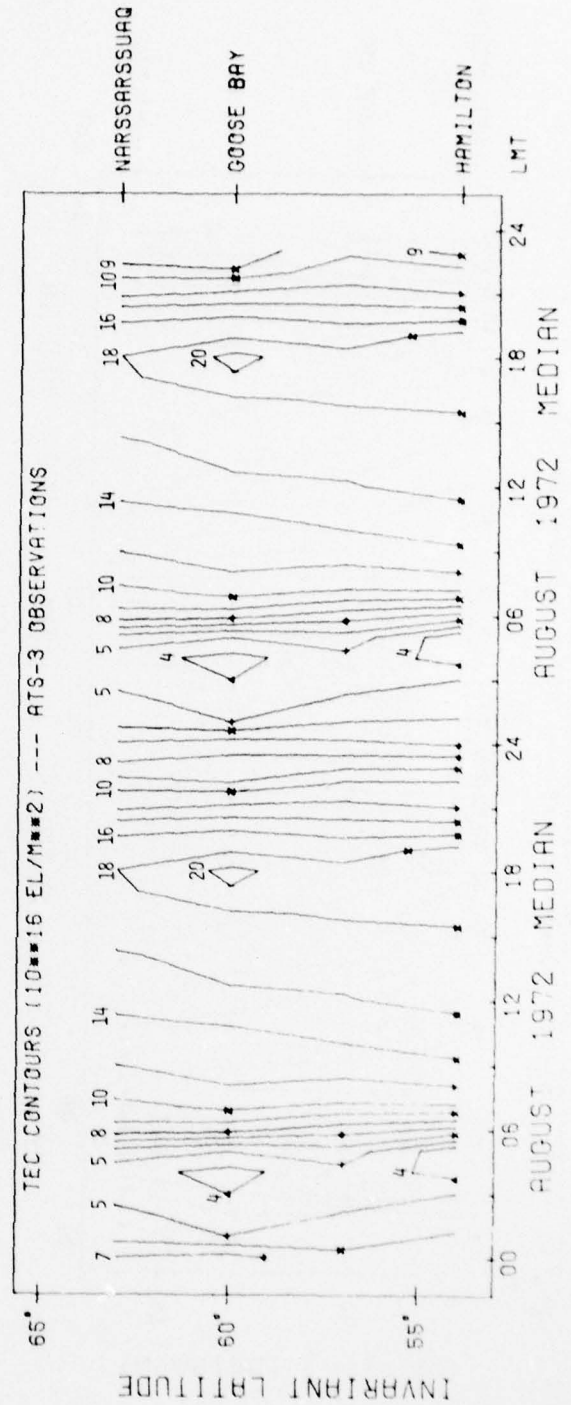
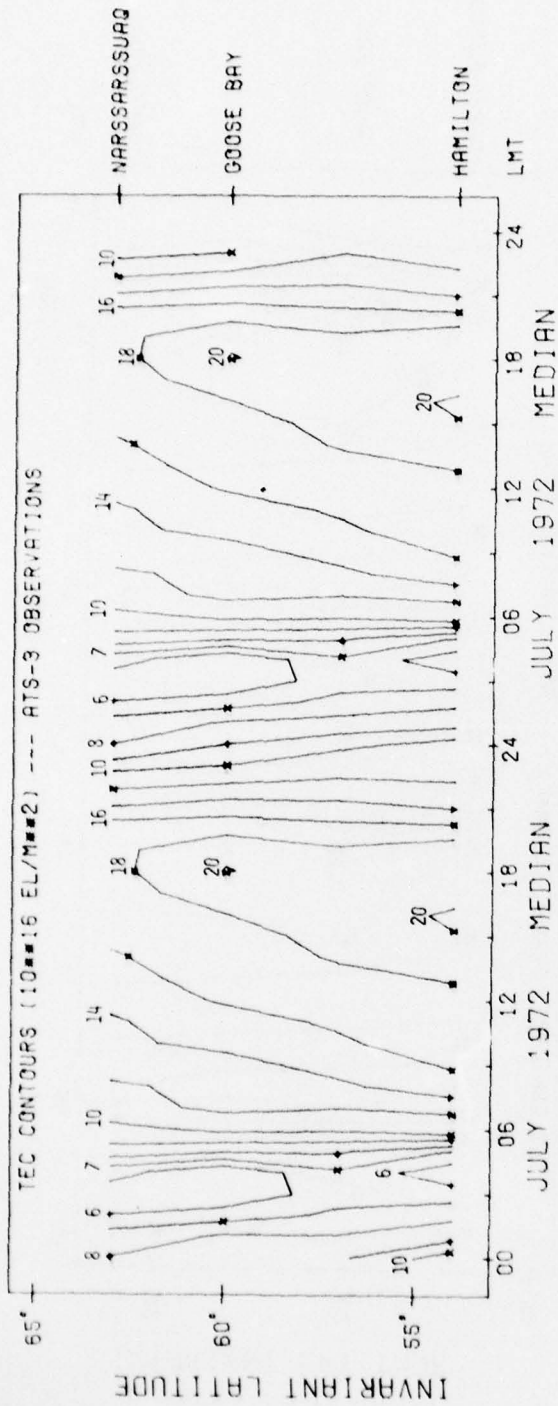


FIGURE 34b.

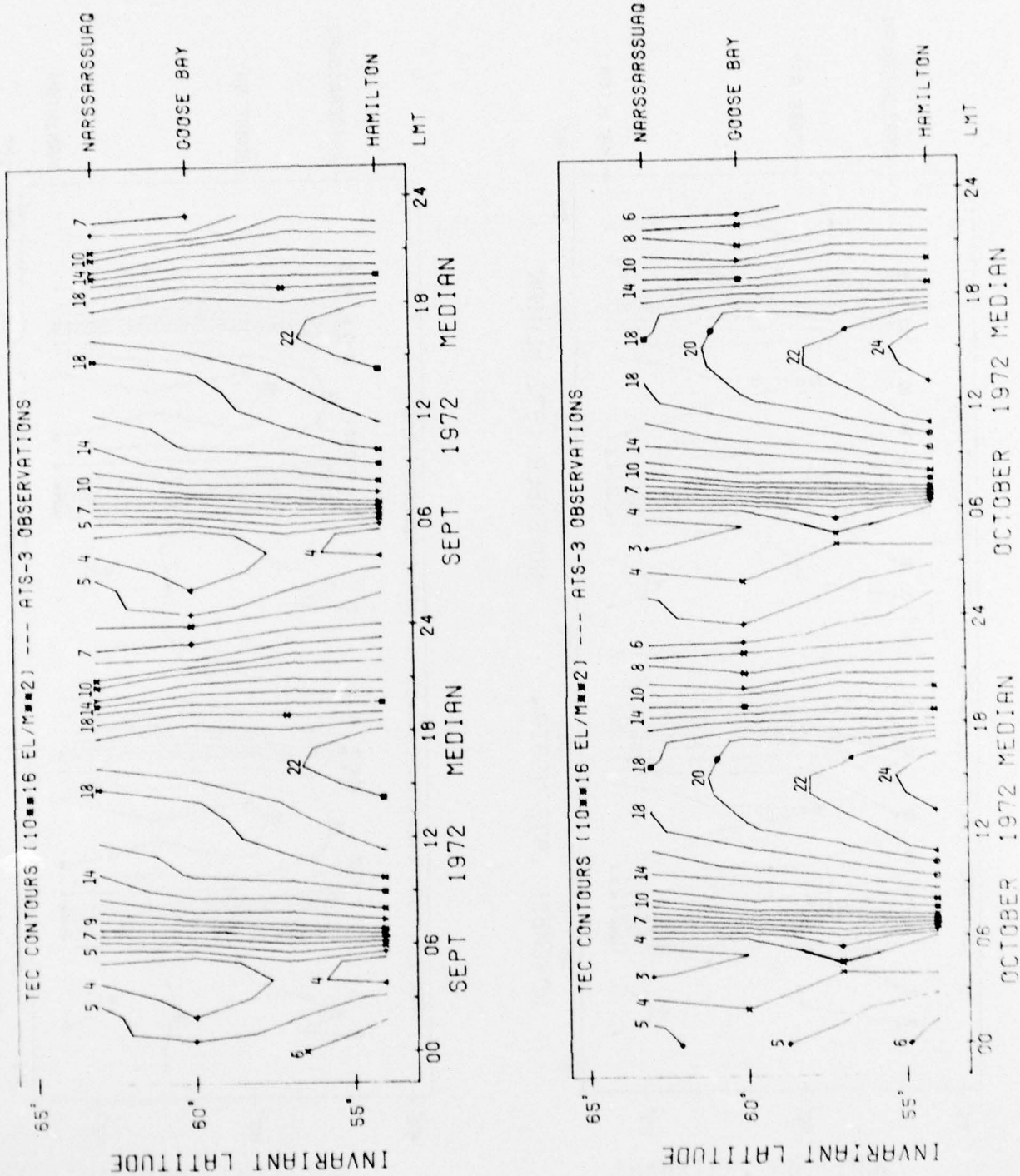


FIGURE 34c.

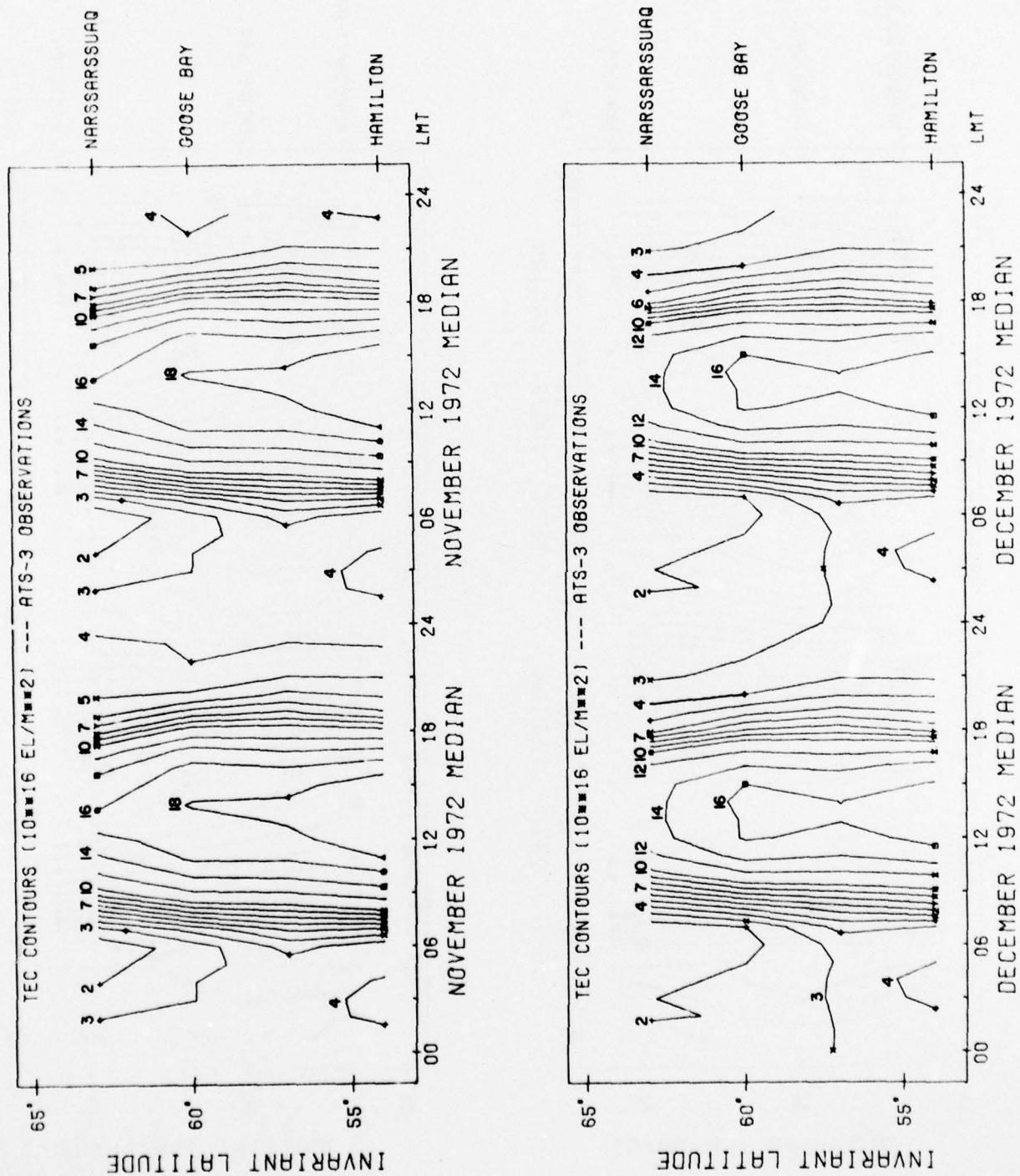


FIGURE 34d.

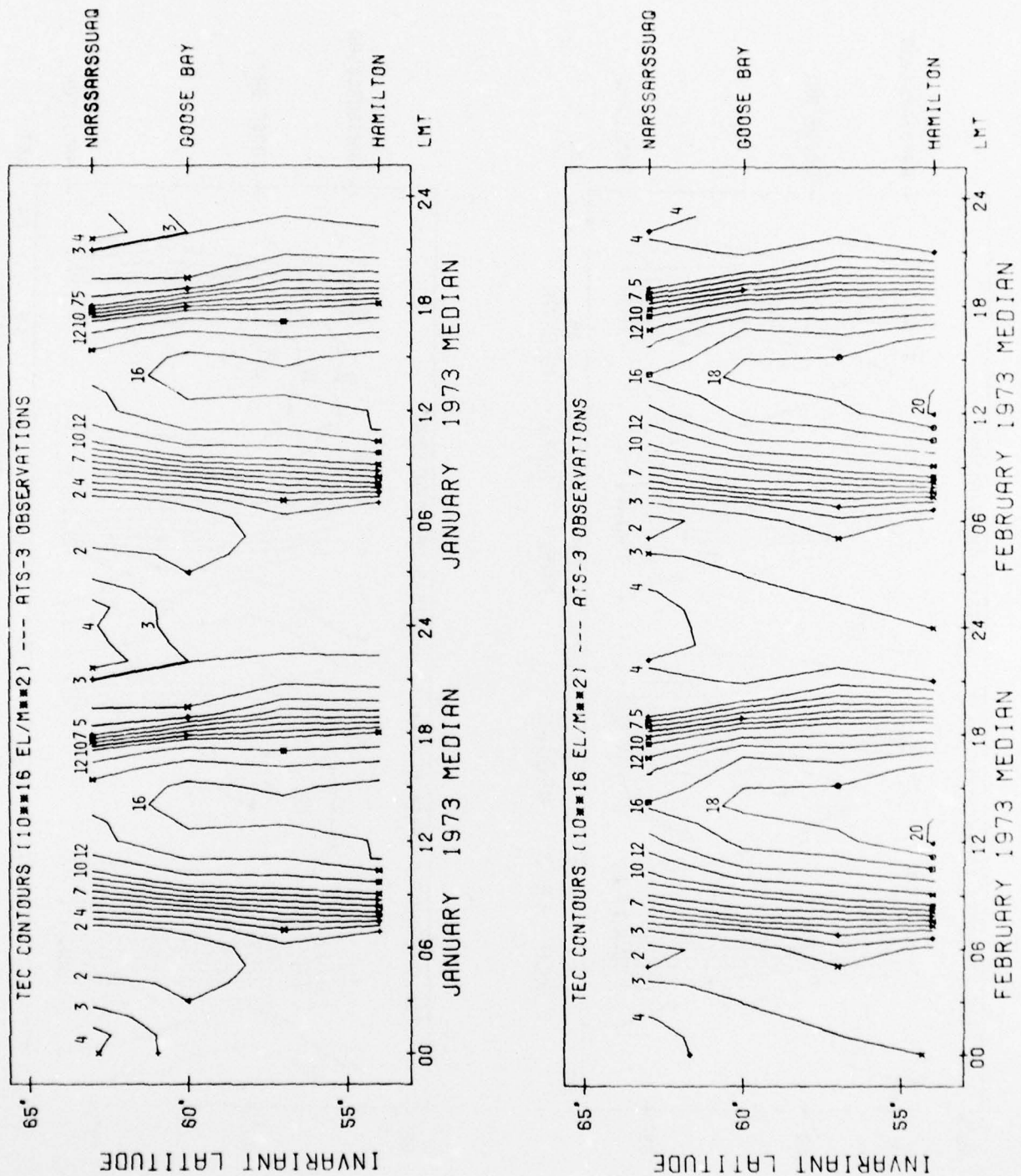


FIGURE 34e.

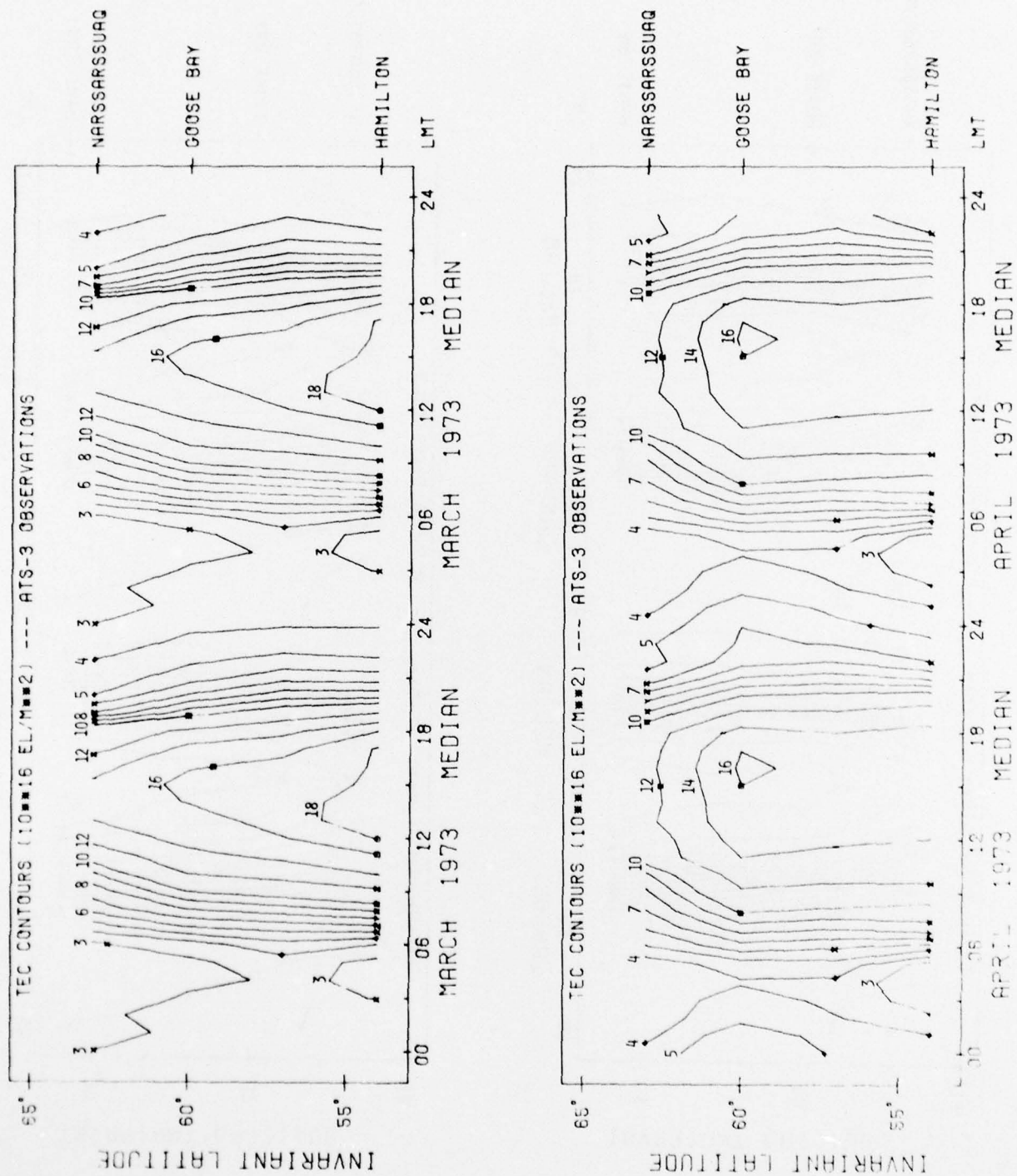


FIGURE 34f.

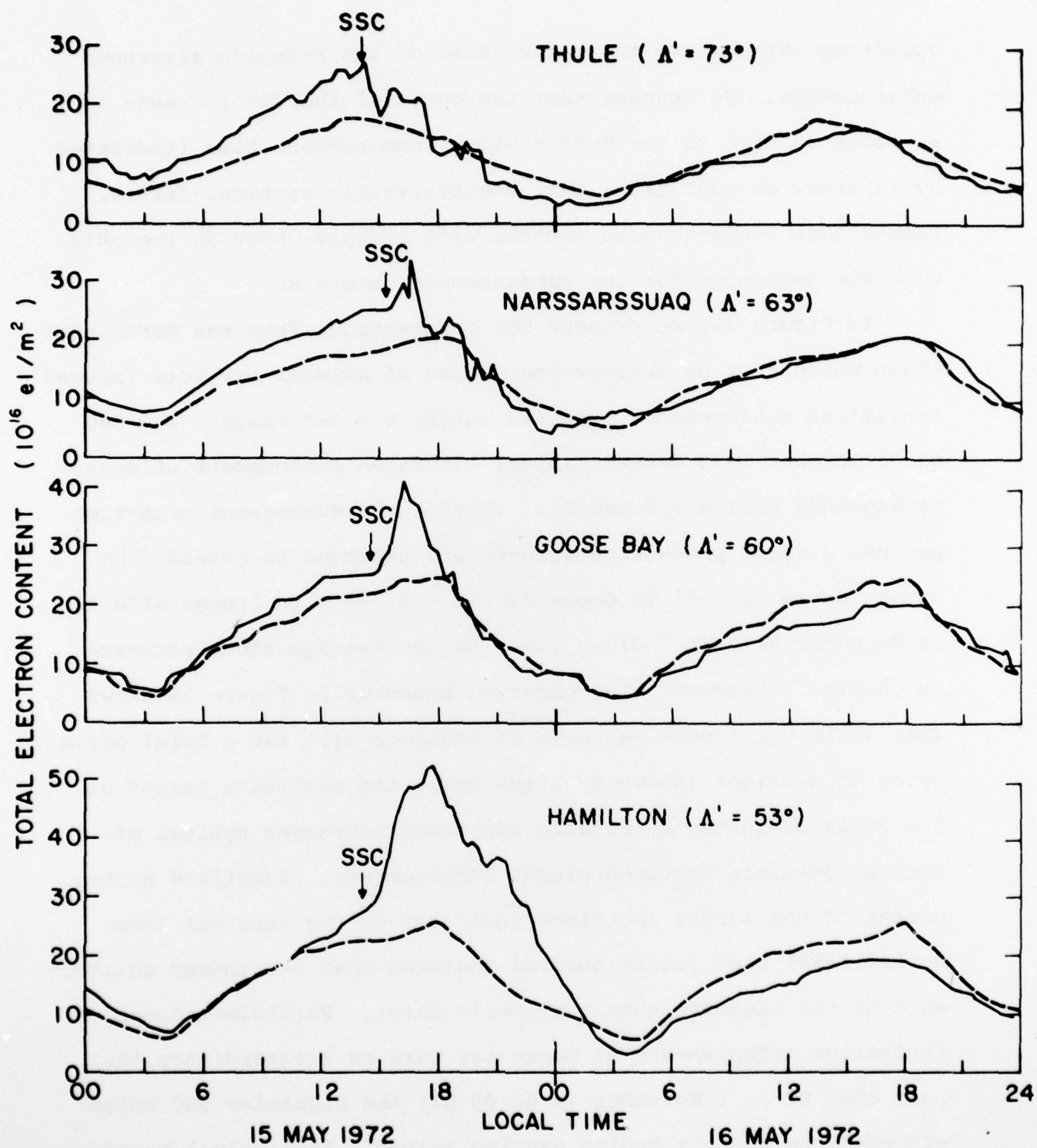


FIGURE 35.

uplifting effects are the major cause of the F-region afternoon enhancements. We suggest that the onset of the TEC increase is so close in time to the Sudden Storm Commencement time (indicated by an arrow at each site) that electrodynamic vertical drifts, rather than storm-induced neutral wind effects, provide the only possible mechanism for the enhancements observed.

In Figure 36, we present TEC observations from the meridional chain which show an extraordinary case of auroral particle induced ionization enhancements over the entire  $L = 3-5$  range. The SSC on 31 October 1972 caused typical afternoon enhancement effects at Sagamore Hill and Goose Bay. During the subsequent nighttime period, auroral production effects are expected to extend from Narssarssuaq ( $L \approx 5$ ) to Goose Bay ( $L \approx 4$ ) -- with trough effects at Sagamore Hill ( $L \approx 3$ ) -- i.e., as the average storm patterns in Chapter 3 suggest. The observed behavior in Figure 36 shows that while the trough was seen at Sagamore Hill for a brief period prior to midnight (shown by black dot), the nighttime period at  $L \approx 3$  was dominated by erratic nighttime increases typical of auroral particle produced plasma enhancements. Satellite photographs of the aurora (at times indicated by the vertical lines marked DAPP) show active auroral features that are indeed equatorward of the Sagamore sub-ionospheric point. Particle-induced ionization enhancements at Goose Bay were so extraordinary that near 0600 UT on 1 November ( $\approx 02:00$  LT) the nighttime TEC value exceeded the monthly median daytime values! Statistical based storm-time predictions have little hope of forecasting such extraordinary behavior.

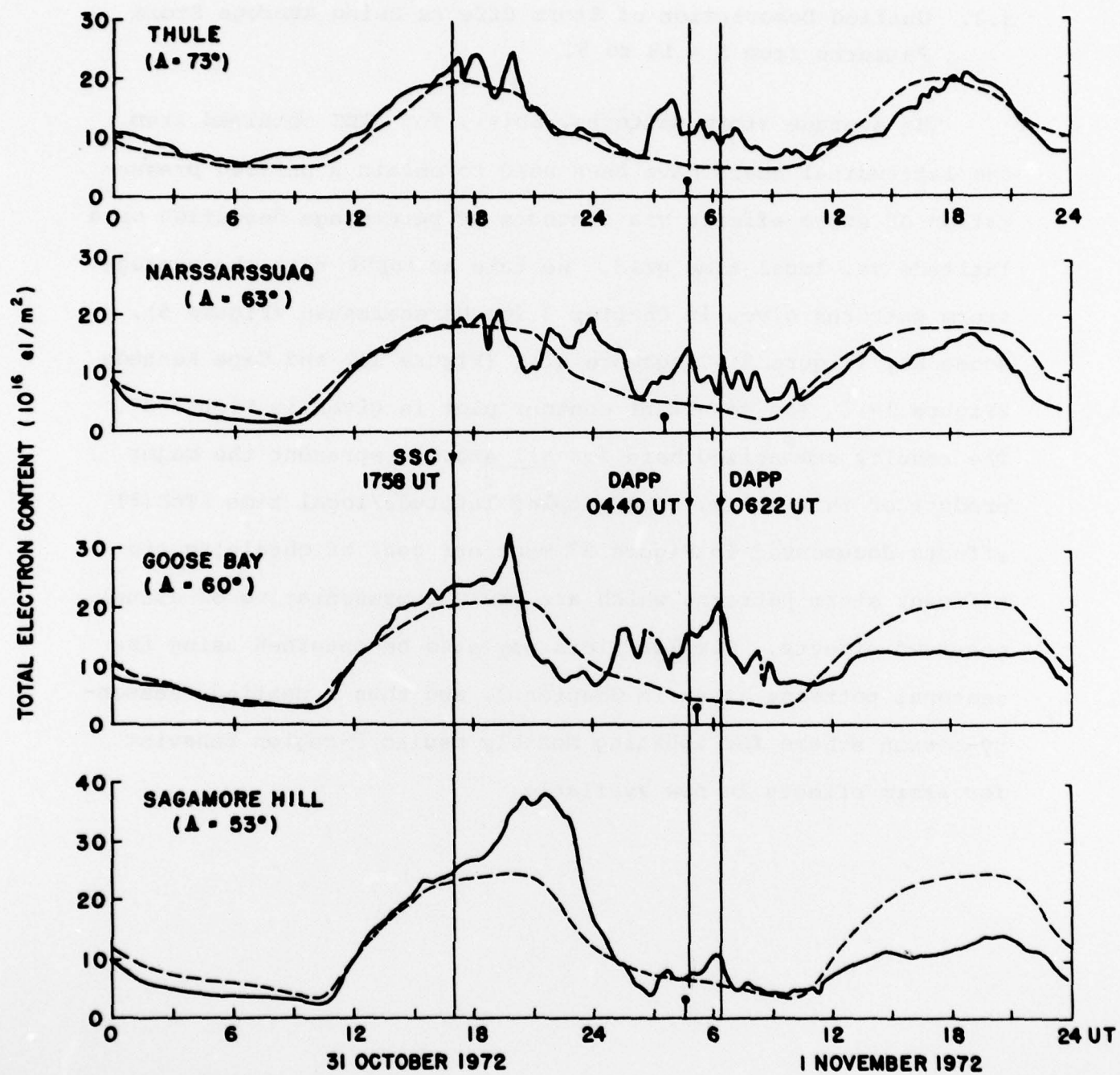


FIGURE 36.

### 5.3. Unified Description of Storm Effects Using Average Storm Patterns from $L \approx 1\frac{1}{2}$ to 5.

The average storm patterns,  $SD(\%)$ , for  $\Delta TEC$  obtained from the latitudinal chain have been used to obtain a unified presentation of storm effects via contours of percentage deviation on a latitude vs. local time grid. We take as input data the average storm patterns given in Chapter 3 for Narssarssuaq (Figure 5), Goose Bay (Figure 8), Sagamore Hill (Figure 11) and Cape Kennedy (Figure 17). The resultant contour plot is given in Figure 37. The results summarized here for all storms represent the major product of this study. The coupled latitude/local time  $\Delta TEC(\%)$  effects documented in Figure 37 meet our goal of obtaining significant storm patterns which are truly representative of actual observed effects. Similar plots may also be obtained using the seasonal patterns given in Chapter 3, and thus a unified, season-by-season scheme for updating monthly median F-region behavior for storm effects is now available.

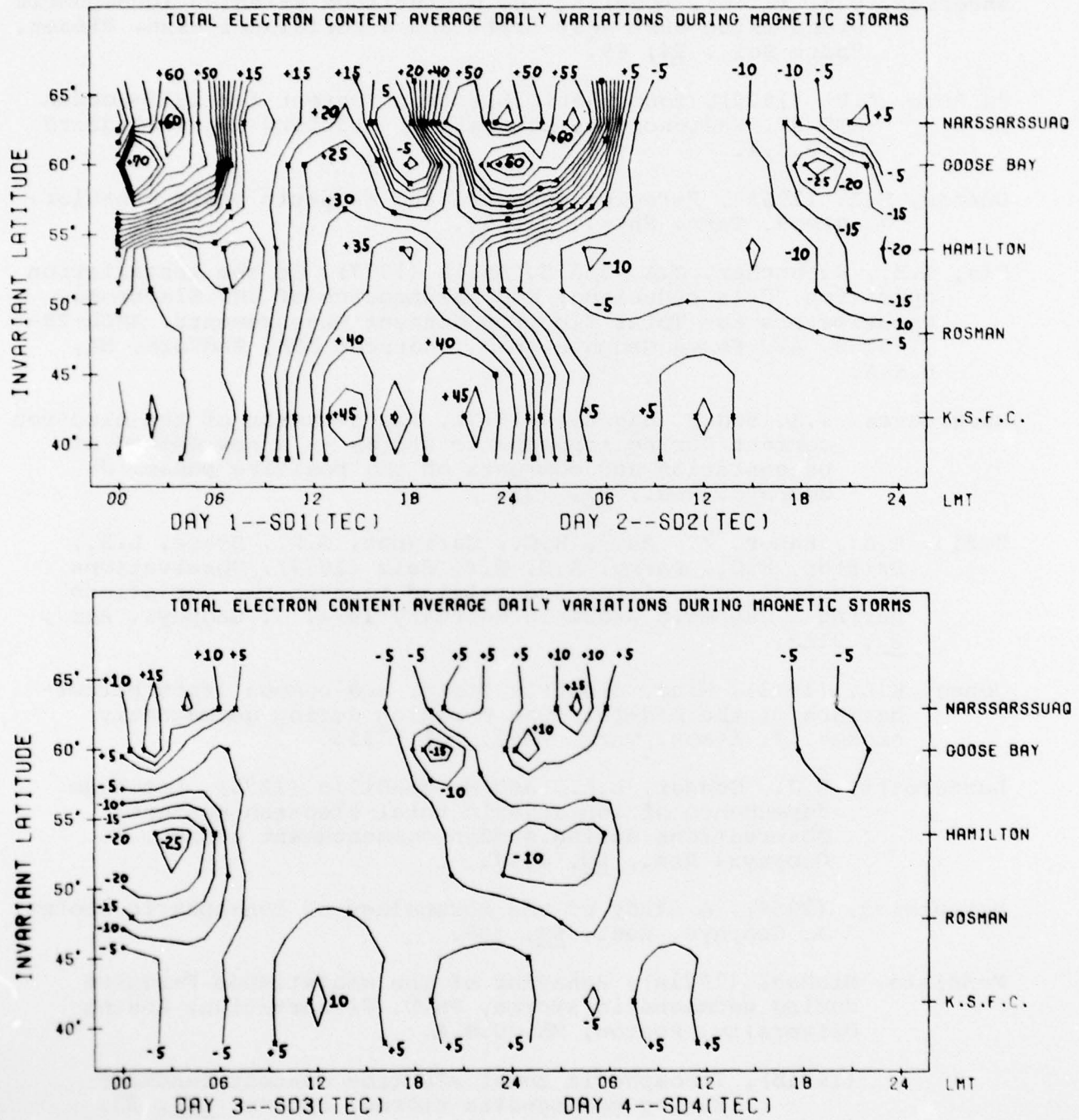


FIGURE 37

## 6. LIST OF REFERENCES

- Anderson, D.N. (1976), Modeling the midlatitude F-region ionospheric storm using east-west drift and a meridional wind, Planet. Space Sci., 24, 69.
- da Rosa, A.V. (1972), Ionospheric Electron Content for 1971-Rosman (ATS-3), Radioscience Laboratory, Stanford Univ, Stanford CA, U.S.A.
- Duncan, R.A. (1969), F-region seasonal and magnetic storm behavior, J. Atmos. Terr. Phys., 31, 59.
- Eis, K.E., Klobuchar, J.A. and C. Malik (1977), On the installation, operation, data reduction, and maintenance of VHF Electronic Polarimeters for Total Electron Content measurements, AFGL-TR-77-0130, Air Force Geophys. Lab., Hanscom AFB, Bedford, MA, U.S.A.
- Hargreaves, J.K. and F. Bagenal (1977), The behavior of the electron content during ionospheric storms -- a new method of presentation and comments on the positive phase, J. Geophys. Res., 82, 731.
- Hedin, A.E., Bauer, P., Mayr, H.G., Carignan, G.R., Brace, L.H., Brinton, H.C., Parks, A.D. D.T. Pelz (1977), Observations of neutral composition and related ionospheric variations during a magnetic storm in February 1974, J. Geophys. Res., 82, 3183.
- Jones, K.L. (1973), Wind, electric field, and composition perturbations of the mid-latitude F-region during geomagnetic storms, J. Atmos. Terr. Phys., 35, 1515.
- Lanzerotti, L.J., Cogger, L.L., and M. Mendillo (1975), Latitude dependence of ionospheric total electron content: Observations during sudden commencement storms, J. Geophys. Res., 80, 1287.
- Matsushita, (1959), A study of the morphology of ionospheric storms, J. Geophys. Res., 64, 305.
- Mendillo, Michael (1971a), Behavior of the midlatitude F-region during geomagnetic storms, Ph.D. dissertation, Boston University, Boston, MA, U.S.A.
- (1971b), Ionospheric total electron content behavior during geomagnetic storms, Nature, 234, 23.

- (1973), A study of the relationship between geomagnetic storms and ionospheric disturbances, Planet. Space Sci., 21, 349.
- (1975), Review of Positive Ionospheric Storms: Observations and Theory, Proceedings of COSPAR Sym. Sat. Beacon Studies of Ion. Struc. and ATS-6 Data, IZMIRAN, Moscow, U.S.S.R.
- (1976a), Satellite beacon studies of global F-region disturbances effects, Proceedings of COSPAR Sym. on Geophys. Use of Sat. Beacon Observations, Boston University, Boston, MA, U.S.A.
- (1976b), The construction of storm-time corrections for ionospheric F-region parameters and their application to trans-ionospheric group-path delay, AFGL-TR-76-0057, Air Force Geophysics Lab, Hanscom AFB, Bedford, MA, U.S.A.
- Mendillo, M., Buonsanto, M.J. and J.A. Klobuchar (1977), Distortions of the winter nighttime ionosphere at L = 4, J. Geophys. Res., 82, 3223.
- (1976), The construction and use of storm-time corrections for Ionospheric F-region parameters, Proc. of Sym. on Effects of the Ionosphere on Space Systems and Communications, J.M. Goodman (ed), Naval Res. Lab, Washington, D.C.
- Mendillo, M. and C.C. Chacko (1977), The base-level ionospheric trough, J. Geophys. Res., 82, 5129.
- Mendillo, M., Hawkins, G.S. and J.A. Klobuchar (1975), A sudden vanishing of the ionospheric F-region due to the launch of Skylab, J. Geophys. Res., 80, 2217.
- Mendillo, M., H. Hajeb-Hosseini and J.A. Klobuchar (1974), Ionospheric disturbances: evidence for the contraction of the plasmasphere during severe geomagnetic storms, Planet. Space Sci., 22, 223.
- Mendillo, M. and J.A. Klobuchar (1974), An atlas of the midlatitude F-region response to geomagnetic storms, AFCRL Tech. Report No. 0065, Hanscom AFB, Bedford, MA, U.S.A.
- (1975), Seasonal effects in ionospheric storms, Proc. COSPAR Sym. Sat. Beacon Studies of Ionospheric Structure and ATS-6 Data, IZMIRAN, Moscow, U.S.S.R.

- Mendillo, M., Papagiannis, M.D. and J.A. Klobuchar (1969), A Seasonal effect in the mid-latitude slab thickness variations during geomagnetic storms, *J. Atmosph. Terr. Phys.*, 31, 1359.
- (1970), Ionospheric storms at mid-latitudes, *Radio Sci.*, 5, 895.
- (1972), Average behavior of the midlatitude F-region parameters  $N_T$ ,  $N_{max}$ , and  $\tau$  during geomagnetic storms, *J. Geophys. Res.*, 77, 4891.
- Obayaski, T. (1964), *Research in Geophysics*, Ch. 14, ed. Odishaw, The MIT Press, Cambridge, MA, U.S.A.
- Papagiannis, M.D., Hajeb-Hosseinih and M. Mendillo (1975), Changes in the ionospheric profile and the Faraday factor M with Kp, *Planet. Space Sci.*, 23, 107.
- Prolss, G.W. and K.H. Fricke (1976), Neutral composition changes during a period of increasing magnetic activity, *Planet. Space Sci.*, 24, 61.
- Schodel, J.P., Mendillo, M., daRosa, A.V., Klobuchar, J.A., Roelofs, T.H., Fritz, R.D., Essex, E.A., Flaherty, B.J., Hibberd, F.H., Kersley, L., Koster, J.R., Liszka, L. and Y. Nakata (1974), A global description of the F-region during the ionospheric storm of December 17, 1971, *J. Atmosph. Terr. Phys.*, 36, 1121.
- Titheridge, J.E. (1972), Determination of ionospheric electron content from the Faraday rotation of geostationary satellite signals, *Planet. Space Sci.*, 20, 353, 1972.